HOKKAIDO UNIVERSITY

Title	GROWTH OF RUTILE AND TRIRUTILE SINGLE CRYSTALS BY THE FLOATING ZONE METHOD
Author(s)	Higuchi, Mikio
Degree Grantor	北海道大学
Degree Name	博士(工学)
Dissertation Number	乙第4665号
Issue Date	1994-12-26
DOI	https://doi.org/10.11501/3080071
Doc URL	https://hdl.handle.net/2115/32675
Type	doctoral thesis
File Information	4665.pdf

Hokkaido University Collection of Scholarly and Academic Papers : HUSCAP

GROWTH OF RUTILE AND TRIRUTILE SINGLE CRYSTALS BY THE FLOATING ZONE METHOD

MIKIO HIGUCHI

1994

*There is no **perfect** single crystal. The **perfect** single crystal can be theoretically imagined only at 0 K, which you can never reach. Therefore, actual crystals, even a silicon crystal for semiconductor devices, should involve intrinsic defects more or less. So, do you give up to grow the **perfect** single crystal? The answer should be "No", even though you surely know that is impossible. You have to keep on trying to grow better single crystals, believing those crystals to be of use for all the mankind.*

CONTENTS

Chapter 1	**General Introduction**	1
1.	Properties of Rutile Single Crystals	6
2.	Possible Other Materials for Polarizer	12
3.	Outline of the Floating Zone Method as a Growth Technique of Rutile Single Crystals	17
4.	Outline of this thesis	29
	References	31
Chapter 2	**Growth of Low-Angle Grain Boundary Free Rutile Single Crystals by the Floating Zone Method**	33
1.	Introduction	34
2.	Experimental	35
3.	Results	43
4.	Discussion	56
5.	Summary and Conclusions	65
	References	66
Chapter 3	**Effects of Aliovalent Cations on Decoloration of Floating Zone Grown Rutile Single Crystals**	68
1.	Introduction	69
2.	Experimental	70
3.	Results	71
4.	Discussion	81
5.	Summary and Conclusions	89
	References	90
Chapter 4	**Solid-Liquid Interface Shapes in the Floating Zone Growth of Rutile Single Crystals**	92
1.	Introduction	93
2.	Experimental	94
3.	Results and Discussion	95
4.	Summary and Conclusions	105
	References	106

Chapter 5 **Characterization of the Floating Zone Grown Rutile Single Crystals as Polarizer** 107

1. Introduction 108
2. Concept and Measurement of the Extinction ratio 109
3. Fabrication of Prisms 114
4. Results and Discussion 120
5. Summary and Conclusions 125

Chapter 6 **Floating Zone Growth and Characterization of $MgTa_2O_6$ and $NiTa_2O_6$ Single Crystals** 127

1. Introduction 128
2. Experimental 129
3. Results and Discussion 130
4. Summary and Conclusions 150

References 152

Chapter 7 **Conclusions** 153

Acknowledgements 158

Chapter 1

General Introduction

The first people who used optical communication were probably ancient Chinese. They used a *beacon* as a signal. The meaning of the beacon was decoded by its colors and shapes. The *beacon* towers were placed at intervals of 4–5 km, and the raid of enemy was rapidly informed from the border to the capital. Although the amount and speed of the communication by the beacon are of course much less than those of the modern communication, the idea that optical signals were used as communication media should be admired.

As the amount of information is increased and more rapid communication is required, the communication means have been improved. In order for that, the development of new materials and devices has been indispensable. The inventions of laser in 1960 and optical fiber in 1970 brought great evolution to optics technology. These two inventions were subsequently combined with microelectronics to form a new technology field so–called "opto–electronics". The optical communication system is a representative device of opto–electronics technology, and this system has already expelled electric communication system from the long distance and large scale communication. In near future, the optical communication system will displace the electric communication system in all the wired communication, even home telephones.

A variety of single crystals are necessary in modern optical devices, since, in single crystals, there are no grain boundaries, which usually deteriorate the essential properties of materials. Table 1 summarizes the single crystal materials which are used for the optical devices. The optical communication system basically comprises a laser–diode as a signal source, an optical fiber as a communication medium and a photo–diode as a signal receiver. In practice, however, a number of other devices are of course necessary to keep the quality of signal as high as

Table 1. Optical properties and applications of single crystal materials.

optical property	single crystal materials	application
transparency	KBr, NaCl, CaF_2	window
birefringence	SiO_2, $CaCO_3$, TiO_2	polarizer
fluorescence	$CaWO_4$, CsI, LiF	phosphor
photo–conduction	CdS, InSb	photo–diode
light emitting	GaAs, GaP, GaAlP, GaN, SiC	light emitting diode
	Cr:Al_2O_3, Nd:$Y_3Al_5O_{12}$, GaAlAs	laser
	$Bi_4Ge_3O_{12}$, NaI	scintillator
	ZnSe, ZnS	electro–luminescence
electro–optic effect	$LiNbO_3$, $LiTaO_3$, $Bi_{12}SiO_{20}$	optical modulator
acousto–optic effect	$PbMoO_4$, TeO_2	optical modulator
magneto–optic effect	$Y_3Fe_5O_{12}$, $(YbTbBi)_3Fe_5O_{12}$	optical isolator

possible. For example, an optical isolator is an important device to prevent the incidence of reflected light to the laser diode so that stable lasing is realized. Fig. 1 illustrates the principle of the optical isolator. A basic optical isolator comprises a Faraday rotator, a magnet and two polarizer.

As shown in table 1, iron garnet single crystals are used as a Faraday rotator in an optical isolator because of their excellent magneto–optic effect. Yttrium iron garnet (YIG) single crystals are also used for microwave resonator and magnetic bubble memory devices. Thus, intensive research work has so far been done to prepare both bulk and thick–film YIG single crystals of high quality. Also, a variety of the chemical compositions of iron garnet has been examined to design better Faraday rotator which has a larger rotation angle in a constant magnetic field.

In contrast to Faraday rotator materials, little research work has been done for the development of polarizer materials. There are two reasons. One is that high quality calcite single crystals are still available in natural resources, and the other is that the polarizer materials does not have any attractive functions besides generating polarized light. However, calcite single crystals have some disadvantages to use in optical communication system as discussed later. Accordingly, the demand for other materials which have large birefringence has been increasing in recent years.

Rutile (TiO_2) is one of the most promising materials as polarizer and the floating zone method is a promising technique to grow high quality rutile single crystals. Also, other oxide which have rutile or rutile–related structure may have attractive optical properties, such as large birefringence and refractive index. The purpose of this study is to establish the growth technique of rutile single crystals

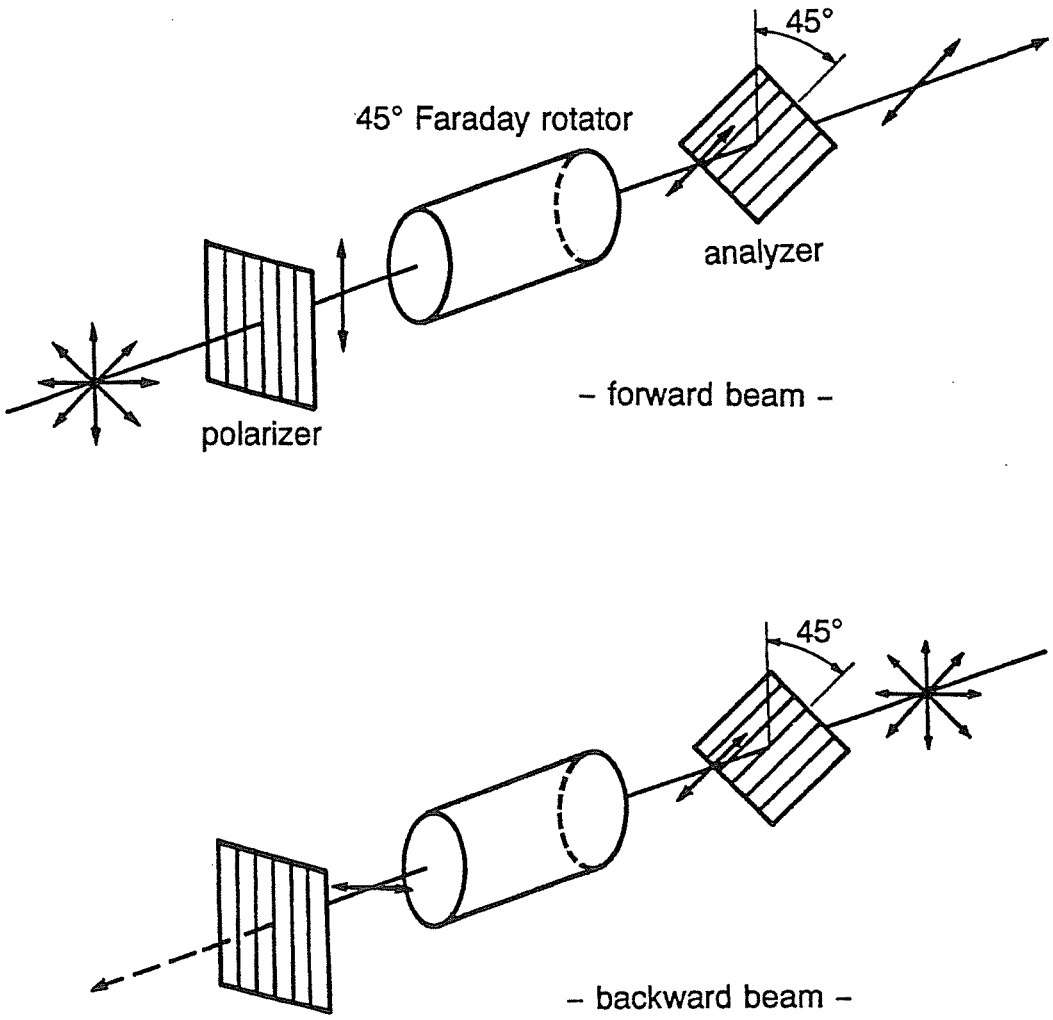

Fig. 1. Principle of the optical isolator.

by the floating zone method and to search for new polarizer materials. The following sections give detailed descriptions on rutile single crystals, other candidates as polarizer materials and the floating zone method.

1. PROPERTIES OF RUTILE SINGLE CRYSTALS

The first artificial growth of rutile single crystals was done by the Verneuil flame fusion technique in 1940'S [1]. The main use of the Verneuil–grown rutile single crystals was for gem stones as imitation diamonds, which were called "night stone" and were highly valued at that time. However, the imitation diamond was soon replaced by other materials, that is, strontium titanate ($SrTiO_3$), rare–earth garnet: yttrium aluminum garnet ($Y_3Al_5O_{12}$) or gadolinium gallium garnet ($Gd_3Ga_5O_{12}$), and finally cubic zirconia (stabilized ZrO_2) was found to be the best for imitation of diamond. Until 1980's, when another important use was found, there was no use for rutile single crystals except for research of basic properties of rutile.

When rutile single crystals are used as imitation diamonds, only large refractive index is remarked; however, rutile has exceptionally large birefringence (double refraction), which is much larger than that of calcite or quartz single crystals which have conventionally been used as polarizer materials. At early 1980's, Shirasaki et al. developed an optical isolator in which rutile single crystals were used as polarizers [2]. After that, rutile single crystals has been replacing calcite in a variety of optical devices. This section deals with the physical and chemical properties of rutile single crystals as compared with calcite and quartz single crystals.

1.1. Thermal stability with respect to crystal growth

Rutile is one of the modifications of titanium dioxide (TiO_2). The other modifications under atmospheric pressure are known as anatase and brookite. Rutile is the only stable phase in three modifications in all the temperature range (form 0 k to congruent melting temperature of 1840 °C) and the other two modifications can exist only metastable phase. This make it possible to grow rutile single crystals directly from the melt. On the other hand, the thermal properties of calcite and quartz, which have been conventionally used for polarizer, are as follows:

Calcite ($CaCO_3$) is thermally unstable, that is, the dissociation pressure of $CaCO_3$ reaches 1 atm at 900 °C to release CO_2. It is therefore impossible to grow $CaCO_3$ single crystals by melt growth techniques unless extremely high CO_2 pressure is applied; moreover, even if so, the grown crystal will be aragonite–type, which is one of the modifications of $CaCO_3$;

Quartz (SiO_2) does not dissociate, but SiO_2 undergoes phase transitions with increasing temperature, i.e. α–quartz → β–quartz → β–tridymite → β–crystobalite. These phase transitions are reversible but very sluggish (practically irreversible), and thus tridymite and crystobalite exist as metastable phase. Also, even melt growth of β–crystobalite is impossible since SiO_2 does not crystallize directly from the melt but form glass due to the extremely high viscosity at the melting temperature.

These facts may limit the growth technique for calcite and quartz single crystals, that is, calcite and quartz must be grown below 900 °C and 573 °C, respectively. The solution growth, especially hydrothermal growth is the best way

to grow these crystals. In fact, high quality quartz single crystals, which are served not only in electronic devices but also in optical devices, are grown by the hydrothermal technique in industrial scale [3]. On the other hand, the artificial growth of calcite has not been established despite a number of studies [4,5], and thus the supply of calcite single crystals depends on only natural resources.

1.2. Optical properties as polarizer materials

Optical properties of rutile, calcite and quartz are listed in table 2. The most important requirement for polarizer materials is that birefringence should be as large as possible in order to design smaller polarizers. From this point of view, rutile seems to be the most promising material because of the largest birefringence in these three materials. Also, the large refractive indices of rutile contribute to fabricate smaller polarizers.

The optic character, whether positive (rutile and quartz) or negative (calcite), does not matter in the design of polarizers. On the other hand, the optical activity, which quartz has, should be taken into account for polarizer design. It is needless to say that the optical activity is undesirable property for polarizer materials.

The absorption edge is not an important factor when the application is limited to optical communication, because the wavelength bands of around 1.3–1.5 μm are usually used. However, shorter wavelength, e.g. ultraviolet region, is preferred for memory devices to increase the memory density. Rutile may not be a suitable material in such devices, since rutile has the absorption edge of 420 nm and completely absorbs ultraviolet radiation. Calcite will be used in such devices because of its absorption edge of 210 nm. Quartz is the only material in these three for the use in vacuum ultraviolet region.

Table 2. Optical properties of rutile, calcite and quartz

		rutile	calcite	quartz
refractive index	n_o	2.616	1.658	1.544
(λ=598nm)	n_e	2.903	1.486	1.553
birefringence		0.287	0.172	0.009
optic character		+	−	+
optical activity		−	−	+
absorption edge (nm)		420	210	150

Summarizing the optical properties of these three materials, rutile is the most promising for polarizers. Calcite has comparable optical properties to rutile. The only advantage of quartz is that the crystal can be used in vacuum ultraviolet region.

1.3. Miscellaneous properties as practical polarizer materials

In practical devices, the optical properties are not the only factor to determine whether the material is suitable or not. The mechanical and chemical properties are also important. Table 3 shows the Mohs hardness, cleavage and the chemical stability of rutile, calcite and quartz.

Hardness is important factor in processing the crystals. As one of the disadvantages of calcite, it is significantly soft and skilled technique is indispensable to process the calcite single crystals. In contrast, rutile and quartz have moderate hardness, that is, not so hard as corundum and also not so soft as calcite.

Cleavage is also important factor in the processing of crystals. A quartz crystal has no cleavage plane because its structure is consisted of SiO_4 tetrahedra which link 3–dimensionally in the crystal. Accordingly, quartz does not have any cleavage plane. The crystal structure of calcite is considered to be a modification of rock salt structure, in which Na^+ and Cl^- is replaced by Ca^{2+} and CO_3^{2-}. In a NaCl crystal, the cleavage plane is (100), which correspond to (1011) plane in calcite structure. Accordingly, a calcite single crystal is easily and completely cloven on the (1011) plane. Rutile also has a cleavage plane of (110), but a rutile single crystals is not easily cloven by the mechanical shock. There is thus no problem on cleavage in the processing of rutile single crystals.

Table 3. Miscellaneous properties of rutile, calcite and quartz

	rutile	calcite	quartz
Mohs hardness	6.5	3	7
cleavage	(110)	(1011)	none
chemical stability	excellent	poor	excellent

Although the optical devices are usually not used in severe conditions, those devices are required to assure a long-term stability. In particular, junction devices which connect a long-distance optical communication are used under the sea, and are accordingly not easy to be fixed or replaced. The most possible factor to deteriorate the devices may be the attack of moisture. Therefore, each element (crystal) should have a strong durability to water. Calcite has a little solubility in water. On the other hand, rutile is very stable to water and also other acids. This fact is the strongest motive to use rutile single crystals replacing calcite single crystals, although appreciably large single crystals with high optical quality is still available in natural resources.

2. POSSIBLE OTHER MATERIALS FOR POLARIZER

As mentioned in the previous section, calcite ($CaCO_3$) and quartz (SiO_2) single crystals have conventionally been used for polarizers. The most advantageous point for these materials is that large single crystals can be easily obtained, that is, large calcite single crystals are abundant in the natural resources, and large quartz single crystals have been commercially grown by the hydrothermal method. The fact that these crystals can be steadily supplied supports to use these materials in practical devices, although each material has disadvantages as discussed in the previous section. In the same section, rutile is also discussed as a promising polarizer material which compensate the disadvantages of calcite and quartz.

The most important requirement for polarizer materials is needless to say that their birefringence should be as large as possible. In table 4, the optically uniaxial crystals which have large birefringence are summarized including calcite, quartz

and rutile. Also, refractive index for ordinary ray and birefringence of the materials are illustrated in fig. 2. Following describes features of these materials mainly from the viewpoint of crystal growth.

Paratellulite (TeO_2):

This crystal is possible to grow by the Czochralski method [6], although the evaporation is intensive. Accordingly, appreciably large single crystals are obtainable. The crystal structure of TeO_2 is of distorted rutile type. Birefringence is 0.157, which is comparable to that of calcite. However, the performance as polarizer will be limited because of the optical activity (optical rotatory power).

$NaNO_3$:

$NaNO_3$ has the same structure as calcite. Birefringence is 0.248. On the contrary, refractive index is appreciably small. Accordingly, extremely small polarizers can be fabricated. However, $NaNO_3$ can not be used in practical devices because of deliquescence.

Magnesite ($MgCO_3$):

Magnesite has larger birefringence of 0.191 than that of calcite, of which structure is the same as magnesite. However, large single crystals of magnesite are not available in natural resources and artificial single crystal growth of magnesite is also difficult.

Hematite (Fe_2O_3):

Large single crystals of hematite is difficult to grow since Fe^{3+} ions are easily reduced to Fe^{2+} at high temperature. Because of the strong color, this crystal can not be used in the visible region, although its birefringence (0.28)

Table 4. Refractive index and birefringence of various optically uniaxial crystals

crystal	refractive index		birefringence	space group	remarks
	n_o	n_e			
calcite ($CaCO_3$)	1.658	1.486	0.172	*R3c*	
quartz (SiO_2)	1.544	1.553	0.009	$P3_121$	optical activity
rutile (TiO_2)	2.615	2.911	0.296	$P4_2/mnm$	
paratellulite (TeO_2)	2.274	2.430	0.156	$P4_12_12$	optical activity distorted rutile
$NaNO_3$	1.585	1.337	0.248	*R3c*	deliquescence calcite–type
magnesite ($MgCO_3$)	1.700	1.509	0.191	*R3c*	calcite–type
hematite (Fe_2O_3)	2.94	3.22	0.28	*R3c*	strong brownish red
YVO_4	1.958	2.168	0.210	$I4_1/amd$	
cassiterite (SnO_2)	1.997	2.093	0.096	$P4_2/mnm$	rutile–type
tapiolite ($FeTa_2O_6$)	2.27	2.42	0.15	$P4_2/mnm$	brownish yellow trirutile–type

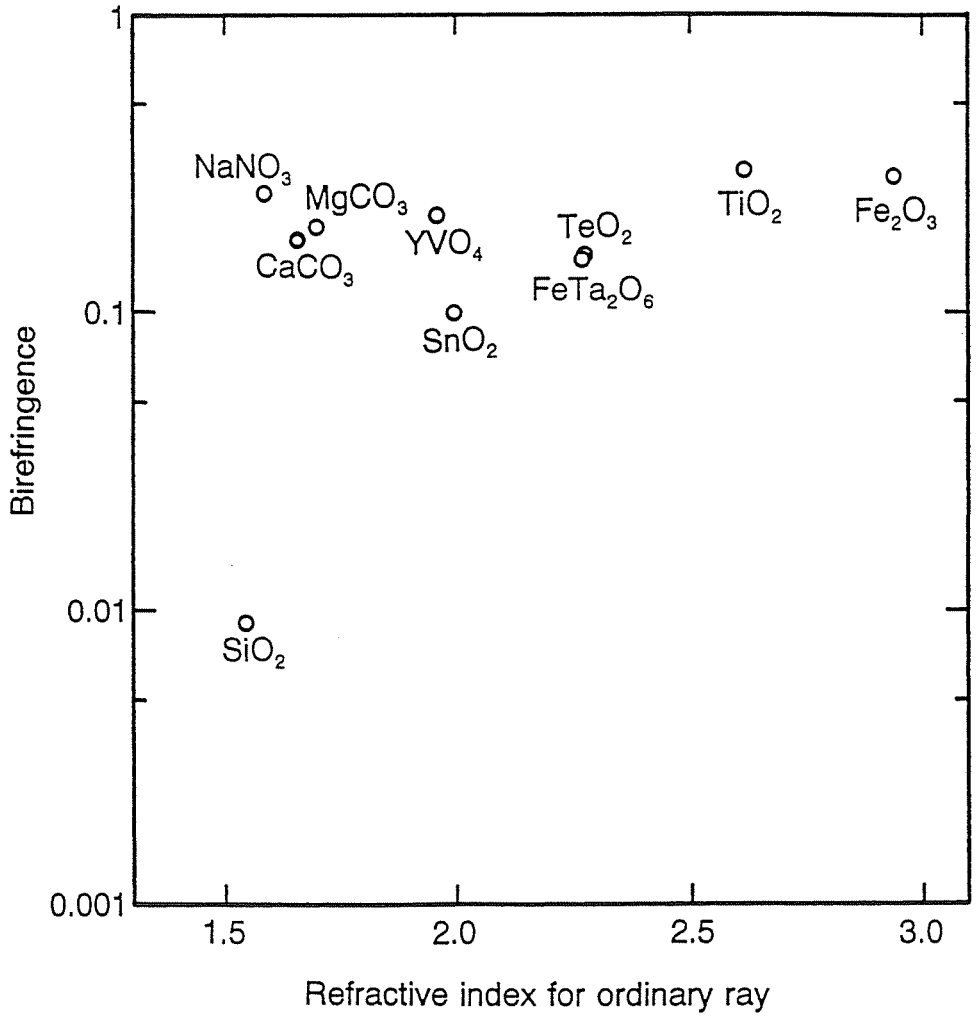

Fig. 2. Refractive index for ordinary ray and birefringence of optically uniaxial crystals.

is comparable to that of rutile. The crystal structure is of corundum type.

YVO_4:

The Czochralski growth of YVO_4 has recently been developed by Kuwano et al [7]. The crystal structure of YVO_4 is the same as zircon ($ZrSiO_4$). The birefringence of YVO_4 is 0.210, which is intermediate between those of calcite and rutile. Although processing is difficult because of strong cleavage, YVO_4 is, as well as rutile, a promising material for polarizers.

Cassiterite (SnO_2):

Cassiterite has the same structure as rutile. The birefringence of cassiterite is 0.096, which is appreciably smaller than that of rutile but is still much larger than that quartz. The crystal growth of SnO_2 is difficult because of high vapor pressure.

Tapiolite ($FeTa_2O_6$):

Tapiolite has the trirutile structure, which is a superstructure of rutile. The birefringence of tapiolite is 0.15, which is comparable to that of calcite. For the crystal growth of tapiolite, oxygen partial pressure must be strictly controlled to keep the valence state of iron to be 2+.

Classifying these materials on the basis of their structures, most materials belong to calcite or rutile type structure. In addition to these materials, there are a number of materials which have calcite or rutile type structure, although the optical properties of all the materials are not known. The new candidates as polarizer materials should may be in these materials, since those materials are expected to have large birefringence on the basis of their structures. From the viewpoint of crystal growth, the melt growth is obviously the best way to steadily

obtain large single crystals. However, the carbonate materials are impossible to grow directly from the melt because of high dissociation pressure of CO_2 at relatively low temperature. On the other hand, most trirutile type crystals are possible to grow from the melt since these materials melt congruently. Accordingly, the development of new polarizer materials should be done intensively on the materials with trirutile type structure.

3. OUTLINE OF THE FLOATING ZONE METHOD AS A GROWTH TECHNIQUE OF RUTILE SINGLE CRYSTALS

3.1. Possible techniques for the growth of rutile single crystals

An appreciable number of crystal growth techniques have so far been developed. The growth techniques are used properly on the basis of the thermal properties of the crystals to be grown. Fig. 3 illustrates the flow chart to select the growth techniques of bulk single crystals. The economical factor is, of course, important, but this factor is neglected in this flow chart. Each technique may involve subdivided techniques, which are also neglected.

It is a quite common knowledge that melt growth technique using a crucible, if possible, is the best way to grow large-scale, bulk single crystals. In fact, large semiconductor and oxide single crystals are commercially produced by the Czochralski method, and ferrite and halide single crystals are grown by the Bridgman method [8,9]. However, all the materials are not grown by those methods, even if the material melts congruently and a crucible is available. Rutile is a typical material which is difficult to grow by the Czochralski and Bridgman method.

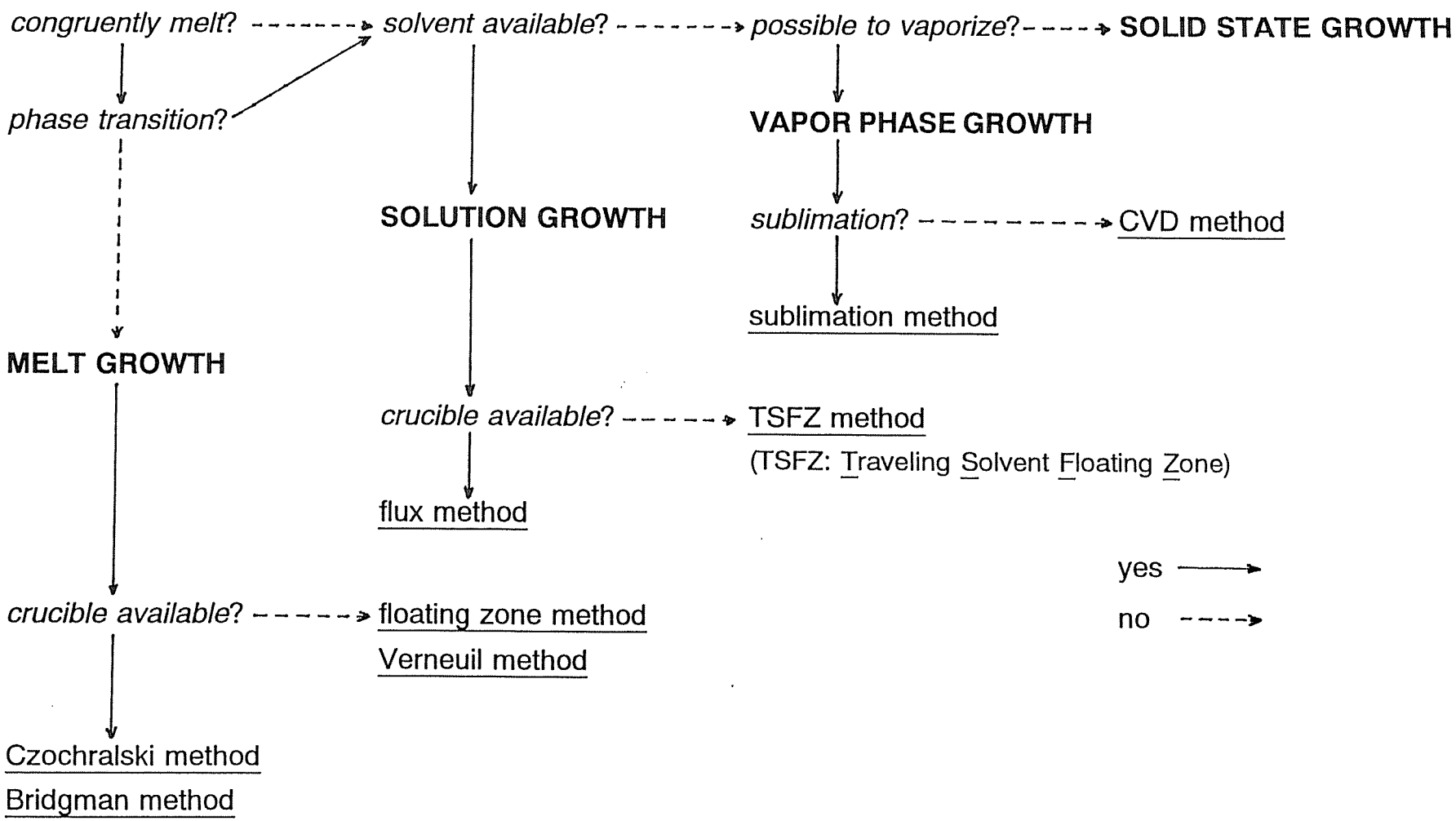

Fig. 3. Flow chart for the selection of bulk crystal growth techniques.

Iridium (Ir) is the only crucible material which can be used at the melting temperature of rutile (about 1840 °C) without the reaction with TiO_2 melt. The iridium crucible is extremely expensive as compared with platinum crucibles (of course, even platinum is not inexpensive), and thus the Bridgman method can not be applied since the crucible should usually be broken to take out the grown crystal. On the other hand, some researchers have been tried to grow rutile single crystals by the Czochralski method, but no one has succeeded to establish the conditions for steady growth of rutile. Machida et al concluded that in the Czochralski growth of rutile the control of crystal diameter is very difficult due to the anomalous convection in the melt [10]. The appearance of the Czochralski grown rutile single crystals were either twisted or hollow–shell shape. Accordingly, a crucible–free melt growth technique should be employed for the growth of rutile single crystals.

As shown in fig. 3, both the floating zone method and the Verneuil method are representative crucible–free melt growth techniques. In fact, rutile single crystals have been commercially produced by the Verneuil method. In the following section, the features of the floating zone method is described in comparison with the Verneuil method.

3.2. Features of the floating zone method

3.2.1. Basic concept of the floating zone method

The floating zone method is a kind of zone melting. A long boat is necessary for the ordinary zone melting, in which the growth system is aligned horizontally, whereas no container is necessary and the growth system is aligned vertically. Fig. 4 illustrates the basic concept of the floating zone method. The heat is

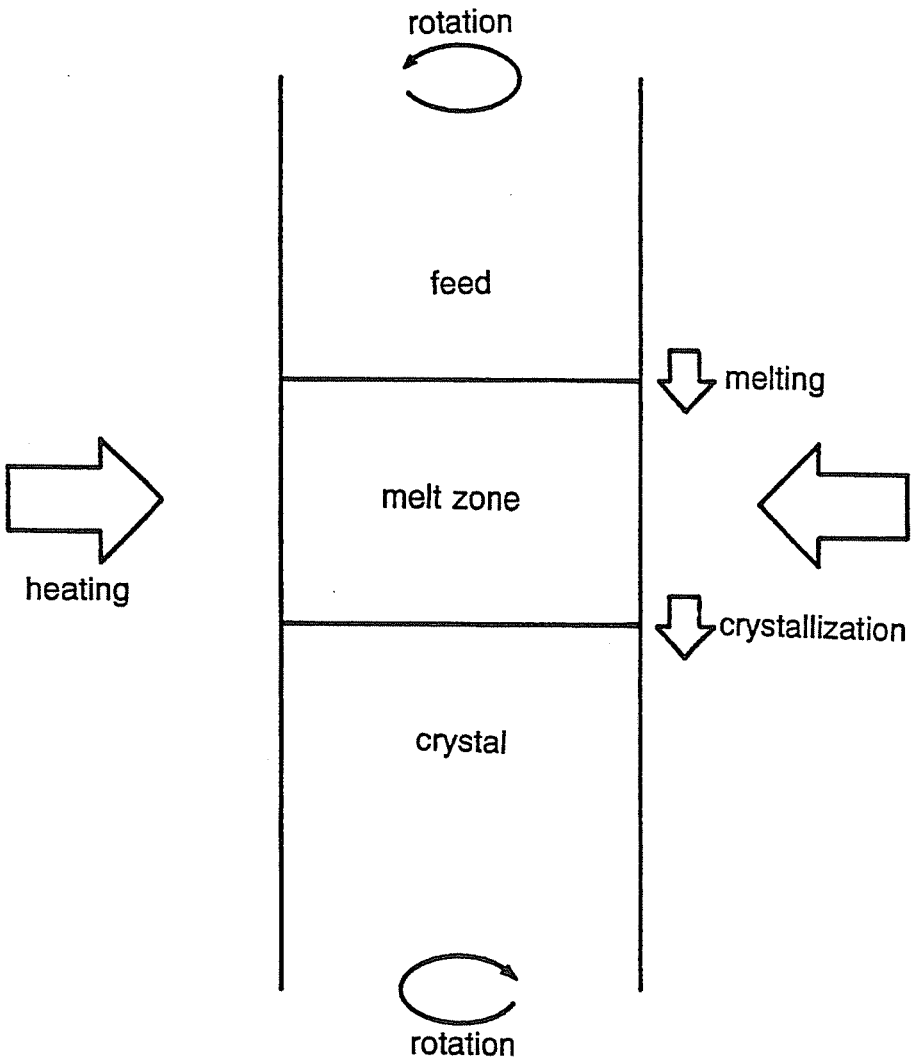

Fig. 4. Basic concept of the floating zone method.

concentrated to one point in space by some technique to form melt zone, which is literally floated and held in space only by the surface tension of the melt itself. Therefore, if the heated region is too long, the melt zone will collapse due to the increased self–weight. Crystal growth is effected by moving melt zone up or down, when melting occur at the interface between the feed rod and the melt zone, and simultaneously solidification occur at the interface between the melt zone and the crystal. Both the feed rod and the crystal are usually counter–rotated in order to homogenize the melt zone thermally and compositionally.

3.2.2. Heating devices of the floating zone method

A variety of heating devices have so far been developed for the floating zone method. The primary purpose of the devices is to efficiently concentrate the heat to one point in space to realize a narrow melt zone which does not collapse due to the self–weight. Most heating sources are probably available for the floating zone method, for example, resistance heater, rf heating, laser beam, electron beam, flame, lamp image, etc. Each of these heating devices should have both merits and demerits. From the industrial viewpoint, the rf heating and the lamp image techniques are suitable, since a long–term stability is possible in both two techniques. In fact, one tenth of silicon single crystals, which are specified to be as pure as possible, are commercially grown by the rf heating floating zone method. The disadvantage of the rf heating is that dielectric materials can not be grown. Therefore, the rf heating can not be applied to grow rutile single crystals since rutile is an insulator, at least, at room temperature. On the other hand, a dielectric material can be grown by the lamp image method, if the material absorbs the infrared radiation. Even if the material itself is transparent to the infrared radiation, a feed rod will be heated. That is because the feed rod is

usually polycrystalline and the infrared radiation is scattered at the grain boundaries to be converted to thermal energy. Once molten part is formed, the melt absorbs the radiation very well, since the electron state of the melt should be different from that of solid.

3.2.3. Comparison between the floating zone method and the Verneuil method

As discussed above, the possible growth technique for rutile single crystals is limited to either the Verneuil method or the floating zone method (especially by the lamp image). The Verneuil method is also known as the flame fusion method and was originated by Verneuil at early 1900'S [11]. In the beginning, the Verneuil method was developed to grow ruby (single crystal of chromium-doped corundum). After that, the Verneuil method has been modified and sophisticated to be used for the crystal growth of a variety of materials [12]. Fig. 5 shows a schematic diagram of the Verneuil method. Powder is melted by passing through the flame, which is produced by the mixture of oxygen and hydrogen gases, and fall on a growing crystal, at the top surface of which thin molten layer is formed. Crystal growth is effected by slowly pulling down the crystal with some rotation. The basic concept of the Verneuil method is similar to the floating zone method. The only difference is the feed, that is, the feed is just powder in the Verneuil method and the feed is a solid (usually sintered) rod in the floating zone method.

Table 5 summarizes the comparison of the floating zone method using lamp image heating and the Verneuil method. Detailed descriptions on each item are given as follows:

i) Operation (crystal diameter control)

Both the floating zone method and the Verneuil method do not have any

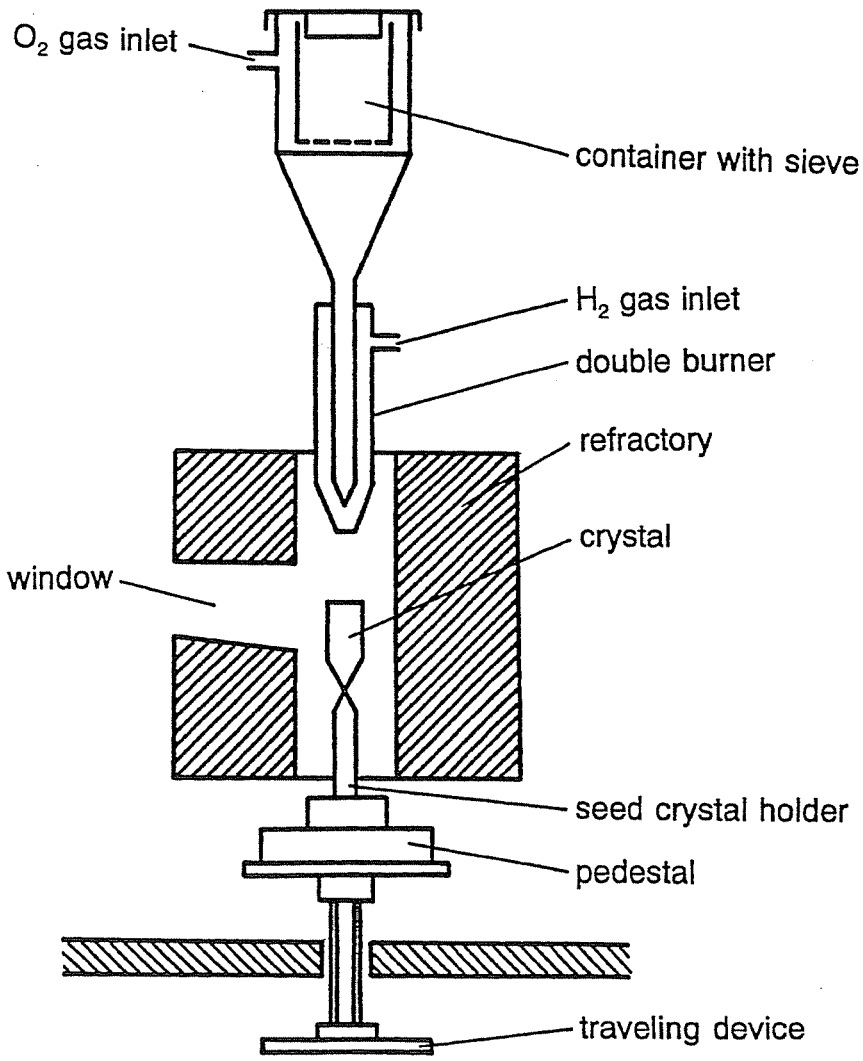

Fig. 5. Schematic diagram of the Verneuil method.

Table 5. Comparison between the floating zone method* and the Verneuil method

	floating zone method	Verneuil method
operation	easy	difficult
atmosphere control	easy	very difficult
crystal quality	good	poor
crystal size	up to 20 mm	up to 50 mm
price of apparatus	expensive	inexpensive

* the lamp image method

effective means of feedback, like a load cell in the Czochralski method, to control crystal diameter. Thus, the crystal diameter control should be done by the operator who has to keep on observing the situation of crystal growth to control the lamp power in the floating zone method, or to control mixing ratio and flow rate of fuel gas in the Verneuil method. In the floating zone method, however, to keep steady crystal diameter is not very difficult since a feed rod with uniform diameter is used although the preparation of the feed rod is indispensable. In the Verneuil method, it is very difficult to keep steady growth run, because the falling rate of the powder is not always constant and the temperature of the flame may be fluctuated by a little fluctuation of the mixing ratio and flow rate of the fuel gas. Accordingly, the operator of the Verneuil method is required a long-term training.

ii) Atmosphere control

The atmosphere, especially oxygen partial pressure, is often a very important factor in the crystal growth, e.g. oxygen partial pressure should be kept as low as possible for the metallic materials. In the Verneuil method, the growth atmosphere is almost determined by mixing ratio of the fuel gases and the growth system is not isolated from ambient. It is therefore impossible to control the growth atmosphere in the Verneuil method. On the contrary, the infrared radiation makes it possible to heat through a quartz tube so that the growth system can be completely isolated from ambient. Thus, the growth atmosphere is very easily varied from strong reducing atmosphere to high oxygen partial pressure.

iii) Crystal quality

In the melt growth, the dislocation density is determined by the thermal

environment to which the grown crystal is subjected. In the floating zone method, a grown crystal can not avoid to be subjected to considerably steep temperature gradient and it is thus difficult to obtain dislocation–free crystals like the Czochralski method. In the Verneuil method, a grown crystal is enveloped in the flame, which produce shallow temperature gradient, but the flame is usually put off after the crystal growth is completed and the crystal is thereby undergoes quenching and therefore strong thermal stress. Consequently, the Verneuil grown crystals usually have much larger dislocation density than the floating zone grown crystals.

iv) Crystal size (diameter)

In both the floating and the Verneuil methods, the melt is located on the top of a growing crystal. It is therefore not easy to increase the crystal diameter since the amount of the melt should be increased, followed by collapsing due to increased self–weight. In the case of the Verneuil method, corundum single crystals up to 50 mm in diameter can be grown, but 25 mm is a limit diameter for rutile single crystals. Large–size silicon single crystals above 100 mm in diameter are easily grown by the rf heating floating zone method, but it is not easy to increase the crystal diameter by the lamp image floating zone method as discussed in Chapter 5. The crystal diameter will be limited up to 20 mm in order to perform a stable growth run for any materials.

v) Price of apparatus

From the economical viewpoint, the price of the apparatus is an important factor to determine the price of the grown crystals. The Verneuil method is an economically excellent technique for the melt growth. The apparatus is basically constituted of a feed container, a gas burner, refractories and a

simple moving device. All these parts are inexpensive. On the other hand, the price of the image furnace is very expensive as compared with the Verneuil furnace.

Summarizing the comparison between the floating zone method and the Verneuil method, the floating zone is advantageous if the crystal quality is given priority, and the Verneuil method is favorable if the economical viewpoint is stressed.

3.2.4. Previous studies on single crystal growth by the floating zone method with an infrared convergence type heater

Since Akashi et al. had developed very sophisticated image furnaces for floating zone method [13], a variety of materials have been grown using this type apparatus. The following materials, which can not be grown by the Czochralski method, have been targeted:

a. Materials of which melting temperature is extremely high.
b. Materials which should be grown under an extremely low or high oxygen partial pressure.
c. Materials which melt incongruently.

In the cases a and b, a crucible is not available, and in the case of c, the Czochralski growth is principally impossible.

Sakurai et al. successfully grew Sm_2O_3–ZrO_2 solid solution single crystals, of which melting temperature was 2400 °C at least, by using a Xe–arc lamp of 5.4 kW as a heat source [14]. Kitazawa et al also reported the floating zone growth of refractory materials, such as $La_2Zr_2O_7$ (2300 °C), Y_2O_3 (2440 °C), ZrO_2–CaO (2600 °C), CaO (2600 °C) and $Y_2Zr_2O_7$ (2800 °C) [15]. These martials are

probably difficult to grow even by the Verneuil method since the melting temperatures are too high to melt by the flame.

Fayalite (Fe_2SiO_4) and ilmenite ($FeTiO_3$) congruently melt at 1205 °C and 1400 °C, respectively, but no crucible is available for these materials because strong reducing atmosphere is necessary to keep the valence state of iron to be 2+. Takei et al successfully applied the lamp image floating zone method to grow this material [16]. The growth atmosphere used was the mixture of CO_2 and H_2, in which platinum crucible can not be used even though the melting temperature of those materials are much lower than that of platinum.

The above-mentioned materials are certainly important for the basic study. However, the industrial application of the lamp image floating zone method has been limited to yttrium iron garnet (YIG) single crystals. YIG is a typical material which melts incongruently and the single crystals of YIG had conventionally been grown by the flux method. Kimura et al successfully grew YIG single crystals by the traveling solvent floating zone (TSFZ) method, in which the melt composition was Fe_2O_3 excess of 15–25 mol% [17]. The melt can coexist with the solid YIG. The basic idea to apply this method to grow YIG single crystals had already been proposed by Abernethy et al [18]. However, the quality of the crystals grown by Abernethy et al was poor since the growth apparatus was not suitable for the TSFZ method. The development of the sophisticated lamp image furnace made it possible to grow YIG single crystals by the TSFZ method. The TSFZ method is considered to be a modified self-flux method. A long-term slow cooling, which means slow growth rate, is usually necessary for the flux method; in the TSFZ method, however, the growth rate is relatively high, i.e. 1–1.5 mm/hr, because of a considerably steep temperature gradient at the solid-liquid interface.

4. OUTLINE OF THIS THESIS

As mentioned in the previous section, rutile has excellent optical, mechanical and chemical properties, and the demand for rutile single crystals has therefore been increasing to use as polarizers in a variety of optical devices. It is of urgent necessity to grow rutile single crystals of high optical quality. The floating zone method is one of the most promising techniques, which replace the Verneuil method, to grow rutile single crystals. The floating zone method is also attractive in materials research since the expense and the work involved are relatively small. Nevertheless, there have so far been no detailed reports on the growth of rutile single crystals by the floating zone method. Also, few research work has been made to grow trirutile type double oxides, and their optical properties have therefore not been clarified.

On these background, the purpose of this study has been directed to establish the growth technique of rutile single crystals of optical grade by the floating zone method and to clarify the optical properties of trirutile type double oxides. The growth conditions to obtain rutile single crystals by the floating zone method are discussed and the optical quality of the crystals as polarizer materials is examined. The trirutile type double oxides, of which birefringence is unknown but is expected to be large, are grown by the floating zone method and their optical properties are investigated. Following is the outline of this thesis:

Chapter 1 describes the general introduction of this study, including the importance to develop new polarizer materials, some properties of rutile as a polarizer material, other possible materials for polarizer, and outline of the floating zone method as possible technique to grow rutile and trirutile single crystals.

Chapter 2 describes the growth conditions to obtain low–angle grain boundary free rutile single crystals. The low–angle grain boundaries are the major cause to deteriorate the extinction ratio, which is most important index to evaluate the quality of the crystal as a polarizer. The effects of oxygen partial pressure, dopant and growth direction are examined to suppress the formation of low–angle grain boundaries.

Chapter 3 deals with the effect of aliovalent cations of the decoloration of rutile single crystals. The coloring of rutile is responsible to the absorption in near infrared region, in which the optimum wavelength bands for optical communication are present. The relation between the point defects and the diffusivity of oxide ions in the rutile crystal is discussed.

Chapter 4 deals with the liquid–solid interface shapes in the floating zone growth of rutile single crystals. In the floating zone method, the control of interface shapes is very important to grow large diameter single crystals. The interface shapes are investigated as a function of rotation rate, growth direction and crystal diameter. The relation between the growth conditions and interface shapes is discussed on the basis of the convection and thermal conduction in the melt.

Chapter 5 deals with the optical quality of the floating zone grown rutile single crystals. The extinction ratio of the prisms fabricated from the crystals is determined to evaluate the quality of the crystals as practical polarizers.

Chapter 6 deals with the floating zone growth and properties of $MgTa_2O_6$ and $NiTa_2O_6$ single crystals, which have the trirutile structure. The optimum growth conditions to obtain $MgTa_2O_6$ and $NiTa_2O_6$ single crystals are discussed. The

properties of $MgTa_2O_6$ and $NiTa_2O_6$ single crystals are clarified and compared with those of rutile single crystals. The potentiality of $MgTa_2O_6$ and $NiTa_2O_6$ single crystals as polarizer materials is also discussed.

Chapter 7 gives the conclusions of this thesis on the growth of rutile and trirutile single crystals by the floating zone method and their optical properties.

REFERENCES

1. Y. Nakazumi, *Seramikkusu*, **3** (1968) 731.
2. M. Shirasaki and K. Asama, *Appl. Opt.*, **21** (1982) 4296.
3. J. Asahara and K. Nagai, *Seramikkusu*, **15** (1980) 170.
4. D. R. Kinloch, R. F. Belt and R. C. Puttbach, *J. Crystal Growth*, **24/25** (1974) 610.
5. C. Belin, *J. Crystal Growth*, **34** (1976) 341.
6. S. Miyazawa, *J. Crystal Growth*, **49** (1980) 515.
7. Y. Kuwano and S. Saito, *Electronic Ceramics*, **24** (1993) 11.
8. H. Takei, *Nihon Kessho Gakkai-shi*, **31** (1989) 89.
9. S. Kimura and K. Kitamura, *J. Ceram. Soc. Jpn.*, **101** (1993) 22.
10. H. Machida and T. Fukuda, *J. Crystal Growth*, 112 (1991) 835.
11. A. Verneuil, *Compt. Rend.*, **135** (1902) 791.
12. Y. Nakazumi, "Kessho Kogaku Handbook", Kyoritsu Shuppan (1971) 892.
13. T. Akashi, K. Matsumi, T. Okada and T. Mizutani, *IEEE Trans.*, **Mag-5** (1969) 285.
14. O. Sakurai, Y. Yokotani, K. Uematsu, N. Mizutani and M. Kato, *Nihon Kagakukai-shi*, (1981) 1396.

15. T. Kitazawa, K. Nagashima, T. Mizutani, K. Fueki and T. Mukaibo, *J. Crystal Growth*, **39** (1977) 211.
16. H. Takei, *J. Crystal Growth*, **43** (1978) 463.
17. S. Kimura and I Shindo, *J. Crystal Growth*, **41** (1977) 192.
18. L. L. Abernethy, T. H. Ramsey Jr. and J. W. Ross, *J. Appl. Phys.*, **32** (1961) 376S.

Chapter 2

Growth of Low-Angle Grain Boundary Free Rutile Single Crystals by the Floating Zone Method

1. INTRODUCTION

There are a variety of crystals which are used for optical devices. The most important requirement for those crystals is optical uniformity, which is quantitatively estimated by measuring extinction ratio. For example, the single crystals used for a long distance optical communication should have the extinction ratio of more than 60 dB [1], which is equivalent to that the fluctuation of refractive index in the crystal is up to 10^{-6}. Although this specification is extremely severe, the extinction ratio of the crystals for optical devices should be as high as possible.

The main cause which gives rise to the fluctuation of refractive index is the strain in the crystal. Since TiO_2 melts congruently at 1840 °C, the melt growth technique can be applied. The Czochralski method is an excellent melt growth techniques to prevent the grown crystals from thermal stresses. In fact, dislocation-free GGG (gadolinium gallium garnet) single crystals can be grown by this method [2]. However, the Czochralski method is not suitable for growing rutile single crystals because of the difficulty in controlling the convection of melt [3]. As mentioned in Chapter 1, the Verneuil method is an economically excellent technique to grow refractory oxide single crystals; however, the Verneuil grown crystals are usually strongly strained due to the thermal stress, which is caused by quenching after the crystal growth is completed [4]. Accordingly, the strong strain in the Verneuil grown crystals is inevitable.

In the floating zone method, a grown crystal is not quenched and it is accordingly expected that the dislocation density in the floating zone crystal is much less than that in the Verneuil grown one. However, many low-angle grain

boundaries are formed in the rutile crystal grown by the floating zone method in an oxygen atmosphere, which seems to be reasonable to avoid the reduction at high temperature. The existence of the low-angle grain boundaries is a more serious problem than the strain, since the light propagating in such a crystal is refracted and scattered at the grain boundary to greatly reduce the extinction ratio.

In this chapter, following three items are examined to suppress the formation of low-angle grain boundaries in the floating zone grown rutile crystals:

(1) The effect of oxygen partial pressure,

(2) The effect of dopants, and

(3) The effect of growth direction.

The formation mechanism of the low-angle grain boundaries is also discussed on the basis of the obtained results.

2. EXPERIMENTAL

2.1. General description of crystal growth procedure by the floating zone method

The single crystal growth by the floating zone method commonly follows the flow chart shown in fig. 1. Two steps are involved in the crystal growth by the floating zone method. One is to prepare a feed rod and the other is to grow a single crystal with an image furnace. Following subsections describe detailed experimental procedure for the floating zone growth. This procedure is also employed in the experiments of following chapters with some modification in accordance with the specified purpose of the experiments.

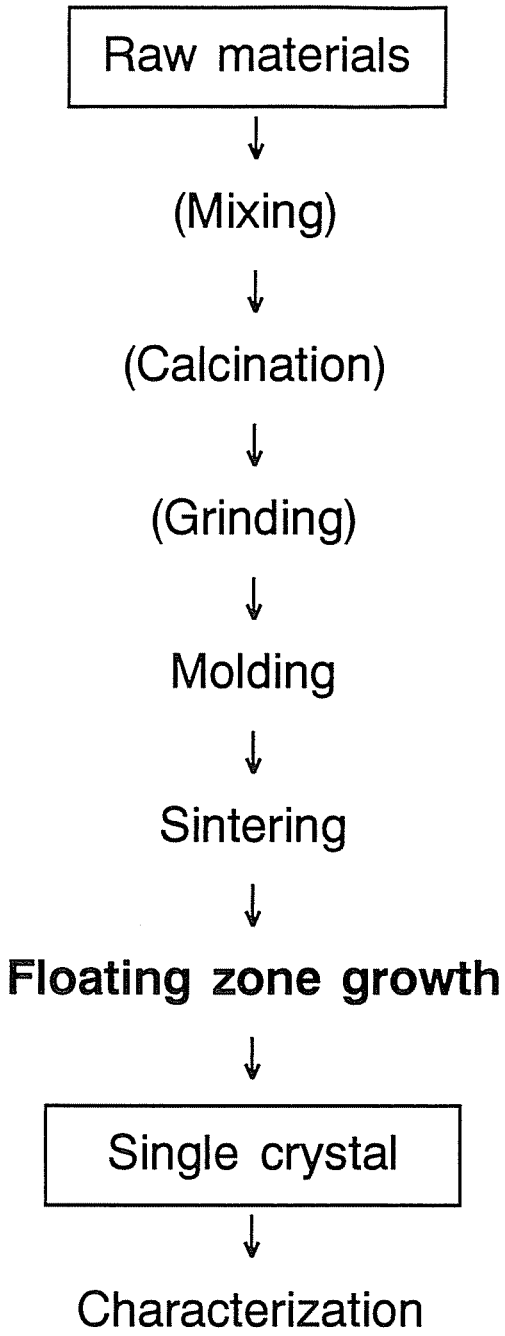

Fig. 1. Flow chart of crystal growth by the floating zone method

2.1.1. Preparation of a feed rod

One of the disadvantages of the floating zone method is the necessity to prepare a feed rod. The requirements for a feed rod is as follows:

i) A feed rod should be straight to avoid the precession movement, which disturbs a stable growth run.

ii) A feed rod should have a uniform diameter to keep constant melt volume and consequently a constant crystal diameter.

iii) A feed rod should have strictly stoichiometric composition for double oxides or uniform chemical composition to avoid compositional change or fluctuation in the melt zone, which might result in the cellular growth because of the constitutional supercooling.

iv) A feed rod should be as dense as possible to avoid the reverse penetration of the melt into the residual pores.

In order to meet the these requirements, a feed should be prepared as carefully as possible in following way.

In the case of the pure rutile, the starting materials, which are purchased from reagent company, can be directly used to prepare a feed rod. In the case of double oxides, however, the ignition loss of the starting materials should be determined before mixing in order to keep the stoichiometry, since the starting materials should adsorb some moisture or other volatile materials. The molding is usually effected by cold isostatic pressing (CIPping). The powder is introduced in a rubber bag, from which air should subsequently be evacuated. After sealing, the rubber bag is pressed under a hydrostatic pressure (usually 100 MPa) so that a cylindrical rod is obtained. The molded rod is then sintered at desired temperature for appropriate duration in a vertical tube furnace. For sintering, zone firing, which

means to pass the rod up and down through the hottest zone in the furnace, is performed to avoid the inhomogeneity of density due to the temperature gradient along vertical direction. The sintered rod is finally served to floating zone growth.

2.1.2. Growth apparatus

The growth apparatus used in this study is an infrared convergence type image furnace (Nichiden Machinery Ltd.: type SC–4B), of which prototype was developed by Akashi et al. Fig. 2 shows a schematic diagram of the image furnace. This furnace has gold–plated double ellipsoidal mirrors, at the focal point of which halogen lamps are placed. The emitted infrared light from the lamp is almost converged to the other focal point of the ellipsoid to form the melt zone. This apparatus has following advantages:

i) Heating is effected through a quartz tube, which isolates the growth system from ambience atmosphere, so that the growth atmosphere can be easily controlled.

ii) The melt zone can be directly monitored on the screen so that invaluable information on crystal growth can be obtained.

iii) The heat source (halogen lamp) has little power fluctuation so that very stable melt zone can be formed.

iv) The emitted radiation is converged from all the direction so that uniform temperature gradient is realized in horizontal direction.

v) Relatively steep temperature gradient can be obtained (fig. 3).

In the specification of this apparatus, the maximum temperature of 2150 °C is guaranteed by using halogen lamps of 3.5 kW. In fact, a cobalt–doped spinel ($Co:MgAl_2O_4$) single crystal is easily grown by using this type apparatus [5].

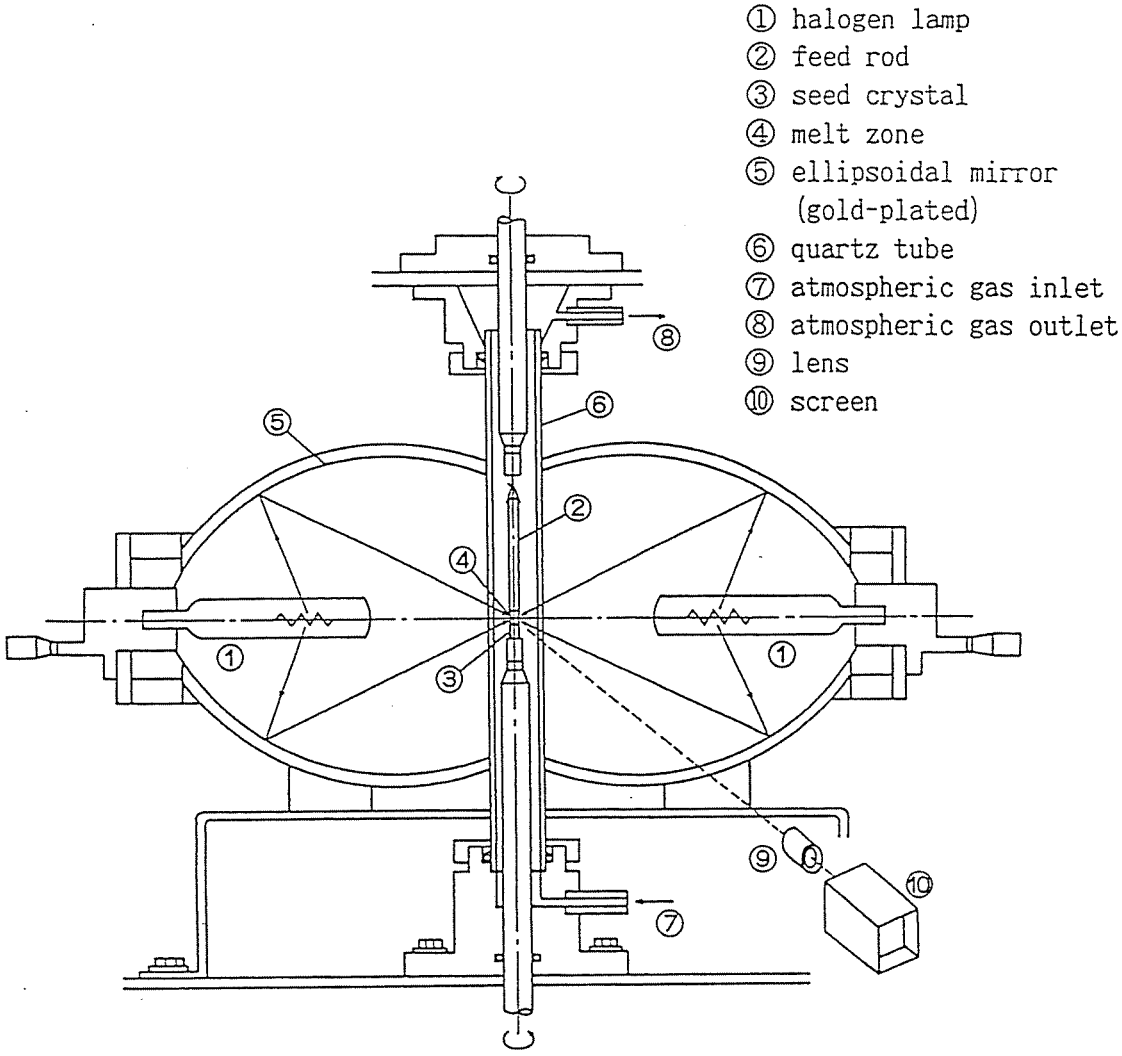

Fig. 2. Schematic diagram of the image furnace used in this study.

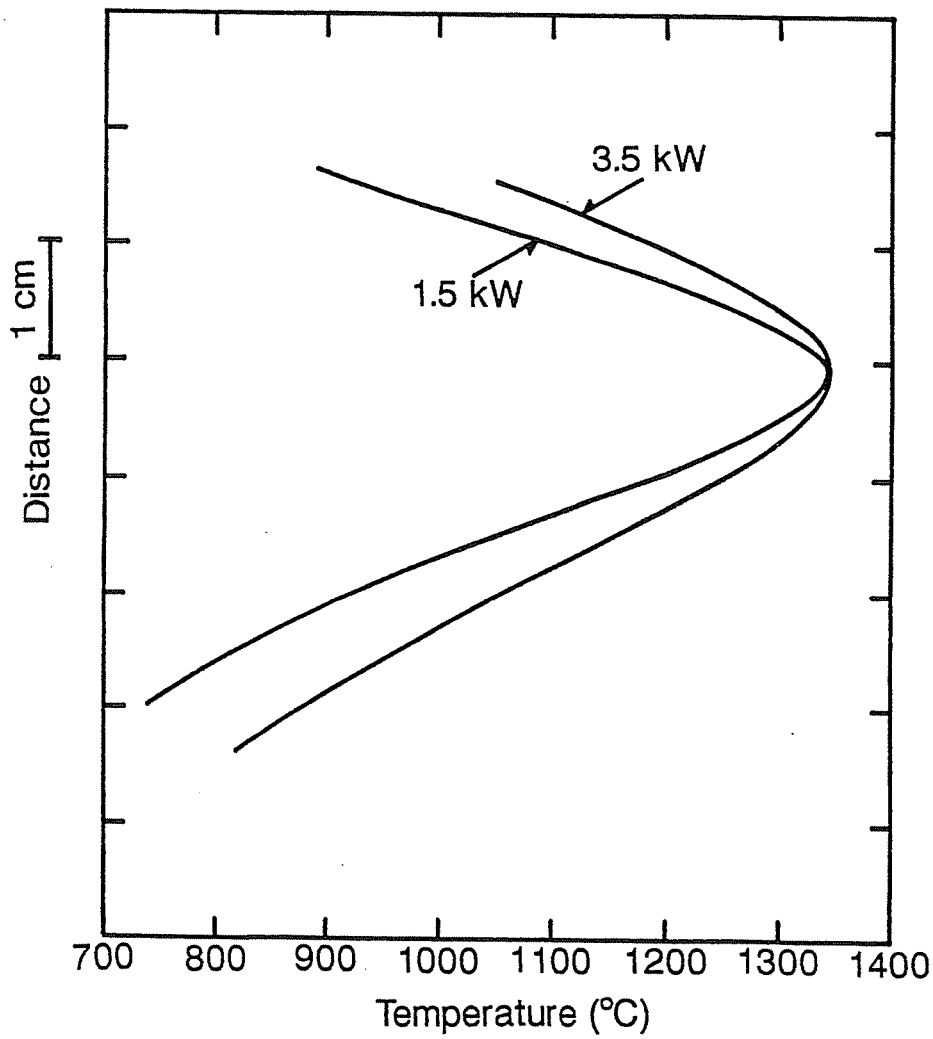

Fig. 3. Vertical temperature gradient in the image furnace.

2.1.3. Crystal growth procedure by the floating zone method

The crystal growth by the floating zone method is usually effected by moving a feed rod and a seed crystal downwards. If upwards, the diameter of a growing crystal will be get thinner and thinner because the meniscus shape at the solid–liquid interface of upper part is bent to the inside due to the balance between the surface tension and the gravity. Thus, a feed rod is suspended from the bottom of the upper shaft and a seed crystal is fixed to the top of the lower shaft. The feed rod is usually not fixed to avoid breaking out when the feed rod and the growing crystal contact because of the shortage of heating power.

The tip of the feed rod is firstly melted to form a droplet like a half–ball or a dome. The molten part is joined to the seed crystal to form a melt zone by adjusting the gap length between the feed rod and the seed crystal. The feed rod and the seed crystal should be counter–rotated at appropriate rotation rates. There are two purposes of the rotation: one is to make thermally uniform environment in the radial direction for the melt zone since the lamp image does not make cylindrically symmetric temperature gradient around the melt zone; the other is to agitate the melt zone to transfer the heat which is absorbed at the surface of the melt and to attain the uniformity in chemical composition. After joining the feed rod and the seed crystal, the melt zone is kept for 5–10 min before moving down to complete the wetting of melt to the seed crystal. The feed rod and the seed crystal are then moved downwards at an appropriate rate to grow a crystal.

In order to keep steady growth run, appropriate lamp power should be supplied to the melt zone. If the power is insufficient, the contact between the feed rod and the growing crystal frequently occur, which cause the instability of the melt zone. On the other hand, excessive lamp power results in the collapse of

the melt zone due to the increased self-weight. Also, the meniscus shape at the growing interface is important to keep a constant crystal diameter. The tangential of the meniscus at the interface should be parallel to the tangential of the growing crystal. Thus, careful power control should be done to keep a constant zone length and a constant meniscus shape by observing the image of the melt zone on the screen.

After growing a desired length, the feed rod and the grown crystal should be separated slowly to avoid the thermal shock. The lamp power is slowly reduced and the gap length between the feed rod and the growing crystal is gradually extended. After the separation, the lamp power is reduced at an appropriate rate which does not give the thermal shock to the grown crystal. Then the crystal growth procedure by the floating zone method is completed.

2.2. Experimental procedure for growing grain boundary free rutile single crystals

The raw materials used in this experiments are as follows: TiO_2 (Fuji Chitan Kogyo, 99.98%), ZrO_2 (Daiichi Kigenso Kagaku Kogyo, reagent grade), Al_2O_3 (Kojundo Kagaku Kenkyusho, 99.9%), SiO_2 (Kojundo Kagaku Kenkyusho, 99.9%) and Lu_2O_3 (Kojundo Kagaku Kenkyusho, 99.9%). When the effect of the oxygen partial pressure was examined, pure TiO_2 powder was directly used for making a feed rod. The effect of the dopants was examined with the addition of 0.5 at% (only in the case of ZrO_2 addition, 0.25–1.0 at% was tried). The pure or doped powder was molded to be a rod in the same way as above-mentioned and sintered at 1200 °C for 3 hours in air. After sintering, the dimension of the rod was 12 mm in diameter and 100 mm long. A Verneuil-grown crystal was used for a seed crystal, which was cut parallel or at an angle of 48 ° with the c-axis after the

determination of orientation by X-ray back Laue technique.

The oxygen partial pressure of growth atmosphere was controlled by the mixture of O_2 and Ar gases (total pressure of 1×10^5 Pa). A pure O_2 stream was used for growing doped crystals to eliminate the effect of the oxygen partial pressure. Other growth conditions were fixed as follows: the growth rate was 5 mm/hr; the rotation rate of both the feed rod and the seed crystal was 30 rpm (counter-rotation); growth direction was *c*-axis or inclined at an angle of 48 ° with the *c*-axis.

For the characterization, the grown crystals were cut to 2 mm thick plates perpendicularly to the growth direction. Both faces of the specimen were then polished to be mirror surfaces. The polished crystals was examined under a polarizing microscope with crossed nicols to observe low-angle grain boundaries.

3. RESULTS

3.1. Effect of the oxygen partial pressure

It is well known that TiO_2 is easily reduced at a high temperature to form a nonstoichiometric compound of TiO_{2-x} [6]. The value of x depends on both temperatures and oxygen partial pressures. If the oxygen partial pressure is high, x will be small at a constant temperature. Accordingly, rutile crystals should be grown under a high oxygen partial pressure to avoid the reduction. However, a rutile crystal grown by the floating zone method under an oxygen pressure of 1×10^5 Pa had many grain boundaries as shown in fig. 4(a). The grains contacted each other with misorientation less than one degree, which was determined by the

X-ray back Laue technique.

The commercially available Verneuil-grown rutile single crystals, which scarcely involves low angle grain boundaries, are usually black and opaque after the growth run [7]. This implies that the crystal must be grown under a considerably low oxygen partial pressure. The black color can probably be attributed to Ti^{3+} ions, which accompany oxygen vacancies for the charge compensation, and the transparency will be restored by subsequent annealing in an oxidation atmosphere. Thus, in the preliminary experiment, a CO_2 stream was tried as a growth atmosphere. CO_2 partially dissociates to give an oxygen partial pressure of about 1×10^3 Pa at the melting temperature of TiO_2 (1820 °C) in equilibrium condition; however, in actual growth system the oxygen partial pressure will be much lower than 1×10^3 Pa since the CO_2 gas flows at a constant velocity. Consequently, the number of low angle grain boundaries in a floating zone grown rutile crystal was drastically decreased by using the CO_2 stream as growth atmosphere. Therefore, the floating zone method, like the Verneuil method, can also produce rutile single crystals without the formation of the misoriented grain boundaries by controlling the oxygen partial pressure.

Fig. 4(b) shows an orthoscopic figure of cross sections of rutile single crystal grown under oxygen partial pressure of 1×10^3 Pa. This crystal had no grain boundaries except for the peripheral region. The upper limit of the oxygen partial pressure for growing grain boundary-free rutile single crystals was up to 3×10^3 Pa. Although the lower limit was not determined in this study, rutile single crystals were grown without grain boundaries under an oxygen partial pressure of 1×10^1 Pa, which is attained by using a pure Ar stream. The as-grown crystals were colored in dark blue because of the oxygen vacancies, but the normal pale

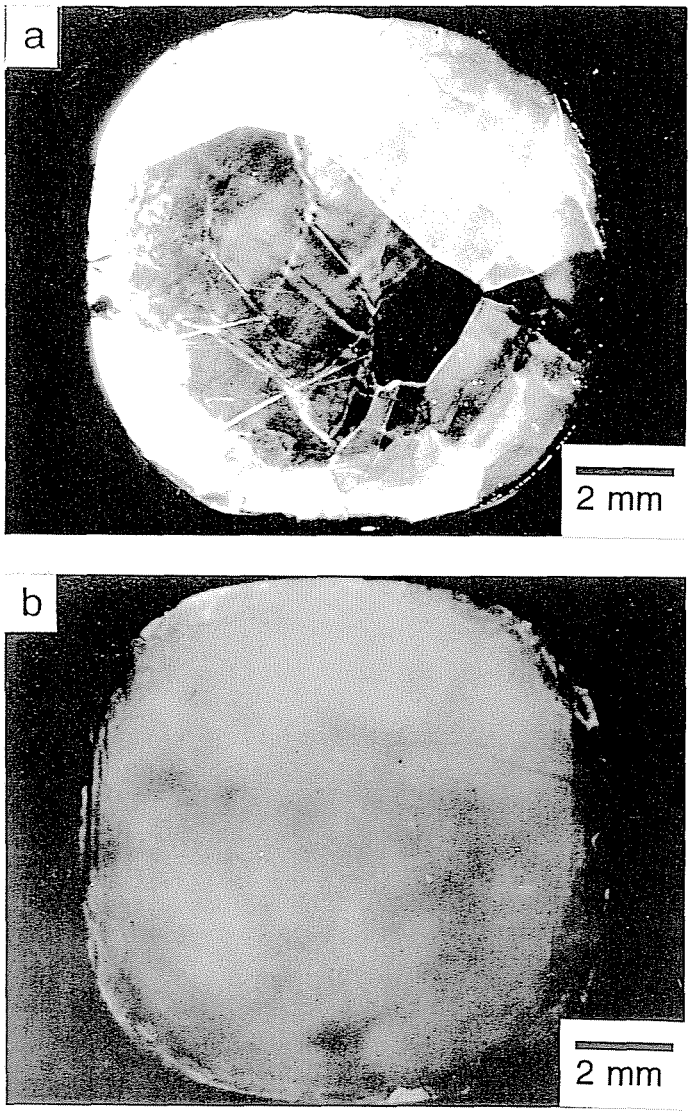

Fig. 4. Polarized microphotographs of the cross sections of rutile crystals grown under different oxygen partial pressure: (a) grown in an oxygen stream; (b) grown under an oxygen partial pressure of 1×10^3 Pa.

yellow color can be restored by annealing in an oxidation atmosphere after the crystal growth (although a long-term annealing is necessary, see Chapter 3).

Fig. 5(a) shows an interference (conoscopic) figure of a rutile single crystal grown by the floating zone method under a low oxygen partial pressure less than 1×10^3 Pa. The isogyers cross at approximately one point and all the isochromatic curves are concentric circles, whereas the isogyers are disordered when there are low angle grain boundaries. Fig. 5(a) is typical for an optically uniaxial crystal and the floating zone grown rutile single crystal accordingly has good optical quality. On the other hand, the interference figure of a commercial rutile single crystal grown by the Verneuil method was that of optically biaxial crystal as shown in fig. 5(b). The commercial crystal would undergo thermal stress, so that it behaved as if it were an optically biaxial crystal.

The etch pit density on the (110) plane of the floating zone grown rutile to clarify the relation between the optical quality and the dislocation density. Fig. 6(a) shows a typical etch pit pattern on the (110) plane of rutile observed with a scanning electron microscope. The geometry of the etch pit was pyramidal with a rectangular basal plane, whose longer and shorter side were parallel to [110] and [001] respectively. This figure reflects the symmetry of the (110) plane of the rutile type structure. Fig. 6(b) shows the distribution of etch pits observed with an optical microscope. The etch pit density on (110) plane was estimated to be $7\times10^4/cm^2$, while a commercial rutile single crystal had about ten times as high etch pit density as the floating zone grown one. The difference in the etch pit densities can be associated with the difference in the interference figures, because the presence of numerous dislocations give rise to the fluctuation of refractive index.

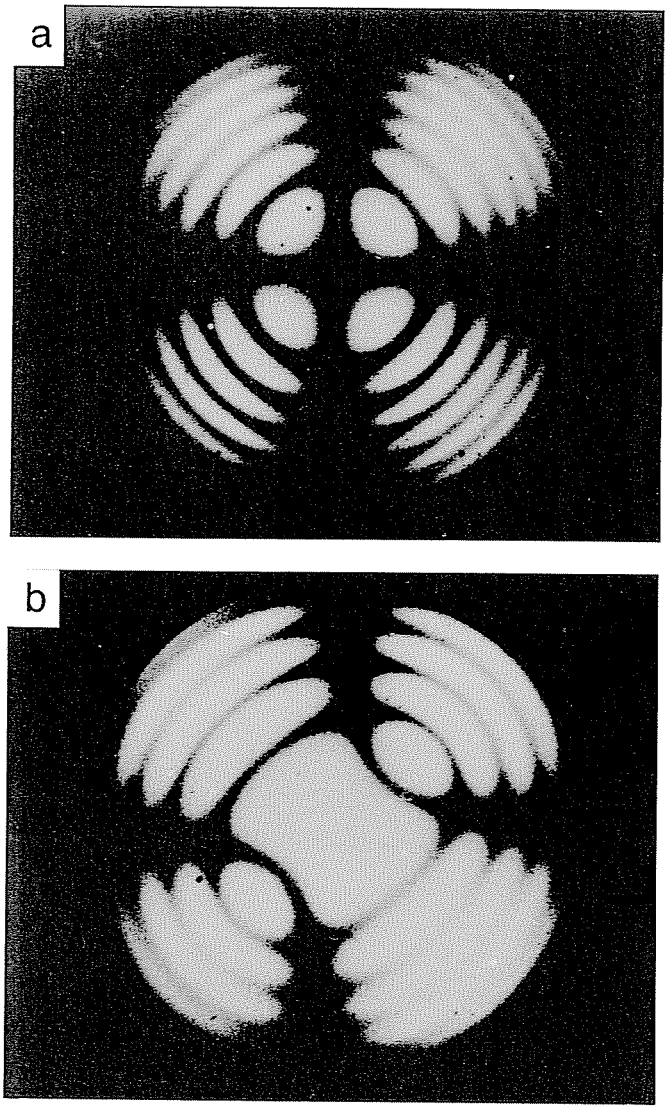

Fig. 5. Conoscopic figures of rutile single crystals: (a) grown in this study by the floating zone method; (b) grown by the Verneuil method.

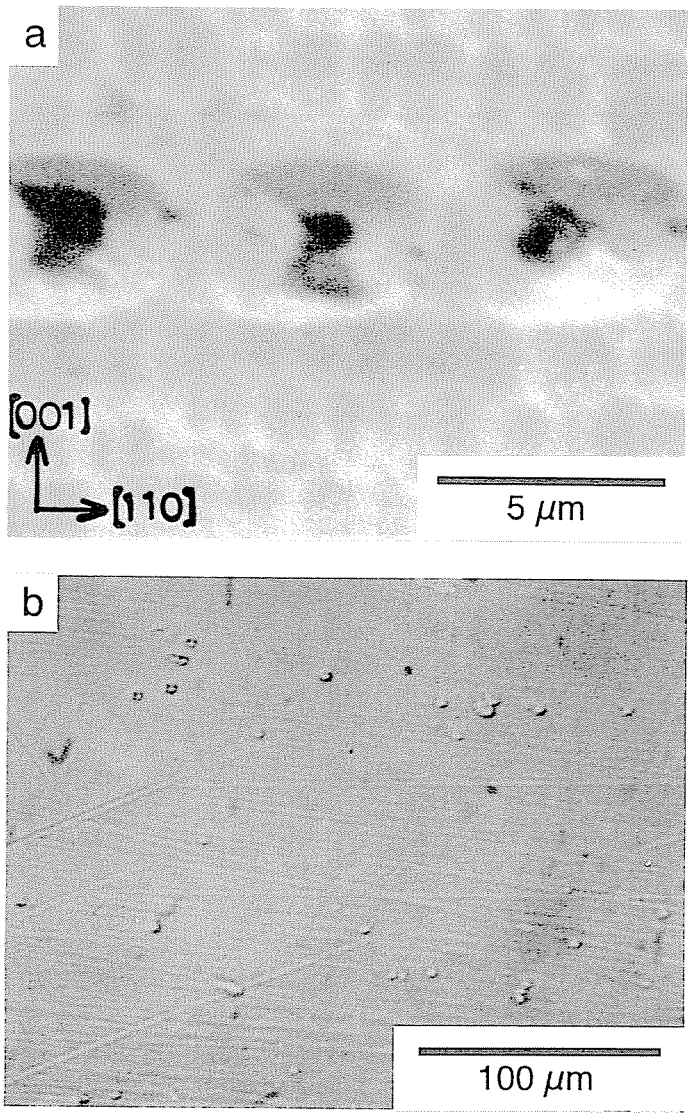

Fig. 6. Etch pit pattern and distribution in the floating zone grown rutile single crystal: (a) observed with a scanning electron microscope; (b) observed with a optical microscope.

3.2. Effect of the dopants

Fig. 7 shows polarized microphotographs of the cross sections of floating zone grown rutile crystals added with different amount of ZrO_2. In the ZrO_2–free crystal, many low–angle grain boundaries were observed, since the growth run was carried out in an oxygen stream. The addition of ZrO_2, however, drastically reduced the number of low–angle grain boundaries. No grain boundaries were found in the crystal containing 0.5 mol% ZrO_2, whereas a few grain boundaries were still observed in the crystal with the addition of 0.25 mol% ZrO_2. A grain boundary free rutile crystal was also grown with the addition of 1.0 mol% ZrO_2.

The most spectacular result by the addition of ZrO_2 was that the as–grown crystal was completely single crystalline even at peripheral region in contrast with the crystal grown under a low oxygen partial pressure. This result clearly indicates the Zr^{4+} ions have the effect to depress the formation of low–angle grain boundaries, since Zr^{4+} ions are expected to distribute over the entire crystal.

The effect of other dopants is shown in fig. 8. Al_2O_3 is an effective dopant to suppress the formation of low–angle grain boundaries next to ZrO_2. In the Al_2O_3–doped (0.4 at%) crystal, a few low–angle grain boundaries exist only at the peripheral region. This is much the same as the crystal grown under a low oxygen partial pressure. The addition of Lu_2O_3 was also effective to reduce the number of low–angle grain boundaries, but not completely: a few boundaries can be observed even in the central part of the crystal. SiO_2 was not a quite adequate dopant; which brought rather bad influence, which is the formation of numerous small bubbles and precipitates.

The ionic radius of each cation used as dopant is presented in table 1 with

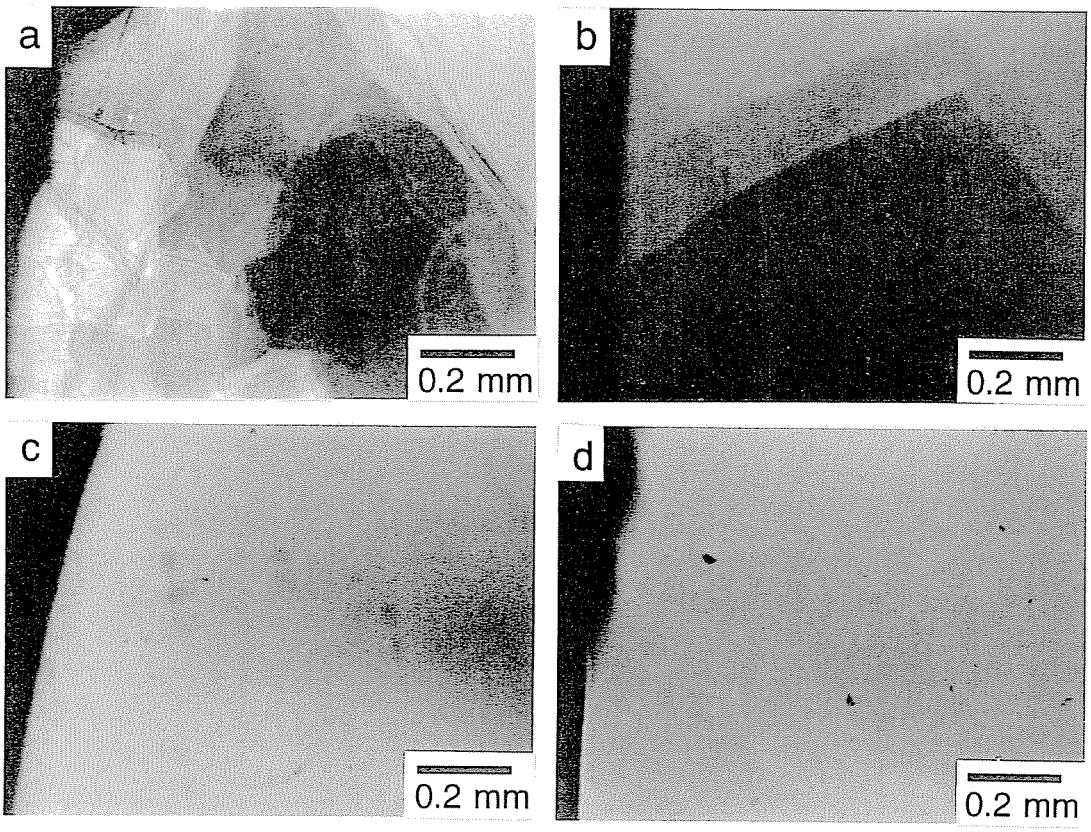

Fig. 7. Polarized microphotographs of the cross sections of ZrO_2–doped rutile crystals: (a) undoped; (b) 0.25 mol% addition; (c) 0.5 mol% addition; (d) 1.0 mol% addition.

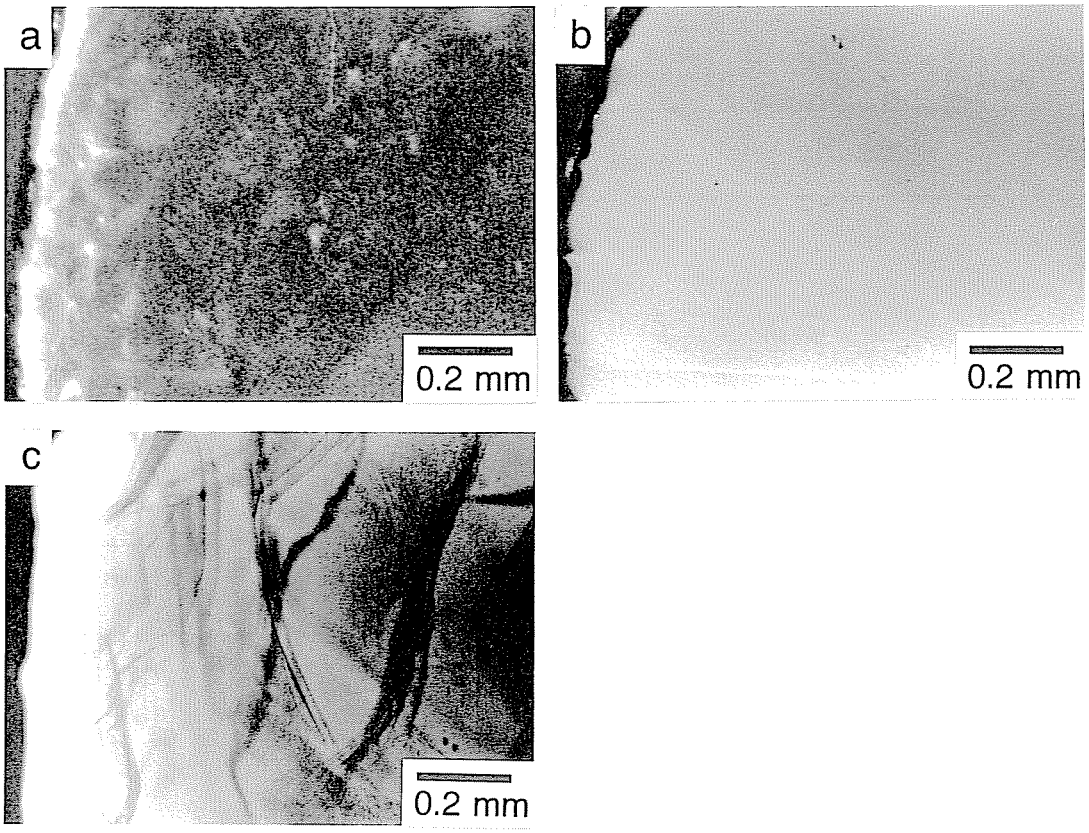

Fig. 8. Polarized microphotographs of the cross sections of rutile crystals added with other dopants: (a) Al_2O_3–doped; (b) Lu_2O_3–doped; (c) SiO_2–doped.

Table 1. Ionic radius of dopant cation and efficiency to suppress the formation of low angle grain boundaries

cation	ionic radius*	R_M/R_{Ti}	efficiency
Zr^{4+}	0.079 nm	1.16	○
Al^{3+}	0.051 nm	0.75	○
Lu^{3+}	0.085 nm	1.25	△
Si^{4+}	0.047 nm	0.69	×
Ti^{4+}	0.068 nm	–	–

* for 6–fold coordination

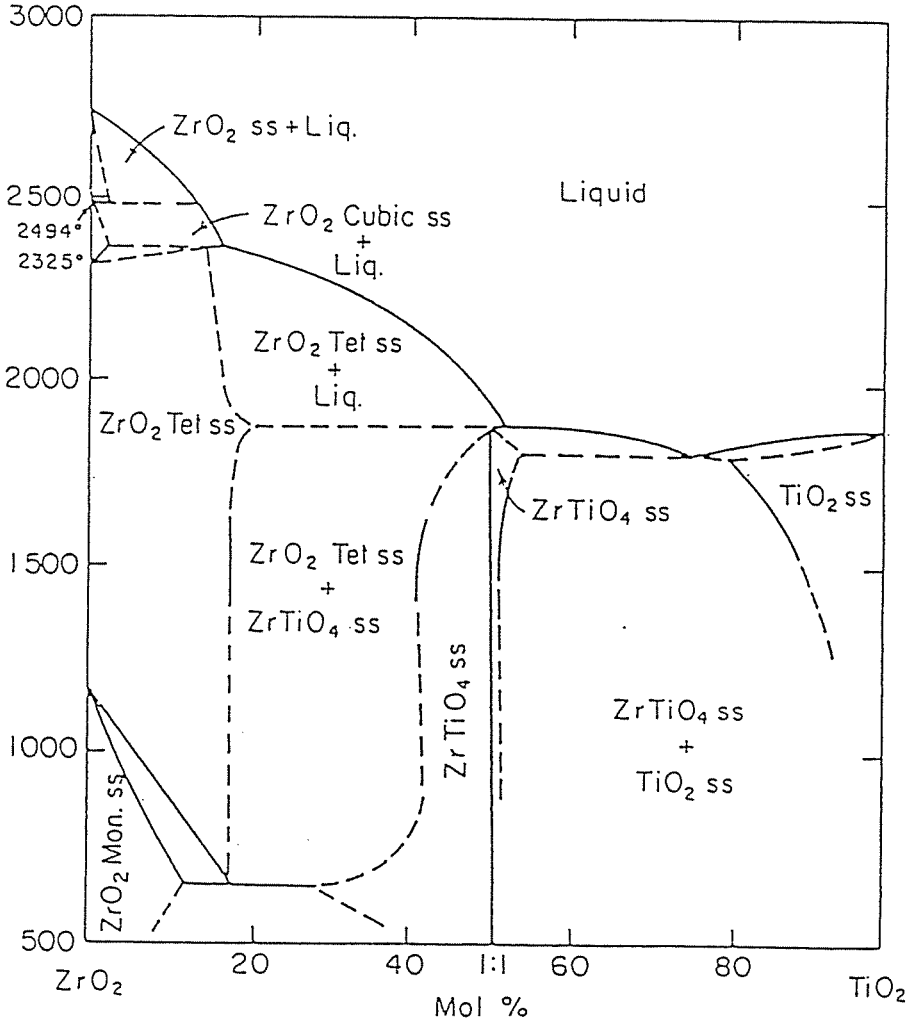

Fig. 9. Phase diagram for the TiO_2–ZrO_2 system (after Noguchi et al [8]).

the efficiency to suppress the formation of low-angle grain boundaries. ZrO_2 can be dissolved up to about 20 mol% in TiO_2 to form a solid solution of rutile as shown in fig. 9 [8]. The ratio of ionic radius of Zr^{4+} to Ti^{4+} is 1.16, which is reasonable value to a form substitutional type solid solution. For other dopants, however, there are no solid solution region at TiO_2 end in reported phase diagrams. Comparing the ionic radius, Al^{3+} is considerably small to substitute Ti^{4+} site, and Lu^{3+} is slightly large. In other crystal structure, however, Al^{3+} and Lu^{3+} can take 6-fold coordination of oxygen and a small amount of Al^{3+} and Lu^{3+} are thus expected to dissolve in TiO_2. As for Si^{4+}, the ionic radius is too small to take 6-fold coordination (except under an ultra-high pressure) and SiO_2 can not dissolve in TiO_2.

The addition of ZrO_2 or Al_2O_3 made it possible to grow rutile single crystals under high oxygen partial pressure. This brought another advantage besides suppressing the formation of low-angle grain boundaries. Fig. 10(a) shows the cross section of rutile single crystal grown at 20 mm/hr in the CO_2 stream. This crystal involves numerous small bubble inclusions. On the other hand, no bubbles can be observed in the Al-doped (0.4 at%) crystal, which was grown at 20 mm/hr in the O_2 stream as shown in fig 10(b). The Al-doped crystal also has no trace of cellular growth, which is often observed in the solid solution crystal grown at a relatively high growth rate. In the case of ZrO_2 addition, the crystal grown at 20 mm/hr also had no bubbles and, of course, low-angle grain boundaries.

3.3. Effect of growth direction

As to be described in Chapter 5, rutile single crystals are often used as parallel plates, of which surface has a variety of specified angles with the optic axis, i.e. c-axis. Thus, the growth along the c-axis is occasionally not

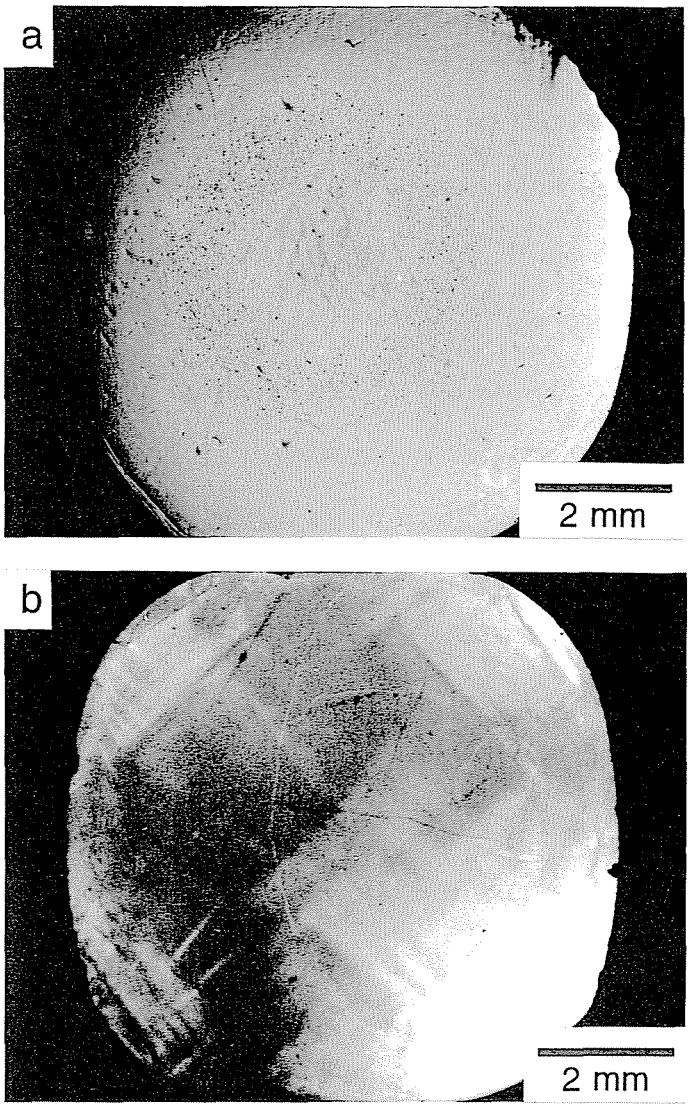

Fig. 10. Optical microphotographs of cross sections of rutile single crystals grown at 20 mm/hr: (a) undoped and grown in the CO_2 stream; (b) Al-doped and grown in the O_2 stream.

advantageous, and the growth parallel to the specified angle is desired in order to effectively process the grown crystals. In section 3.1, a low oxygen partial pressure was found to be effective to suppress the formation of low-angle grain boundaries except for the peripheral region. However, when a seed crystal of which direction was inclined at an angle of 48 ° with the c-axis, a number of low-angle grain boundaries were formed even in the central part as shown in fig. 11(a). On the hand, the ZrO_2-doped (1.0 at%) crystal involves no low-angle grain boundaries even at the peripheral region as shown in fig. 11(b). In the case of Al_2O_3 addition, a number of fiber-like precipitates were observed at the peripheral region and the formation of low-angle grain boundaries could not be suppressed (fig. 11(c)). This result indicates the exsolution of the second phase, which might be Al_2TiO_5, occurred on cooling to reduce the amount of dissolved Al^{3+} in TiO_2.

4. DISCUSSION

The texture constituted of low-angle grain boundaries can be regarded as a lineage structure, which is often observed in metallic crystals grown from the melt [9]. The formation mechanism of the lineage structure is based on the migration and rearrangement of dislocations, so-called polygonization [10]. Fig. 12 shows a schematic diagram of a low-angle grain boundary formed by periodic arrangement of edge dislocations. The texture would not be realized at a high temperature just below the melting point, because the migration of the dislocations is very intensive at such a high temperature. On cooling, the grown crystal is subjected to strong thermal stress because of considerably steep temperature gradient so that dislocations are rearranged to form a ordered configuration in order to relax the thermal stress (fig. 13). The texture is then frozen to room temperature as cooling the crystal, since the dislocations can not migrate at lower

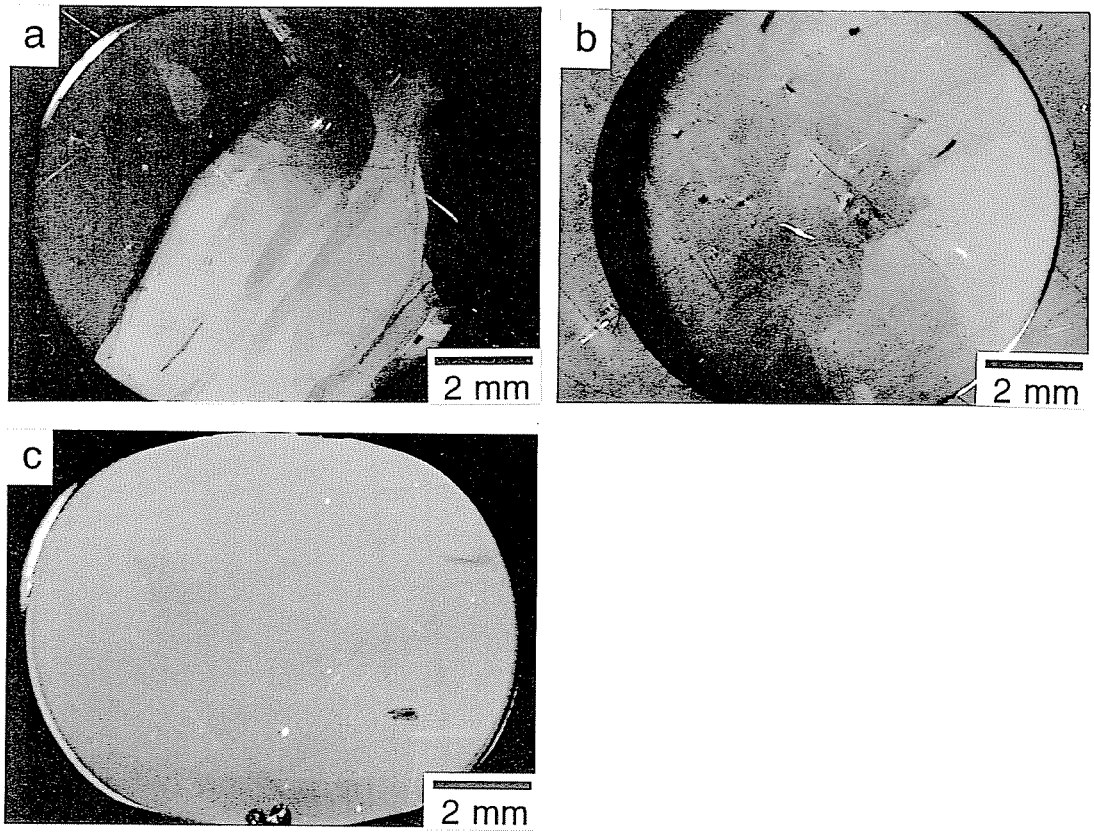

Fig. 11. Polarized microphotographs of the cross sections of rutile crystals of which growth direction was inclined at 48 ° with the c–axis: (a) undoped and grown in the CO_2 stream; (b) ZrO_2–doped and grown in the O_2 stream; (c) Al_2O_3–doped and grown in the O_2 stream.

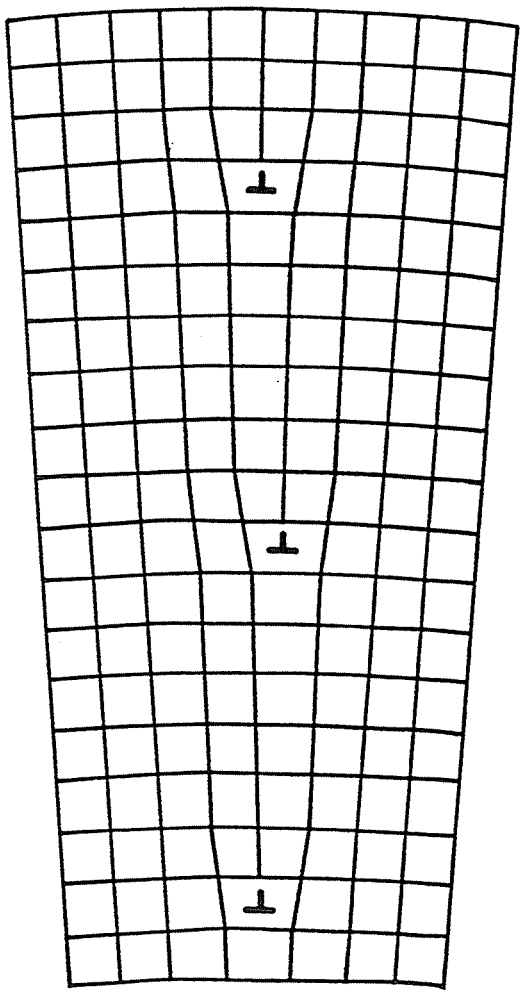

Fig. 12. Schematic diagram of a low-angle grain boundary.

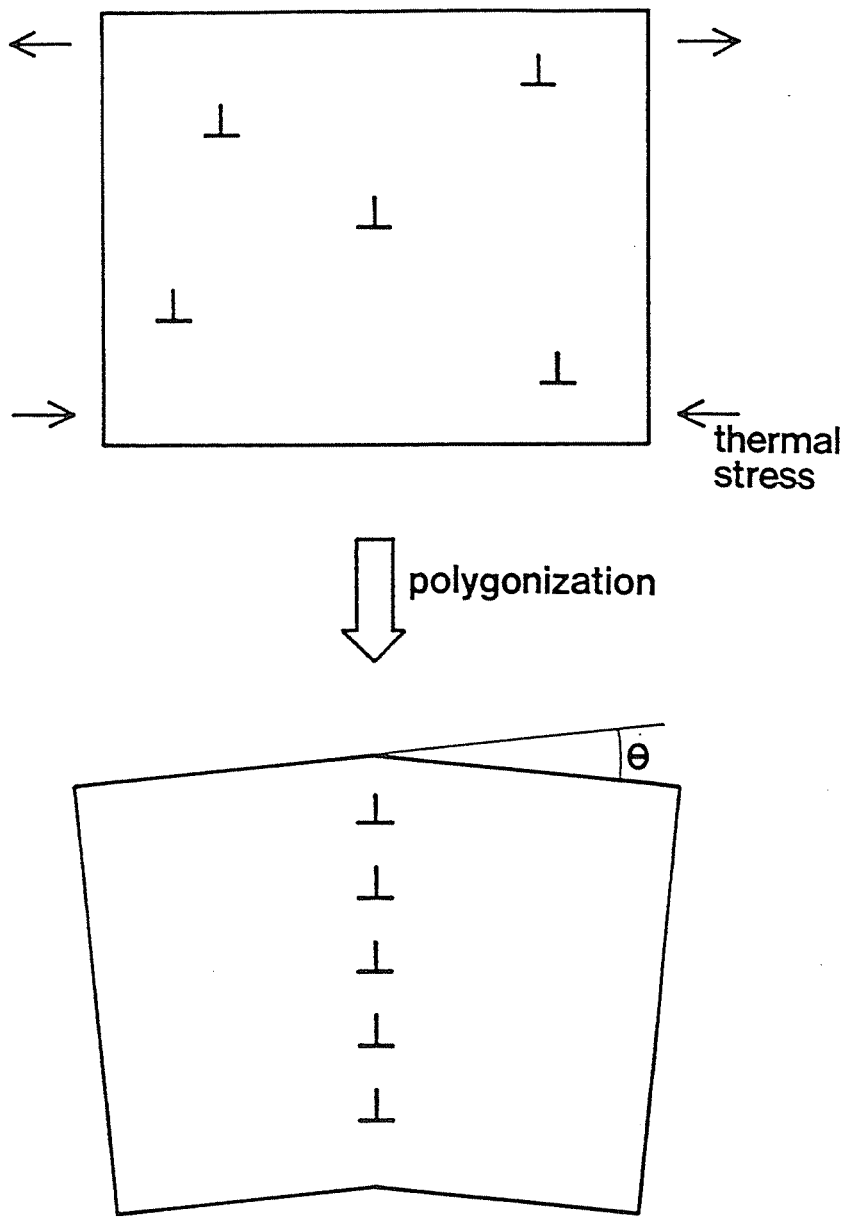

Fig. 13. Schematic illustration for polygonization.

temperatures. Therefore, it is most effective to pin down the migration of dislocations in order to suppress the formation of low–angle grain boundaries.

The addition of a small quantity of impurity, of which size is different from that of the atoms or ions constituting a host crystal, is one of the ways to restrict the migration of dislocations [11]. This is so–called solution hardening. A crystal undergoes tensile and compressive stresses at lower and upper side of the edge dislocation, respectively, as shown in fig. 14(a). If a larger atom is substituted on the lower side an edge dislocation, the strain energy around the dislocation would be reduced (fig. 14(b)). Accordingly, dislocations are pinned down to the positions of impurities and low–angle grain boundaries are consequently not formed. On the basis of this theory, ZrO_2 is an effective and ideal additive to reduce the number of low–angle grain boundaries because the ionic radius of Zr^{4+} is larger than that of Ti^{4+}, i.e. Zr^{4}+: 0.079 nm and Ti^{4+}: 0.068 nm for 6–fold coordinations. When a smaller ion like Al^{3+} is doped, same effect as Zr^{4+} is expected. In this case, Al^{3+} ion will occupy the upper side of the dislocation to relax the compressive stress (fig. 14(c)).

As mentioned in section 3.1, the growth under a relatively low oxygen partial pressure up to 1×10^{3} Pa also effectively suppressed the formation of low–angle grain boundaries, but appreciable subgrains were still observed at peripheral region of a crystal as shown in fig. 4(b).

TiO_2 is easily reduced at high temperatures to form a nonstoichiometric rutile, TiO_{2-x}, which has mixed valence titanium ions, i.e. $Ti^{4+}{}_{1-2x}Ti^{3+}{}_{2x}O_{2-x}$. The Ti^{3+} ions are also expected to pin down the migration of dislocations as well as Zr^{4+} ions, because the ionic radius of Ti^{3+} ion for 6–fold coordinations is 0.076 nm, which is larger than that of Ti^{4+} (0.068 nm) and rather close that of Zr^{4+} (0.079 nm). A

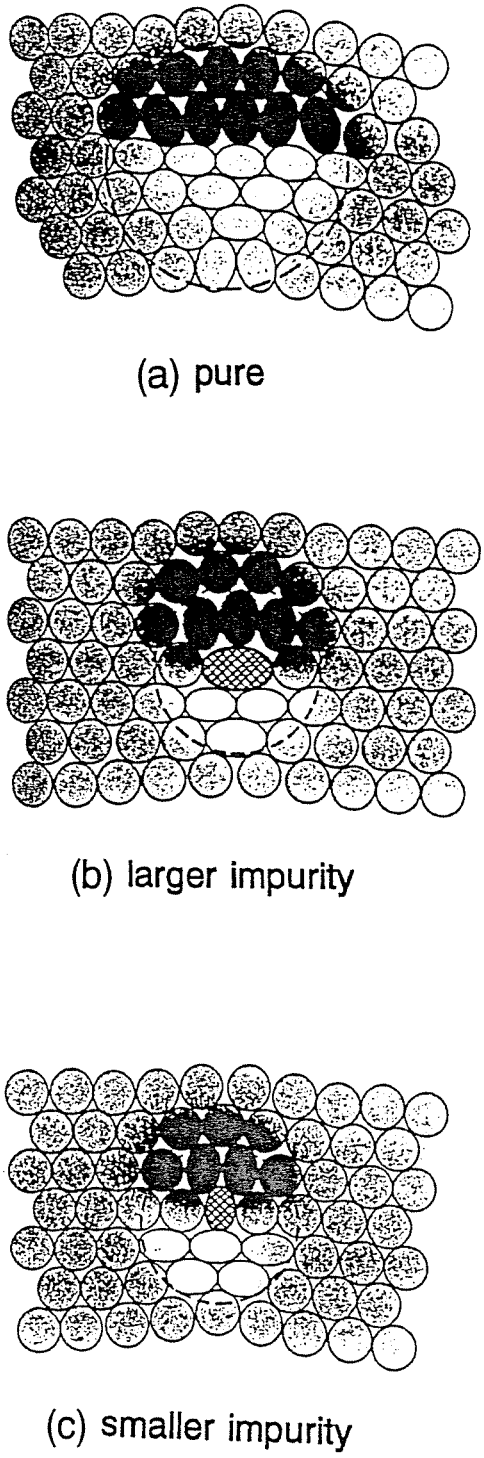

Fig. 14. Schematic illustration for solution hardening.

number of Ti^{3+} ions would be formed just below the melting point of rutile, but the amount of Ti^{3+} ions at such high temperature can not be estimated in the floating zone grown rutile crystal. That is because the grown crystal is oxidized in the course of a growth run, even if the run is carried out under a relatively low oxygen partial pressure. Consequently, the floating zone grown rutile crystal is usually translucent and dark blue but not opaque. On the other hand, a Verneuil grown rutile crystal is usually quenched from a very high temperature just below the melting point, and the amount of Ti^{3+} at the temperature would be frozen, as a result. Thus an as–grown rutile crystal by the Verneuil method is usually black and opaque. According to Sachse, the chemical composition of as–grown rutile crystal by the Verneuil method was $TiO_{1.985}$ [12], which is expected to contain 3 at% Ti^{3+} ions. The amount of Ti^{3+} ions will be sufficient to pin down the migration of dislocations, and thereby a Verneuil grown rutile crystal includes very few low–angle grain boundaries though the crystals would undergo an intense thermal stress by quenching. The floating zone grown rutile is also expected to contain a number of Ti^{3+} ions at high temperatures to depress the formation of low–angle grain boundaries.

The formation of Ti^{3+} ions in a rutile crystal depends not only on temperature but also on oxygen partial pressure and the amount of Ti^{3+} increases with decreasing oxygen partial pressure. Fig. 15 is schematic diagrams for the floating zone growth of rutile crystals under different oxygen partial pressure. Broken lines qualitatively indicate the critical concentration of Ti^{3+} ions which completely suppress the formation of low–angle grain boundaries. In the case of ZrO_2 addition, the critical concentration would be between 0.25 and 0.50 mol%. If dislocations intensively migrate above T_1 because of high thermal energy and the dislocations can not migrate below T_2, the low–angle grain boundaries would be

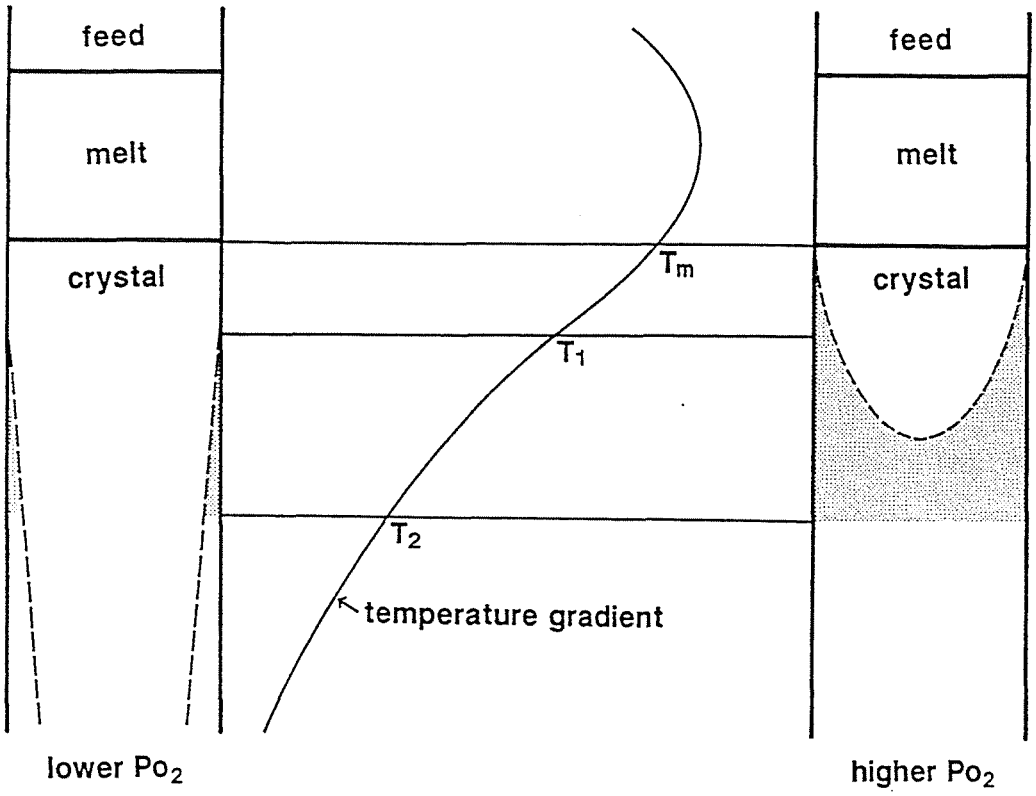

Fig. 15. Schematic diagram of the floating zone growth of rutile single crystals under different oxygen partial pressures. Broken lines indicate the critical Ti^{3+} concentration to suppress the formation of low-angle grain boundaries, which are formed between T_1 and T_2.

formed between T_1 and T_2, and then the texture would be frozen on cooling to room temperature. In the case of growth under a higher oxygen partial pressure, a grown crystal is readily oxidized to decrease Ti^{3+} concentration. If the Ti^{3+} concentration in the entire crystal became below the critical concentration in the region between T_1 and T_2, the low-angle grain boundaries would be formed in the entire crystal. On the other hand, in the case of a lower oxygen partial pressure the oxidation proceeds only at the skin of the crystal. Consequently, the central part of the crystal is widely single crystalline whereas the peripheral region of the crystal includes low-angle grain boundaries. This may be the reason why the low oxygen partial pressure was effective to reduce the number of the low-angle grain boundaries.

It is impossible to avoid the formation of low-angle grain boundaries at peripheral region by only controlling the oxygen partial pressure as growth atmosphere. Moreover, the low-angle grain boundaries formed at peripheral region would occasionally propagate into the central region of a crystal. Therefore, the ZrO_2 addition is more advantageous than the growth under a low oxygen partial pressure to obtain a rutile single crystal which is completely free from low-angle grain boundaries.

When the c-axis was inclined, for example 48 °, to the growth direction, the pure crystal involved a number of low-angle grain boundaries even if the crystal had been grown under a low oxygen partial pressure. Also, the addition of 0.5 at% ZrO_2 was not enough and 1.0 at% ZrO_2 was necessary to completely suppress the formation of low-angle grain boundaries. These result indicate that the thermal stress in the crystal inclined to the c-axis is stronger than that in the crystal grown along the c-axis.

Thermal stress is usually originated from the difference in the shrinkage between the outer and inner regions of the crystal due to the temperature gradient in horizontal direction. When the c–axis is inclined to the growth direction, more stress will occur because of the anisotropy of thermal expansion between along a– and c–axis. In order to relax the enhanced thermal stress, dislocations will readily migrate to form low–angle grain boundaries. Therefore, the growth along the c–axis is the most advantageous to minimize the thermal stresses so that the formation of low–angle grain boundaries are effectively suppressed.

5. SUMMARY AND CONCLUSIONS

The formation of low–angle grain boundaries is the most serious problem in the floating zone growth of rutile single crystals. That is because the low–angle grain boundaries induce the significant fluctuation of refractive index and scattering to the propagating light. In this chapter, the effect of following three conditions on the formation of low–angle grain boundaries was examined: oxygen partial pressure, addition of a small amount of oxides and growth direction.

The formation of low–angle grain boundaries in floating zone grown rutile crystals was effectively suppressed when a relatively low oxygen partial pressure of up to 1×10^3 Pa was used as the growth atmosphere. However, at the peripheral region of the crystals some low–angle grain boundaries were still remained, and when the growth direction was inclined to the c–axis, low–angle grain boundaries were formed even in the central part of the crystals. On the other hand, the addition of a small amount of dopant, especially ZrO_2 (0.5 at%), was remarkably effective to suppress the formation of the low–angle grain boundaries and completely boundary–free rutile single crystals were thereby obtained.

The formation mechanism of low–angle grain boundaries will be based on the polygonization:i.e. dislocations present at a high temperature migrate to form linearly arranged configuration when a grown crystal is subjected to a strong thermal stress. The Zr^{4+} ions, of which radius larger than that of Ti^{4+}, would have a role to pin down the migration of dislocations because of the reduction of strain energy around the dislocations, and the formation of the low–angle grain boundaries are consequently suppressed. Trivalent titanium ions, Ti^{3+}, formed at a high temperature are expected to pin down the migration of dislocations as well as Zr^{4+}, and a low oxygen partial pressure was therefore effective to reduce the number of low–angle grain boundaries except in peripheral region of the crystal.

When the growth direction was inclined to the c–axis, the grown crystal is subjected to a stronger thermal stress to easily form low–angle grain boundaries even under a low oxygen partial pressure. The addition of ZrO_2 is again effective to suppress the formation of low–angle grain boundaries, although 1.0 at% ZrO_2 addition was necessary.

REFERENCES

1. J. Saito, private communication.
2. B. Cockayne and J. M. Roslington, *J. Mater. Sci.*, **8** (1973) 601.
3. H. Machida and T. Fukkuda, *J. Crystal Growth*, **112** (1991) 835.
4. Y. Nakazumi, K Suzuki and T. Yazima, *J. Phys. Soc. Jpn.*, **17** (1962) 1806.
5. K. Hasegawa, private communication.
6. F. Millot, M. G. Blanchin, R. Totot, J. F. Marucco, B. Poumellec, C. Picard and B. Touzelin, *Prog. Solid State Chem.*, **17** (1987) 263.
7. C. H. Moore, *Trans. Am. Ceram. Soc.*, **33** (1950) 140.

8. T. Noguchi and M. Mizuno, *Bull. Chem. Soc. Jpn.*, **41** (1968) 2898.
9. E. Teghtsoonian and B. Chalmers, *Can. J. Phys.*, **30** (1952) 388.
10. A. H. Cottrell, "Dislocation and Plastic Flow in Crystals" (Oxford, 1935).
11. L. H. van Vleck, "Elements of Materials Science and Engineering" (Addison-Wesley, Reading, MA, 1980).
12. H. B. Sachse, *Anal. Chem.*, **33** (1961) 1349.

Chapter 3

Effects of Aliovalent Cations on Decoloration of Floating Zone Grown Rutile Single Crystals

1. INTRODUCTION

It is well known that the wavelength bands of around 1.3 or 1.55 μm is used in the optical communication since the energy loss by the absorption through optical fiber is minimized in this wavelength region [1,2]. The insertion loss through each part is one of the most serious problems in a variety of optical devices. There are two types of insertion losses: i.e. reflection and absorption. The loss by the reflection is usually minimized by anti–reflection coating on the surface of each element; however, the loss by the absorption is inevitable if the element essentially has the absorption at the wavelength of a laser diode which is used.

A rutile single crystal is essentially transparent in a wide wavelength region of 420–5000 nm, in which rutile does not have any absorptions. The intrinsic color of rutile, pale–yellow, is originated on the absorption edge at 420 nm corresponding to blue, which is complementary color for yellow. Therefore, there is no problem to use a rutile single crystal in the optical communications if the crystal does not contain oxygen defects, which color the rutile crystal black or dark–blue.

In Chapter 2, the effect of oxygen partial pressure as growth atmosphere was examined to suppress the formation of low–angle grain boundaries, and a relatively low oxygen partial pressure of up to 1×10^3 Pa was found to be effective to obtain grain boundary free rutile crystals. However, the as–grown rutile crystal obtained under such a low oxygen partial pressure is black or dark–blue, since a number of Ti^{3+} ions and oxygen vacancies are formed at high temperatures. A very long–term annealing, for 10–20 days at 800 °C in an oxidizing atmosphere, is usually

necessary to restore the transparency and the intrinsic color of pale–yellow. Grain boundary free rutile single crystals can also be grown by the addition of small quantity of ZrO_2. However, the as–grown crystals were also dark–blue, even if the crystal growth was effected under an oxygen atmosphere.

According to Aria et al, oxygen tracer diffusivity in Cr–doped rutile was 3 to 8 times larger than that in a pure rutile single crystal [3]. Ikeda et al also reported considerably rapid diffusion of oxide ions in an Al–doped and reduced rutile single crystal [4]. These reports indicates that the addition of trivalent cations is very effective to enhance the diffusivity of oxide ions in rutile.

In this chapter, rutile single crystals to which a small amount of aliovalent (trivalent or divalent) cations was doped was grown by the floating zone method and it was consequently clarified that the addition of the aliovalent cations was effective to obtain decolorized, transparent rutile single crystals. The diffusion mechanism of oxide ions in the rutile crystal is discussed on the basis of obtained results.

2. EXPERIMENTAL

Starting materials used were powders of TiO_2 (Toho Titanium Co., Ltd., 99.9%), Sc_2O_3 (Soekawa Kagaku Co., Ltd, 99.9%), Al_2O_3 (the same as in Chapter 2), Ga_2O_3 (Kojundo Kagaku Kenkyusho, 99.9%) and MgO (Kojundo Kagaku Kenkyusho, 99.9%). The addition of each dopant was 0–0.5 at%. ZrO_2 of 0.4 at% was also codoped in some Sc–doped crystals. The powders of TiO_2 and each dopant was mixed by a wet technique in an agate mortar for 2 hours.

The procedures for preparation of feed rods and floating zone crystal growth were essentially the same way as described in the previous chapter. Growth conditions were as follows: growth rate was 5 mm/hr, rotation rate was 30 rpm for both a feed rod and a seed crystal, and atmosphere was an oxygen stream of 2 liter/min. Some samples were quenched by turning off the lamp power abruptly in the course of steady growth.

After the observation of the color of as-grown crystals, they were cut perpendicularly to the growth direction and polished. The specimen was examined under a polarizing microscope with parallel and cross nicols. Transmittance along the c-axis was measured in the wavelength region of 200-2000 nm using a spectrophotometer (Hitachi-330). For the Al-doped crystal, electrical conductivity was measured along [001] and [110] directions by two probe method in AC and DC field. ICP analysis was also done for the Al-doped crystals, which were used for conductivity measurements.

3. RESULTS

Crystal growth of Sc-doped rutile crystals by the FZ method was successfully performed and cellular growth did not occur in case of the Sc concentrations of up to 0.1 atom%. On the other hand, the penetration of melt into a feed rod was observed in the latter half of the growth run for the crystal of high Sc concentration, e.g. 0.5 atom%. This indicates that there was a large difference in Sc concentration between the melt and the feed rod. As mentioned later, the dissolution of Sc_2O_3 in rutile is very little, and hence Sc would be gradually concentrated in the melt with proceeding growth run. However, the cellular growth was also not observed in case of 0.5 atom%.

Fig. 1 shows as-grown rutile crystal boules obtained by the floating zone method. The Sc-doped (0.1 at%) crystal (a) is transparent and yellowish, which is close to a completely annealed rutile single crystal. The addition of 0.04 at% Sc_2O_3 was also effective to obtain a transparent as-grown crystal. The Sc-free but Zr-doped crystal (b) is dark-blue and translucent, although the crystal growth was done under an oxygen atmosphere. On the other hand, the undoped, pure rutile crystal (c) is transparent, although bluish coloring is still observed.

Fig. 2 shows polished specimen cut from near the tip of the as-grown crystals. Through the Sc-doped crystal (a), background letters "rutile" is clearly visible, while the Sc-free (Zr-doped) crystal (b) is still dark-blue and translucent despite its thickness of approximately 1 mm.

Fig. 3 shows more clearly the effect of Sc-doping on decoloration of a rutile crystal. The sample in fig. 3 was quenched in the course of a steady growth run. The frozen melt part is white and the grown crystal is, despite quenching, transparent and yellowish except the dark-blue region just below the melt zone. This crystal is in contrast with the Sc-free (Zr-doped) crystal in fig. 1 (b), which is dark-blue on the whole, although the crystal was not quenched but normally cooled to room temperature.

Since the ionic radius of Sc^{3+} is just larger than that of Zr^{4+}, i.e. Sc^{3+}: 0.081 nm and Zr^{4+}: 0.079 nm for 6-fold coordination, it was expected that the addition of Sc_2O_3 is also effective to suppress the formation of low-angle grain boundaries. In fact, the number of low-angle grain boundaries was reduced but a few boundaries are involved even in the central part of the crystal as shown in fig. 4(a). The simultaneous addition of ZrO_2 and Sc_2O_3 was effective to grow transparent and grain boundary free rutile single crystals (fig. 4(b)).

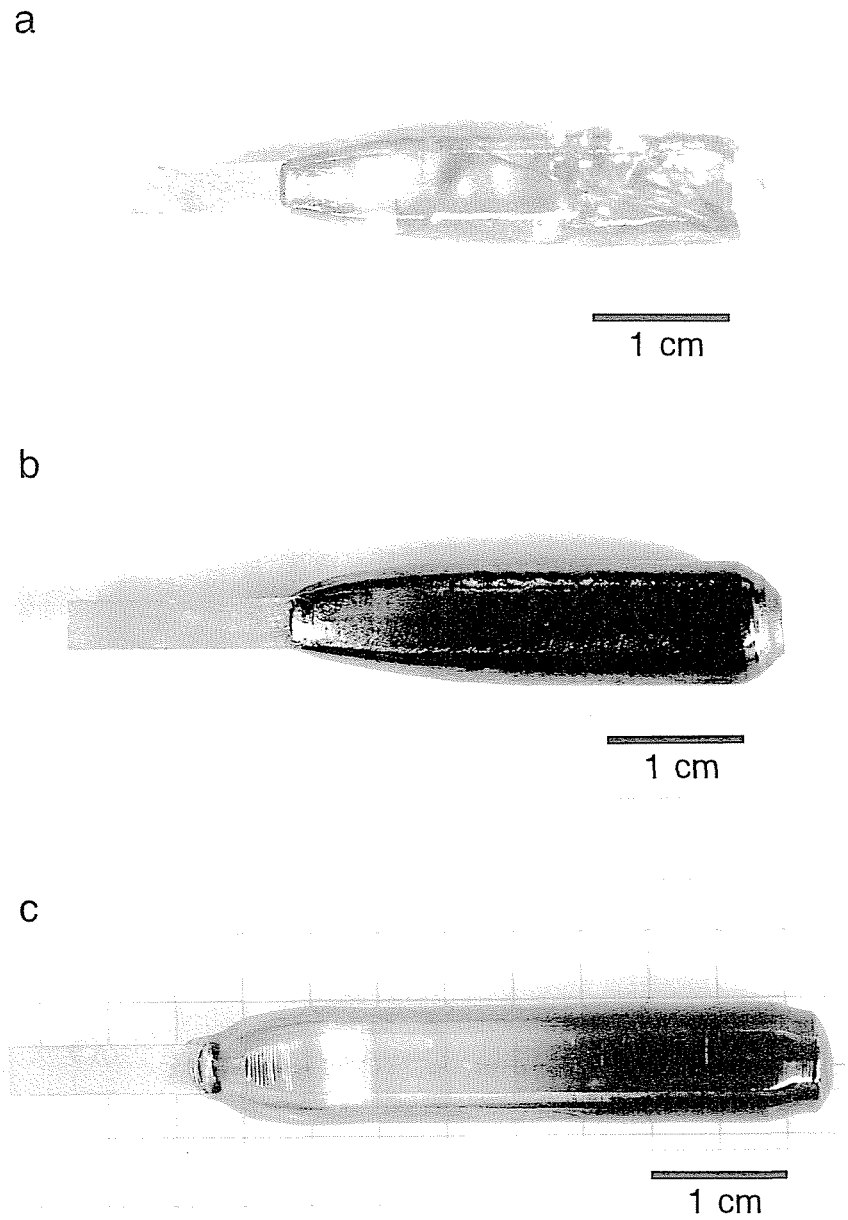

Fig. 1. As-grown rutile crystals obtained by the floating zone method: (a) Sc-doped; (b) Zr-doped; (c) undoped.

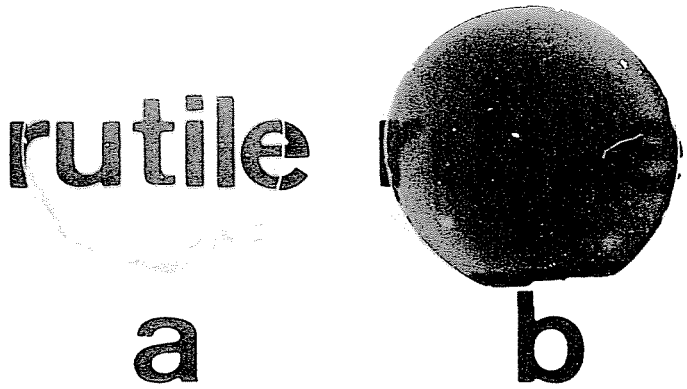

Fig. 2. Cross sections of the as-grown rutile crystals: (a) Sc-doped; (b) Zr-doped.

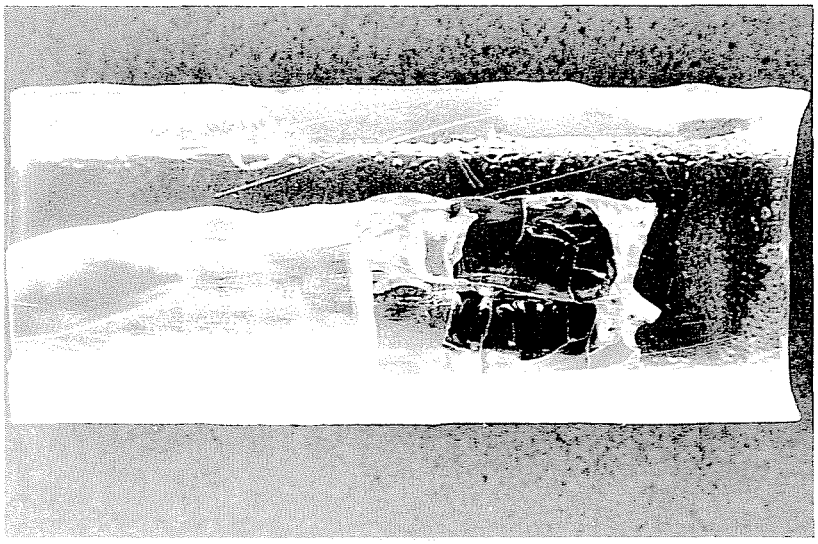

Fig. 3. A quenched specimen of the Sc-doped rutile crystal. The specimen was molded in epoxy resin and cut so as to include the center of the crystal.

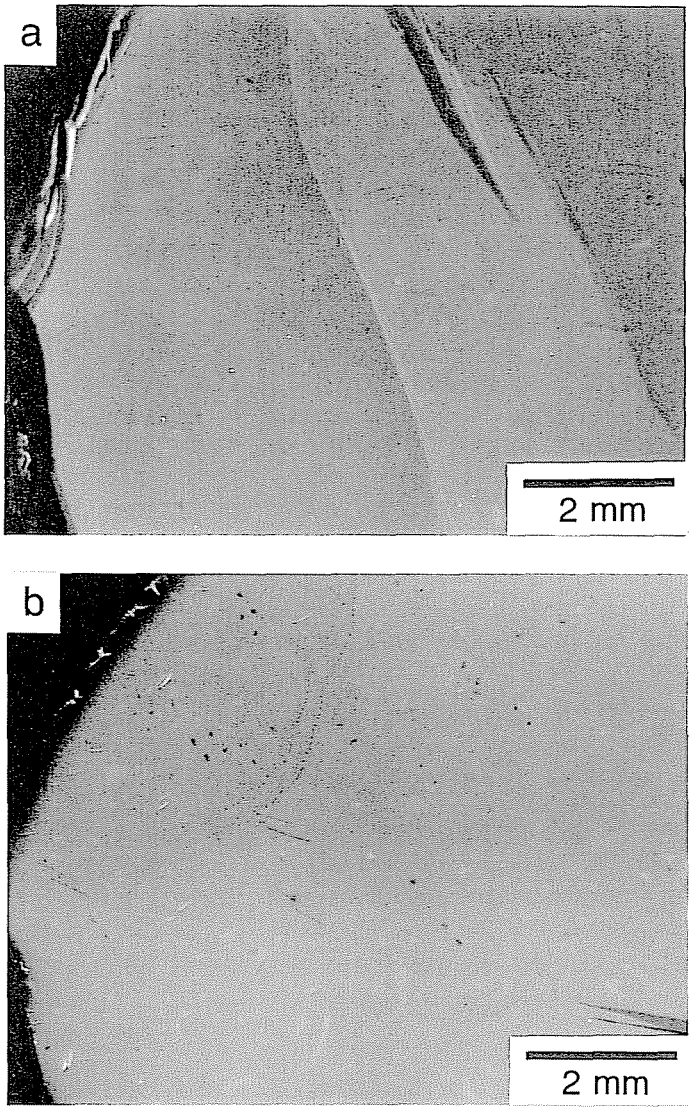

Fig. 4. Polarized microphotographs of cross sections of Sc–doped rutile crystals grown by the floating zone method: (a) only Sc–doped; (b) Zr– and Sc–codoped.

Cracks were occasionally observed in transparent as-grown crystals as shown in fig. 1 (a). The cracks were formed spirally from tip to seed of the as-grown crystals on cooling to room temperature. The cause of the cracks is not clarified, but rapid diffusion of oxide ions may be responsible, since Sc-free rutile crystals, which were dark-blue, were never cracked. After the growth of a Sc-doped crystal, cooling under a low oxygen partial pressure and subsequent annealing were effective to avoid cracks. The duration for the annealing to obtain transparent crystals was significantly shortened, i.e. 20 hours at 800 °C, as compared with the case for Sc-free crystals.

For Ga- or Mg-doped crystals, the same phenomenon as for the Sc-doped crystals was observed, that is, all the as-grown crystals were transparent on the whole. However, the solubility limit of Ga_2O_3 and MgO in TiO_2 seems to be very low so that fiber-like precipitates were observed at the peripheral region of the crystals as-shown in fig. 5.

Al_2O_3 is an effective dopant not only to suppress the formation of low-angle grain boundaries (Chapter 2) but also to obtain a transparent rutile single crystal. Fig. 6 shows an as-grown Al-doped rutile single crystal, which is pale-yellow and completely transparent.

Fig. 7 shows the transmittance of rutile single crystals in the wavelength range of 200-2000 nm. The transmittance of the as-grown, Al-doped rutile single crystal is essentially the same as that of a pure crystal which is fully annealed to eliminate the oxygen deficiency. On the other hand, the as-grown, pure crystal obtained in a CO_2 stream has a strong and broad absorption above 600 nm, where the transmittance is approximately zero. The as-grown, pure rutile crystal is strong dark-blue but not opaque. This is consistent with the spectrum, i.e. a slight

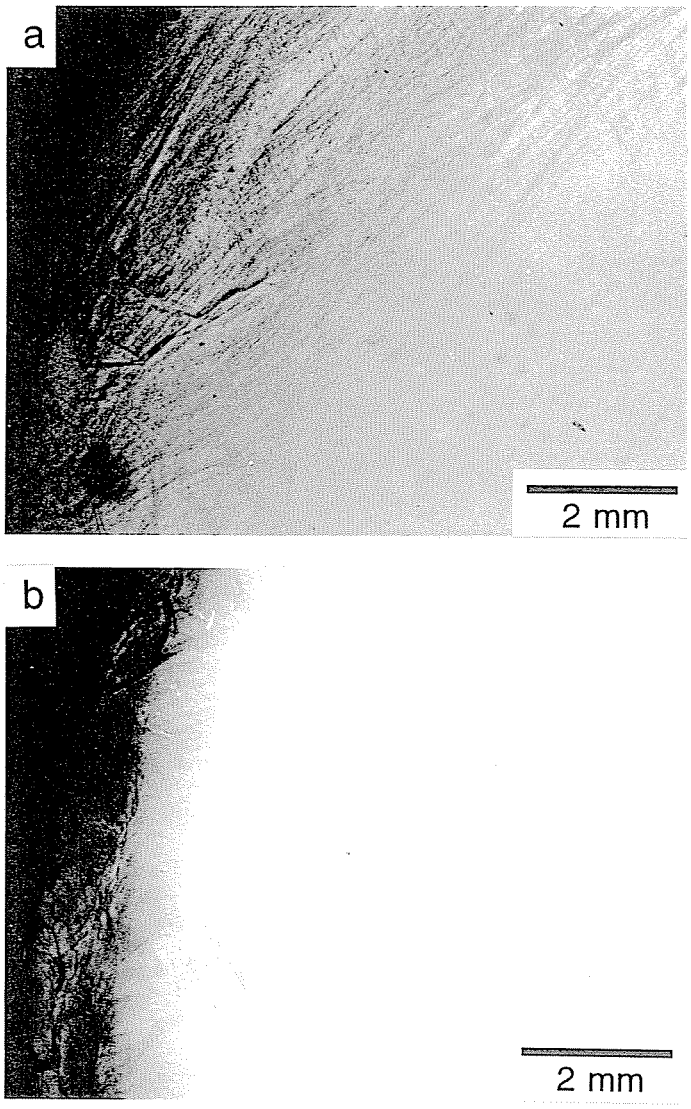

Fig. 5. Optical microphotographs of cross sections of Mg– and Ga–doped rutile crystals: (a) Mg–doped; (b) Ga–doped.

Fig. 6. As-grown, Al-doped rutile single crystal.

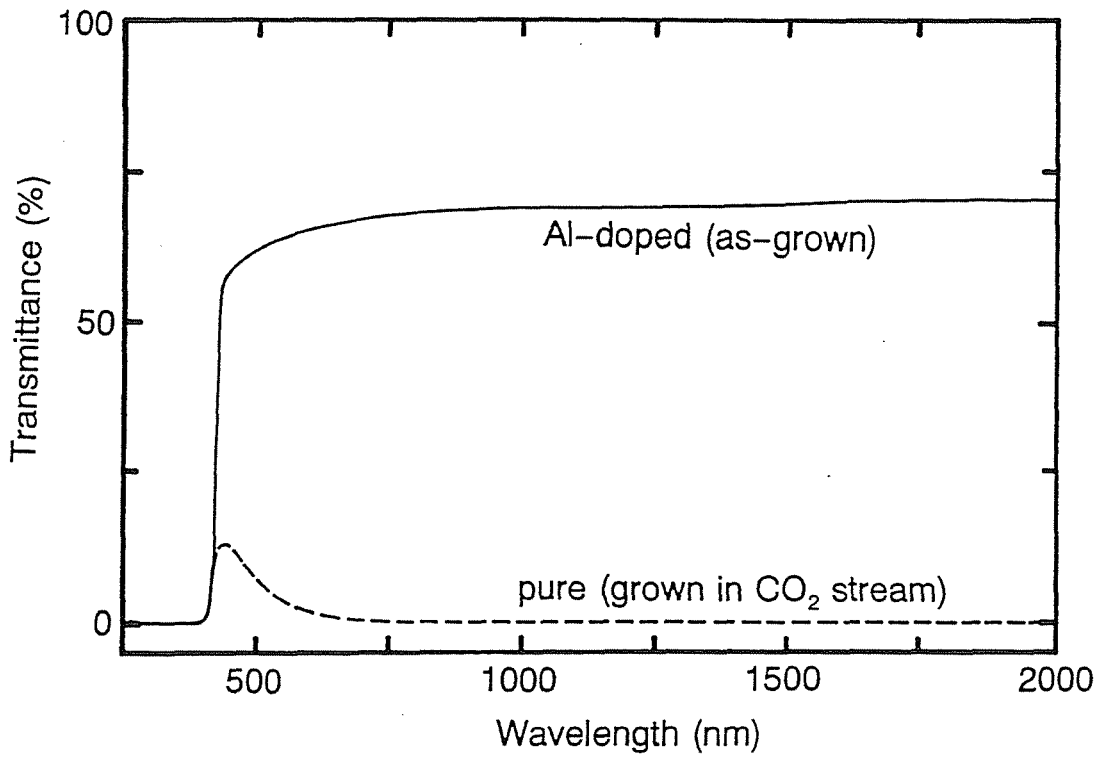

Fig. 7. Transmittance of as-grown rutile single crystals in visible and near infrared regions.

The electrical conductivity of Al–doped and pure rutile single crystals were measured to evaluate the difference in the diffusion rate of oxide ions. Fig. 8 shows the temperature dependance of the conductivity along [001] direction measured in AC and DC fields. For AC field, the conductivity of the Al–doped crystal is larger by one order of magnitude in 600–800 °C than that of the pure crystal which is fully annealed. One the other hand, the conductivity of Al–doped crystal in DC field is much the same as that for AC field throughout the measured temperature range, and there is no remarkable difference between the Al–doped and pure crystals. In the case of [110] direction, the difference in the conductivity in AC field between the Al–doped and pure crystals is not so large as along [001] direction but there is a distinctive difference as shown in fig. 9.

The Al–content in the grown crystals was determined by the ICP analysis to be approximately same as that in the feed rod. Since the samples for the ICP analysis was cut from near the portion used for conductivity measurement, the each crystal used for conductivity measurement should have the same Al–content as nominal composition. Accordingly, the difference in the conductivity should be caused by the Al–content of each crystals.

4. DISCUSSION

As stated above, the coloring of dark–blue or black in a pure rutile crystal grown from the melt can be clearly attributed to the reduction at high temperatures to form trivalent titanium ions, Ti^{3+}, and corresponding oxygen vacancies. The

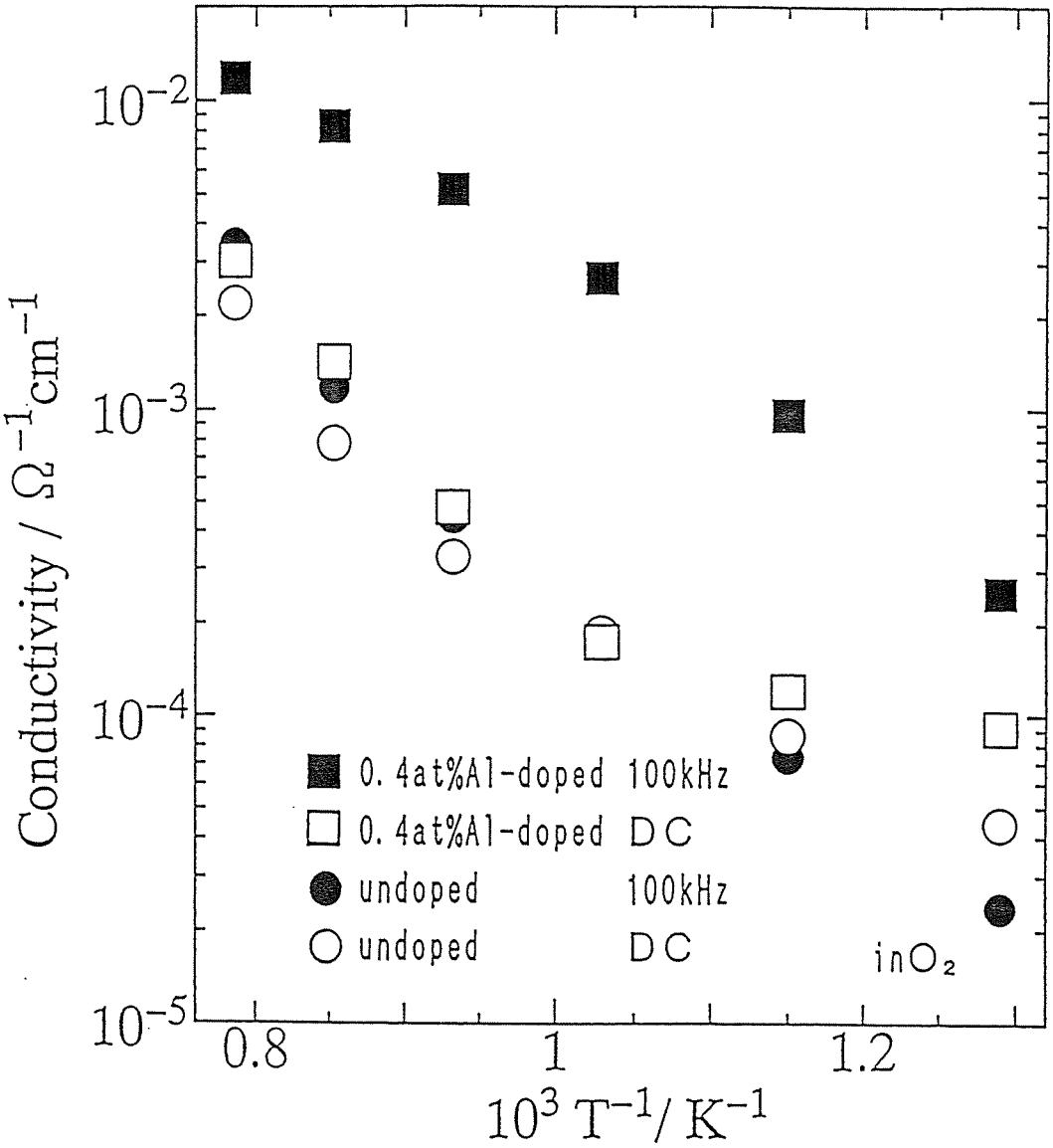

Fig. 8. Electrical conductivity of floating zone grown rutile single crystals along [001] direction.

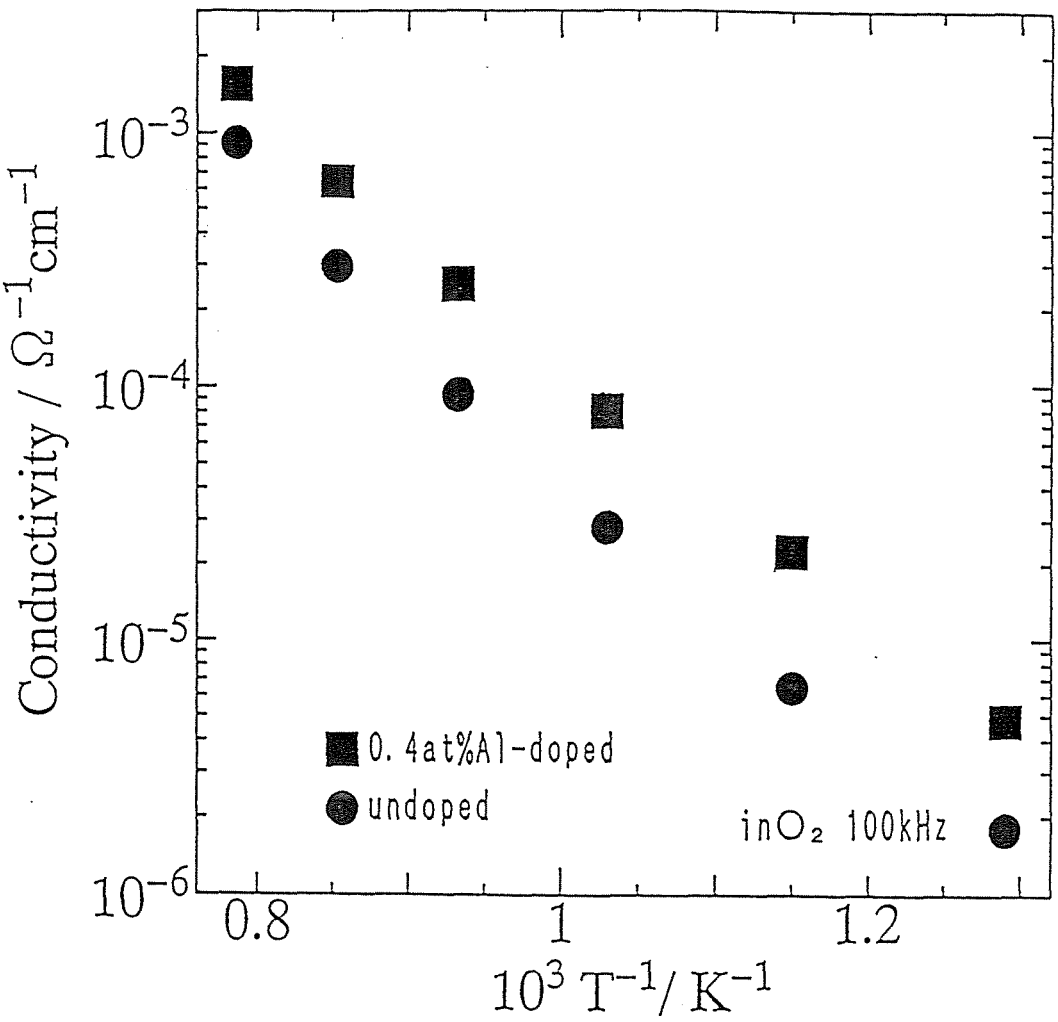

Fig. 9. Electrical conductivity of floating zone grown rutile single crystals along [110] direction.

reduction is inevitable for the melt growth of rutile crystals as far as the growth run is performed under a oxygen partial pressure of up to 10^5 Pa. Accordingly, a transparent rutile crystal can be obtained by post-annealing in an oxidizing atmosphere to diffuse oxide ions over the whole crystal. Diffusion rate usually increases with increasing temperature, and thus it may be advantageous to anneal at as high temperatures as possible. However, the stability of Ti^{3+} increases with increasing temperature even under a high oxygen partial pressure. Therefore, annealing should be done at a relatively low temperature, which was empirically determined to be 800 °C for the rutile single crystals grown under a low oxygen partial pressure up to 10^3 Pa.

At an early stage of annealing, oxide ions would easily diffuse via oxygen vacancies, which are accompanied with Ti^{3+} ions, and the peripheral region of the crystal readily becomes transparent and close to stoichiometric TiO_2, as a result. After that, the oxide ions have to pass through the stoichiometric TiO_2 layer to diffuse inside of the crystal and the diffusion rate is expected to be considerably slow because there are no point defects which allow the oxide ions to diffuse rapidly (fig. 10). Consequently, it takes a long-term annealing for 10-20 days to obtain a thoroughly transparent rutile single crystal.

The diffusion rate of the oxide ion is accelerated not only by the presence of the point defects but also by the presence of dislocations and low-angle grain boundaries, which give another path for the diffusion [5]. As shown in fig. 1(c), the undoped, pure crystal grown in the oxygen stream is not dark blue and transparent because the crystal comprises many low-angle grain boundaries. On the contrary, the Zr-doped crystal is, on the whole, strongly dark-blue and almost opaque as shown in fig. 1(b). This demonstrates that the diffusion rate of oxide

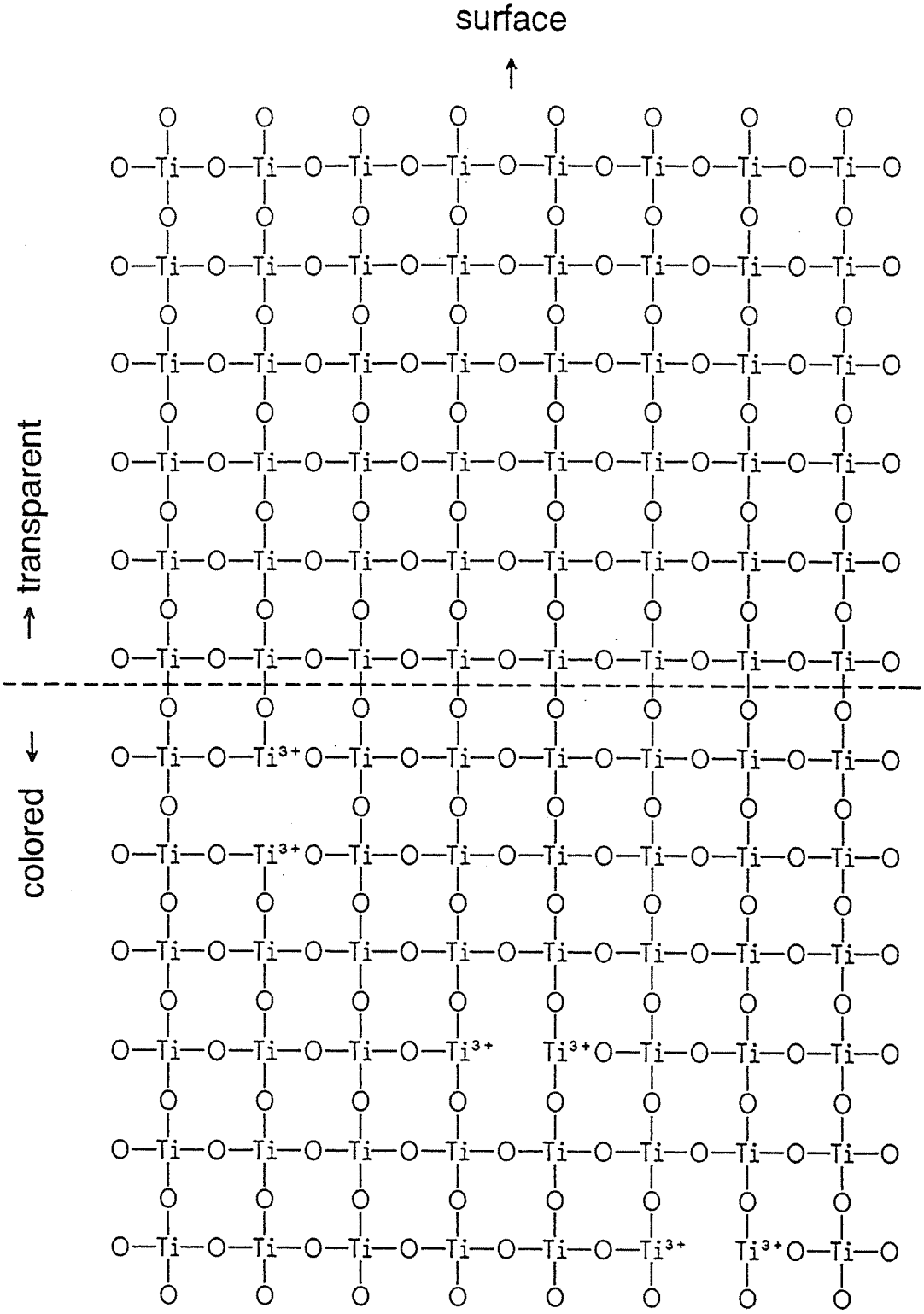

Fig. 10. Two dimensional expression of pure rutile crystal.

ions is remarkably slow in the Zr–doped crystal, which have no low–angle grain boundaries.

The as–grown, Al–doped crystal is pale yellow and completely transparent, although the crystal contains few low–angle grain boundaries. Therefore, the other rapid path for the oxide ion diffusion should be considered. It is well known that Y– or Ca–doped ZrO_2, so–called stabilized ZrO_2, is a good ionic conductor, in which oxide ions are a charge carrier and easily migrate via oxygen vacancies formed for the charge compensation [6,7]. In a similar way, oxide ions are expected to easily migrate in a rutile crystal to which trivalent or divalent ions are doped. If the trivalent ions, e.g. Al^{3+}, substitute Ti^{4+} site in a rutile crystal, oxygen vacancies will result as follows:

$$(1-x)TiO_2 + xAlO_{1.5} \rightarrow Ti_{1-x}Al_xO_{2-0.5x}Vo_{0.5x}$$

where Vo is oxygen vacancy. In similar way, if divalent ions, e.g. Mg^{2+}, substitute Ti^{4+} site, following equation is expected:

$$(1-x)TiO_2 + xMgO \rightarrow Ti_{1-x}Mg_xO_{2-x}Vo_x$$

The oxygen vacancies introduced by the addition of aliovalent ions never disappear, even if Ti^{3+} ions are oxidized to Ti^{4+} (fig. 11). Appreciably rapid and continuous diffusion of oxide ions is therefore expected to occur on cooling, and transparent and yellowish rutile crystals were obtained in the as–grown state, as a result.

The data of conductivity measurement clearly prove the assumption that oxide ions can diffuse more rapidly in Al–doped rutile crystal than in undoped crystal.

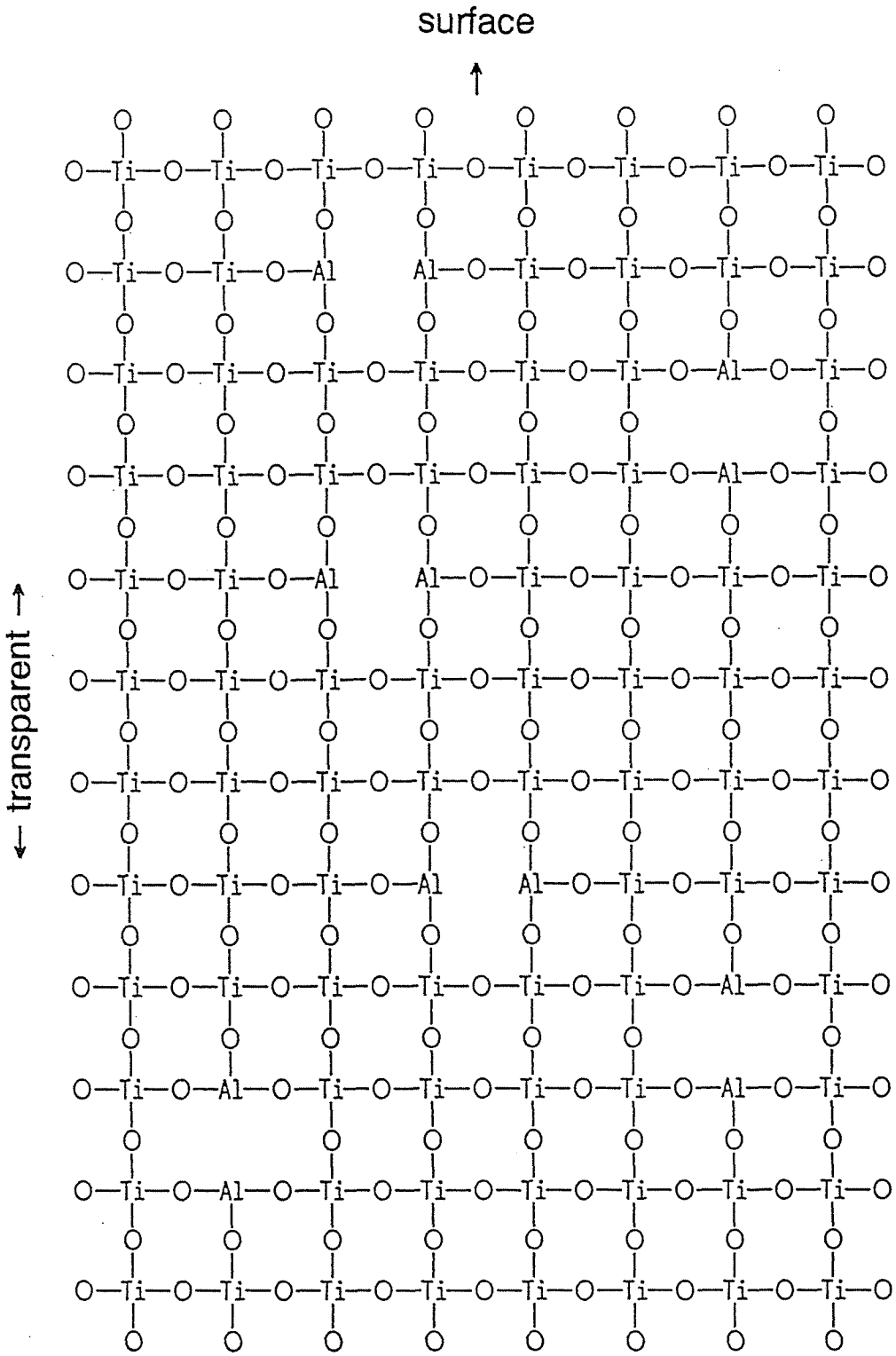

Fig. 11. Two dimensional expression of Al–doped rutile crystal.

In 600–900 °C, the conductivity of Al–doped crystal is larger by one order of magnitude in AC field than that of undoped crystal. In AC field, the conductivity is determined by the mixture of electronic and ionic conduction. In DC field, however, the contribution of ionic conduction for conductivity is negligible, since the carriers, i.e. oxide ions in this case, are polarized and can not migrate. Thus, the conductivity in DC field must be determined only by the electronic conduction. Since the DC conductivity of Al–doped crystal is much the same as that of the undoped crystal, there is no contribution of the Al–doping to electronic conduction. Therefore, the higher AC conductivity of Al–doped crystal than that of undoped crystal is caused by the ionic conduction. Two types of carriers are possible in the Al–doped crystal, that is, O^{2-} ions and Al^{3+} ions. The diffusion rate of Al^{3+} along the c–axis is larger by two orders of magnitude than that perpendicular to the c–axis because the rutile structure has a channel along the c–axis, through which channel the small Al^{3+} ions can easily migrate. Accordingly, if the ionic conduction of Al^{3+} is dominant, the AC conductivity of Al–doped crystal along [110] direction must be approximately same as that of undoped crystal. However, there is distinct difference in AC conductivity between the Al–doped and undoped crystals although the difference is less than that along the c–axis. Therefore, the oxide ions can migrate at an appreciable velocity in the Al–doped crystal, which contributes the higher AC conductivity. There is also anisotropy of the diffusion rate of oxide ions in a rutile crystal. The diffusion rate of oxide ions is generally larger along the c–axis than that perpendicular to the c–axis, but the difference is not so large as the case of Al^{3+}. This is the reason why the difference in the AC conductivity along the c–axis is larger than that along [110] direction.

Generally, the diffusion rate of any kind of species must be higher at higher temperature. In semiconductor such as TiO_{2-x}, however, the contribution of the

intrinsic electronic conduction becomes dominant to determine the conductivity. Accordingly, the difference in the AC conductivity between the Al–doped and undoped crystals becomes smaller above 1000 °C. The temperature range of 600–900 °C, in which the difference in the AC conductivity between the Al–doped and undoped crystals is maximum, corresponds to the empirical annealing temperature, at which a pale–yellow and completely transparent rutile crystal is obtained although a long–term annealing is necessary. This result does not indicate that the maximum diffusion rate of the oxide ions is attained in this temperature range but just indicates that considerably rapid diffusion of the oxide ions still remains in such a relatively low temperature range, in which few Ti^{3+} can survive.

4. SUMMARY AND CONCLUSIONS

The coloring of the floating zone grown rutile crystal is one of the most serious problems, since the colored crystal has a wide absorption band around 1.5 μm, which correspond to the wavelength used in optical communications. The origin of the coloring should be the existence of Ti^{3+} ions, which are reduced from Ti^{4+} at high temperature with oxygen deficiency. In order to oxidize the Ti^{3+} ions, a considerably long–term, e.g. 20 days, annealing in air is necessary if the crystal is grown under a low oxygen partial pressure to avoid the formation of low–angle grain boundaries. However, even if a rutile crystal is grown in the O_2 stream with the addition of ZrO_2, the grown crystal is still dark–blue. In this chapter, the effects of aliovalent (trivalent or divalent) cations on the decoloration of floating zone grown rutile single crystals have been examined.

The addition of any trivalent or divalent cations was effective to obtain transparent, as–grown rutile single crystals. The addition of Sc_2O_3 or Al_2O_3 was

also effective to suppress the formation of low-angle grain boundaries; in particular, the Al-doped crystal had few low-angle grain boundaries. In 200-2000 nm, the transmittance of the as-grown, Al-doped crystal was the same as that of undoped crystal, which was fully annealed to be pale-yellow and transparent.

The most reasonable explanation for this phenomenon is that the diffusion rate of oxide ions is accelerated by the existence of oxygen vacancies, which should be formed by the addition of aliovalent cations for the charge compensation. The AC conductivity of the Al-doped crystal was larger by one order of magnitude than that of the pure crystal in 600-900 °C. The difference may be attributable to the ionic conduction by the oxide ions, which rapidly migrate via oxygen vacancies. The temperature range of 600-900 °C corresponds to the annealing temperature to obtain fully decolorized rutile single crystal. Therefore, the diffusion rate of oxide ions in the Al-doped crystal is still appreciably high at 600-900 °C so that fully decolorized rutile single crystal was obtained during relatively rapid cooling to room temperature for 30 min after the growth run was completed.

In conclusion, oxygen vacancies are effectively formed by the addition of trivalent or divalent cation. Oxide ions are easily diffused via the oxygen vacancies to oxidize Ti^{3+} to Ti^{4+} on cooling and decolorized and transparent rutile single crystals are consequently obtained.

REFERENCES

1. M. Maeno, "Muki Sozai Gijutu Dokuhon", Nikkan Kogyo Shinbun-sha, (1987) 277.

2. R. Yamauchi and K. Inada, "Hikari Erekutoronikusu Zairyo Manyuaru", Optronics-sha, (1986) 151.
3. M. Arita, M. Hosoya, M. Kobayashi and M. Someno, *J. Am. Ceram. Soc.*, **62** (1979) 443.
4. J. A. S. Ikeda, Y.-M. Chiang and B. D. Fabes, *J. Am. Ceram Soc.*, **73** (1990) 1633.
5. Y. Oishi and K. Ando, "Kagaku Sosetsu No. 9", Gakkai Shuppan Center, (1975) 31.
6. W. D. Kingery, J. Pappins, M. E. Doty and D. C. Hill, *J. Am. Ceram. Soc.*, **42** (1959) 393.
7. D. W. Stickler and W. G. carlson., *J. Am. Ceram. Soc.*, **47** (1964) 122.

Chapter 4

Solid–Liquid Interface Shapes in the Floating Zone Growth of Rutile Single Crystals

1. INTRODUCTION

In the melt growth of single crystals, the interface shape between a growing crystal and the melt is one of the most important factors to determine the quality of the grown crystals [1–3]. A concave interface is usually unfavorable, since dislocations are easily concentrated into the central part of crystals, in which cracks often occur [1,2]. On the other hand, an extremely convex shape should also be avoided to reduce thermal stresses [3]. A flat or slightly convex interface shape is therefore desirable for the melt growth. However, practical interface shapes are usually very complicated, since the interface shapes are influenced by many parameters such as temperature gradient, convection in the melt, and thermal conductivity of the melt and crystal. All the parameters influence each other, and they can not be controlled independently. Accordingly, compromised interface shapes are usually adopted. For example, YAG single crystals grown by the Czochralski method have a remarkably convex interface shape to form intentionally a limited core region constituted of {110} facets which deteriorate optical uniformity [4].

In the floating zone growth, an extremely convex interface gives rise to another problem, which is contact between the feed rod and the growing crystal. The contact induces instability or collapse of the melt zone by the wobble of the feed rod when the feed rod is just suspended from the upper shaft. If the feed rod is fixed, the contact causes a more serious problem, that is, the feed rod itself breaks down. This is the reason why a large–diameter crystal is usually difficult to grow by the floating zone method with an infrared convergence type heater.

In the previous chapter, rutile single crystals were successfully grown by the

floating zone method with an infrared convergence type heater; however, the crystal diameters for the stable growth were limited to 12 mm, since the contact between a feed rod and a growing crystal occasionally occurred, followed by the collapse of the melt zone, when the diameter of the growing crystals exceeded 12 mm. Therefore, in order to develop the floating zone growth of large-diameter rutile single crystals, it is very important to examine how the interface shapes are changed when the crystal diameter is increased and what parameter is effective to reduce the height of the interface. There have been no detailed paper on the floating zone growth of rutile single crystals, and thus no report on the interface shapes.

In this chapter, the shapes of solid-liquid interface in the floating zone growth of rutile single crystals were investigated as a function of the rotation rate, the crystal diameter and the growth direction. The relation between the interface shapes and the growth conditions will be discussed on the basis of convection and heat transfer in the growing crystals and the melt zone.

2. EXPERIMENTAL

High purity TiO_2 (Fuji Chitan Kogyo, 99.98%) and reagent grade ZrO_2 (Daiichi Kigenso Kagakukogyo) powders were used as starting materials. ZrO_2 was added with 0.75 wt% to observe growth striations, which would reflect the shape of solid-liquid interface. Feed rods for the floating zone growth were prepared in the same manner as described in the previous chapter. The diameter of the feed rods were 12 mm and 15 mm so as to obtain rutile single crystals 10 mm and 13 mm in diameter. The latter diameter was the limit in this study to perform the stable floating zone growth.

The growth apparatus used was a double–ellipsoid image furnace, which was essentially the same as in the previous chapter except for the halogen lamps. The lamps had a filament of plate–like shape on the whole, whereas commonly used lamps have a helicoid–shape filament. The lamps used in this study would improve the radial thermal distribution. The crystal growth procedure by the floating zone method was the same as described in the previous chapter. Growth conditions were as follows: rotation rate was 30 rpm for the feed rod and 20–60 rpm for the seed crystal, growth rate was 5 mm/hr and the atmosphere was a CO_2 stream of 2 liter/min.

Grown crystals were cut to 2 mm thick plates parallel to the growth direction including the center of the crystals. Both sides of the specimen were mechanically polished and then finished to be mirror surfaces. Growth striations (interface shapes) were examined under a polarizing microscope with crossed nicols.

3. RESULTS AND DISCUSSION

Growth striations of the floating zone grown rutile single crystals were easily observed with the polarizing microscope by the addition of a small amount of ZrO_2 as shown in fig. 1, whereas the striations were not visible in ZrO_2–free crystals. In the case of growing ZrO_2–doped crystals, an appreciable fluctuation of impurity segregation would occur at the growth interface, and stress birefringence which was detectable with the polarizing microscope would be induced, as a result. An interface shape of a quenched rutile crystal was the same as the striation of the ZrO_2–doped crystal grown under the same condition. Accordingly, the interface shapes in the following figures are traced over the growth striations of the ZrO_2–doped crystals.

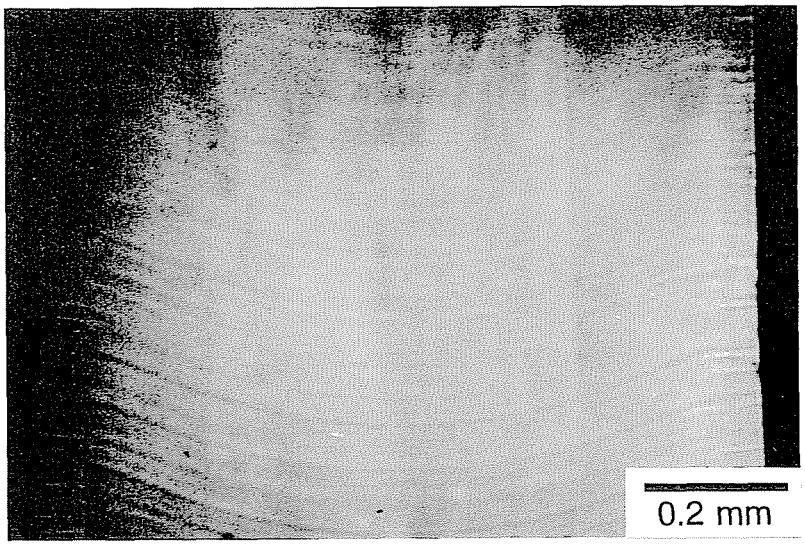

Fig. 1. Polarized microphotographs of a vertical section of Zr–doped rutile single crystal grown by the floating zone method.

In order to evaluate the height of the interface, a term of convexity is used in this chapter. The convexity is presently defined as h/r, where h and r represent the height of the interface and the crystal radius, respectively, as shown in fig. 2.

Fig. 3 shows the effect of the rotation rates on the interface shapes of the 10 mm diameter crystal growth along the c–axis. At 20 rpm, the interface shape is considerably convex toward the melt, and the convexity is 0.61. The convexity of the 10 mm diameter crystal was drastically decreased with increasing rotation rate. A plateau shape, which is favorable for the floating zone growth, was realized at 40 rpm. Finally, the central part of the interface became concave toward the melt at 60 rpm.

For the a–axis crystal 10 mm in diameter, the height of the interface was considerably lower than that of c–axis crystals as shown in fig. 4. The convexity is 0.2 at 20 rpm, which is appreciably favorable shape for the floating zone growth as well as the interface for c–axis crystal at 40 rpm. Also, the interface inversion occurred to form an concave interface even at 40 rpm.

For the 13 mm diameter crystal, the rotation rates was less effective to reduce the convexity than for the 10 mm diameter crystal. Fig. 5 shows the interface shapes of the 13 mm crystal grown along the c–axis. The convexity at 20 rpm is 0.63, which is slightly larger than that of the 10 mm diameter crystal at 20 rpm. At 60 rpm, the interface is still convex to the melt (the convexity is 0.48), and the interface inversion, which was observed in the 10 mm diameter crystal, did not occur in the 13 mm diameter crystal.

As shown in figs. 3, 4 and 5, some of the interfaces are bent at the intermediate position between the center and the edge of the crystals grown at

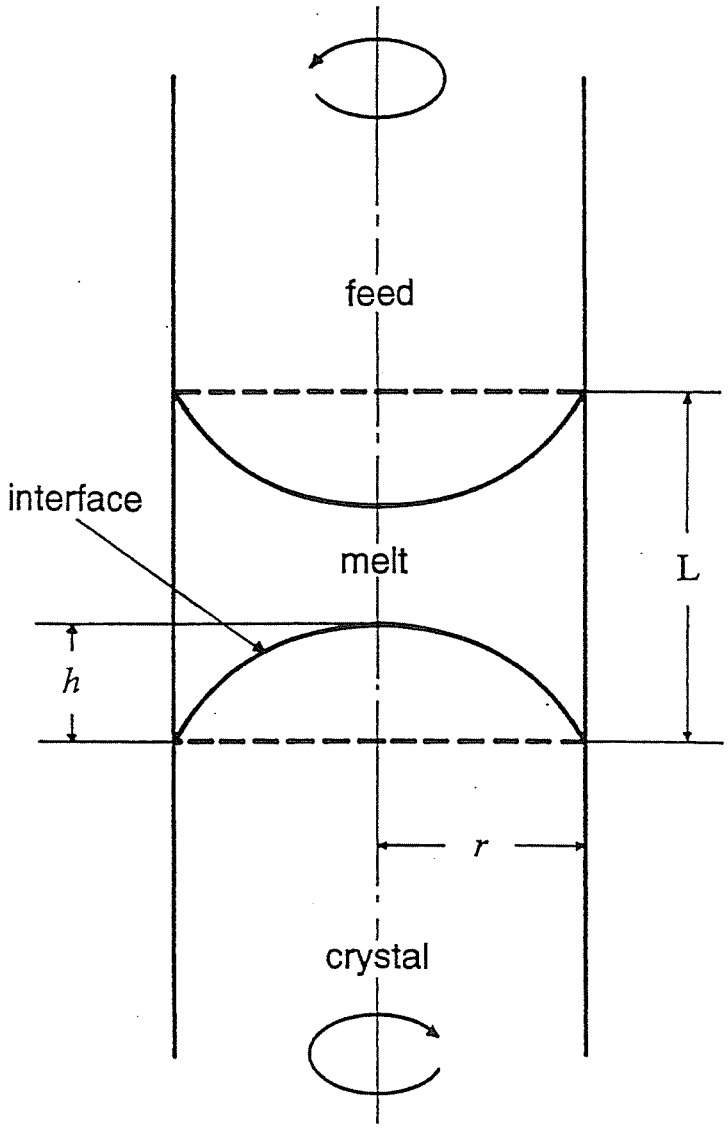

Fig. 2. Schematic illustration of the floating zone growth. L, h and r represent external zone length, height of the interface and radius of the growing crystal, respectively.

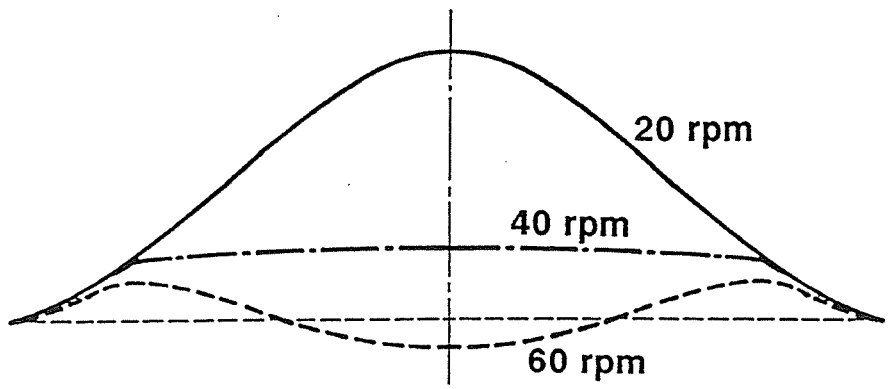

Fig. 3. Effect of the rotation rate on the interface shapes of the 10 mm diameter crystal grown along the c–axis.

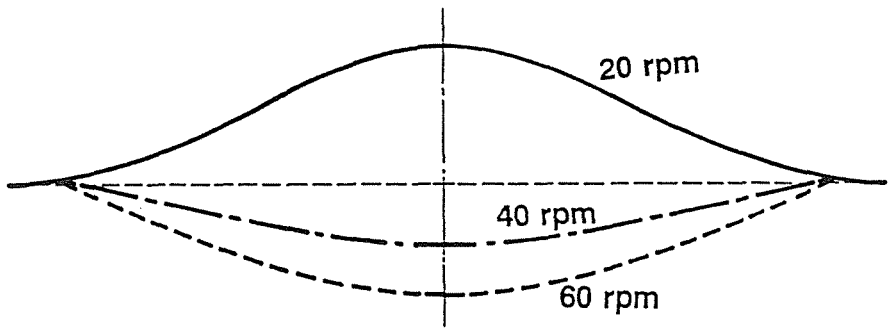

Fig. 4. Effect of the rotation rate on the interface shapes of the 10 mm diameter crystal grown along the a–axis.

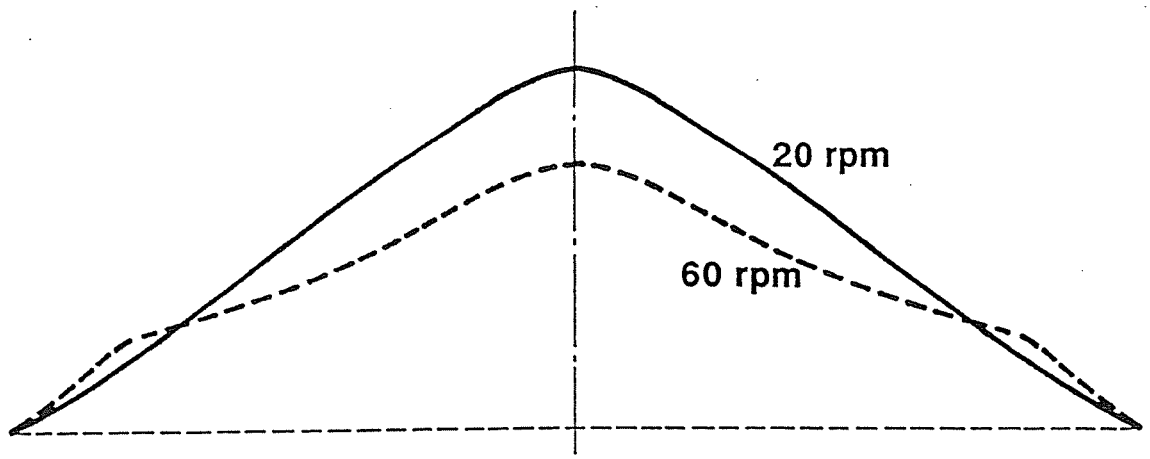

Fig. 5. Effect of the rotation rate on the interface shapes of the 13 mm diameter crystal grown along the c–axis.

high rotation rates, and the interface shapes near the edge are much the same despite of drastic change in the central part. This phenomenon indicates the existence of two types of convections in the melt zone. One will be a Marangoni convection and the other will be a forced convection as shown in fig. 6. There have been many reports on the existence of the Marangoni convection along the free surface of the melt in the floating zone method [5–7]. Because the Marangoni convection is caused by difference in surface tension due to temperature gradients, the convection flows from upper part to lower part along the melt surface. Radiant heat from the lamps will be almost absorbed at the melt surface, and the heat will be transferred into the inner region of the melt zone by convection rather than by conduction. Therefore, the Marangoni convection has an important role to transfer the absorbed radiant heat. On the other hand, the forced convection, which is caused by the crystal rotation, flows from the center to the outer region of the melt zone. Thus, the forced convection has a role to transfer the heat to the central region of the melt zone. The strength of the forced convection is estimated by Reynolds number, i.e. $r^2\omega/\nu$, where ω is the rotation rate of the crystal and ν is the kinematic viscosity of the melt. Therefore, the strength of the forced convection increases with increasing rotation rate so that the convexity of the interface is reduced. In the case of the 10 mm diameter crystal, the high rotation rates were certainly effective to reduce the convexity. Kitamura et al. reported similar effect of rotation rate on the interface shapes of YIG single crystals grown by a traveling solvent floating zone method [8]. The convexity of the interface in YIG single crystals decreased with increasing rotation rate, although the change of the convexity was less than that in the rutile single crystal 10 mm in diameter.

Until the steady state for floating zone growth is attained, the lamp power should be continuously increased even after an constant crystal diameter is

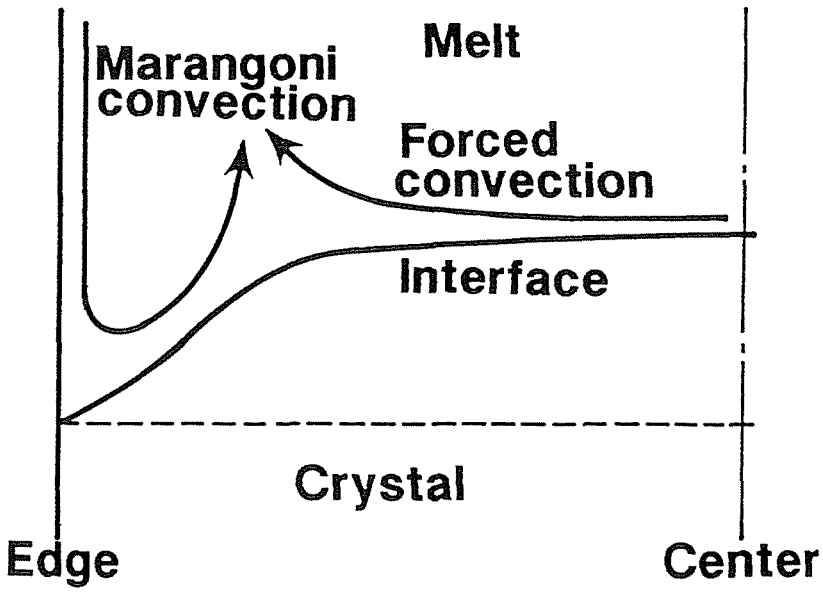

Fig. 6. Schematic illustration of convections in the melt zone.

attained. This phenomenon indicates that appreciable heat in the melt zone is lost by the conduction through the grown crystal. The difference in the convexity between c–axis and a–axis crystals will be explained by the difference in the thermal conductivity along the c–axis and a–axis. Since the thermal conductivity along the c–axis is larger than along a–axis, i.e. 10.4 W/mK and 7.4 W/mK along c– and a–axes, respectively, at room temperature [9], more heat must be lost from the melt zone through the grown crystal in the case of the c–axis crystal growth. This heat loss will consequently result in the increase in the convexity.

Since the Reynolds number is also proportional to the square of the crystal radius, the increase in the crystal diameter is expected to effectively enhance the strength of the forced convection and to reduce the height of the interface, as a result. In the floating zone growth of rutile single crystals, however, the convexity was not reduced but rather increased with increasing crystal diameter. On the contrary, it is often observed in the Czochralski growth of some oxide single crystals, e.g. $Gd_3Ga_5O_{12}$, that the interface shape changes from convex to concave when the crystal diameter is increased to form the shoulder part [10].

This discrepancy is explained by the difference in thermal environment between the floating zone and the Czochralski growth systems. The melt zone in the floating zone method is directly exposed to the atmosphere, and there is usually no thermal insulation. Most of the absorbed radiant heat would readily be lost by radiation. Therefore, the melt volume would severely influence the temperature in the central region of the melt zone. In this study, the melt volume for growing a rutile single crystal 13 mm in diameter was twice as large as that for 10 mm diameter crystal. Therefore, the temperature in the central region of the melt zone for the 13 mm diameter crystal would considerably be lower than that

for the 10 mm diameter crystal, and the forced convection was consequently less effective in the case of 13 mm diameter crystal. On the other hand, in the Czochralski method, a crucible, which is often used as heat source, is embedded in thick thermal insulation. The temperature in the inner region of the melt is thereby comparable with that near the crucible even if a large crucible, which increases the melt volume, is used to grow large-size crystals. The enhanced forced convection has therefore the possibility to form a concave interface when the crystal diameter is increased in the Czochralski method.

4. SUMMARY AND CONCLUSIONS

The interface shapes in the floating zone growth of rutile single crystals were investigated as a function of crystal rotation rate, growth direction and crystal diameter and following results were obtained:

(1) The convexity was decreased with increasing crystal rotation rate in any cases; however, a high rotation rate was less effective to decrease the convexity of the 13 mm diameter crystal than that of the 10 mm diameter crystal.

(2) The c-axis crystal had larger convexity than the a-axis crystal had because of the larger thermal conductivity along the c-axis than along the a-axis.

(3) The existence of the Marangoni convection was implied by the fact that the interface shapes in the peripheral region did not change despite drastic change in the central region.

The convexity in the floating zone growth of rutile single crystals will be increased with increasing crystal diameter, and the contact between a feed rod and

a growing crystal will consequently occur more frequently, which disturb the stable floating zone growth. The supply of excessive lamp power to avoid the contact will result in the collapse of the melt zone due to the increased self–weight. A higher rotation rate above 60 rpm might be effective to reduce the height of the interface, but this is not a practical solution because a higher rotation rate itself will cause the instability of the melt zone due to mechanical vibration. This phenomenon that the height of interface is increased with increasing crystal diameter indeed demonstrates the difficulty to grow large–diameter rutile single crystals by the floating zone method with an infrared convergence type heater.

REFERENCES

1. S. A. Borodin, L. B. Davidova, V. M. Erofeev, A. V. Shanov, S. A. Startsev and V. A. Tatarchenko, *J. Crystal Growth*, **46**, 757 (1979).
2. K. Kitamura, S. Kimura and S. Hosoya, *J. Crystal Growth*, **48**, 469 (1976).
3. K. Kitamura, S. Kimura and K. Watanabe, *J. Crystal Growth*, **57**, 457 (1982).
4. J. Basterfield, M. J. Prescott and B. Cockayne, *J. Mater. Sci.*, **3**, 33 (1968).
5. D. Schwabe, A. Scharmann, F. Preisser and R. Oeder, *J. Crystal Growth*, **43**, 305 (1978).
6. D. Schwabe and A. Scharmann, *J. Crystal Growth*, **46**, 125 (1979).
7. C. W. Lan, Y. J. Kim and S. Kou, *J. Crystal Growth*, **104**, 801 (1990).
8. K. Kitamura, N. Ii, I. Shindo and S. Kimura, *J. Crystal Growth*, **46**, 277 (1979).
9. R. Hishida, "Fain Seramikkusu Jiten", Gihodo Shuppan (1987) 317.
10. B. Cockayne, B. Lent and J. M. Roslington, *J. Mater. Sci.*, **11**, 257 (1976).

Chapter 5

Characterization of the Floating Zone Grown Rutile Single Crystals as Polarizer

1. INTRODUCTION

The basic requirement in communication is to keep the signal level and the signal–noise (S/N) ratio as high as possible. In the optical communication, these requirements are primarily dependant on the quality of each element, i.e. the quality of crystals which are used. In order to keep the signal level, the insertion loss of laser beam should be as low as possible. The insertion loss is attributable to the reflection at the surface and the absorption. The former is principally inevitable for all the materials, but is minimized to be nearly zero by making anti–reflection coating on the surface of the crystals. As for the absorption loss, the rutile single crystal is essentially transparent in a wide wavelength range from 420 nm to about 5 μm, and there is no absorption in this range if the crystal is fully annealed to be free from Ti^{3+} ions. No problem is therefore expected with respect to the insertion loss when fully annealed rutile single crystals are used in optical communications.

On the other hand, the S/N ratio is severely influenced by the one or two dimensional defects in the crystal, i.e. dislocations and low–angle grain boundaries, which are commonly found in the floating zone grown rutile single crystals. The best way to evaluate the quality of the crystals as optical materials is to measure extinction ratio, which is desired to be as high as possible. In the long distance optical communication, for example, each element (crystal) is usually required to have a very high extinction ratio of above 60 dB.

In this chapter, two types of prisms, Glan–Thompson prisms and parallel plates, are fabricated from the floating zone grown rutile single crystals and their extinction ratio is measured. On the basis of obtained results, the possibility to use

the floating zone grown rutile single crystals in practical devices is examined.

2. CONCEPT AND MEASUREMENT OF THE EXTINCTION RATIO

Firstly, a perfect polarizer and a perfect analyzer are assumed, and they are set as shown in fig. 1. The insertion loss is neglected in this discussion. A light beam which is transmitted through the polarizer should vibrate parallel to only one direction, that is, the light is a perfect linearly polarized light. If the analyzer is aligned exactly parallel to the polarizer, the polarizer light should be transmitted through the analyzer without any loss. On the contrary, if the analyzer is aligned exactly perpendicularly to the polarizer, no light can be transmitted through the analyzer. In this case, the extinction ratio is infinite, since the extinction ratio, R_{ext} (dB), is defined by following equation:

$$R_{ext}(dB) = 10 \cdot \log \frac{I_{\max}}{I_{\min}}$$

where I_{max} is the energy of the light transmitted through the analyzer which is aligned parallel to the polarizer (parallel nicols), and I_{min} is the energy of the light transmitted through the analyzer which is aligned perpendicularly to the polarizer (crossed nicols).

Actual polarizers are not perfect and the light transmitted through the polarizer should accordingly involve two components of electromagnetic waves which perpendicularly vibrate each other as shown in fig. 2. In this case, the extinction ratio is finite and represented by the ratio of the amplitude of the major wave to that of minor wave. When a crystal is used as the polarizer, this

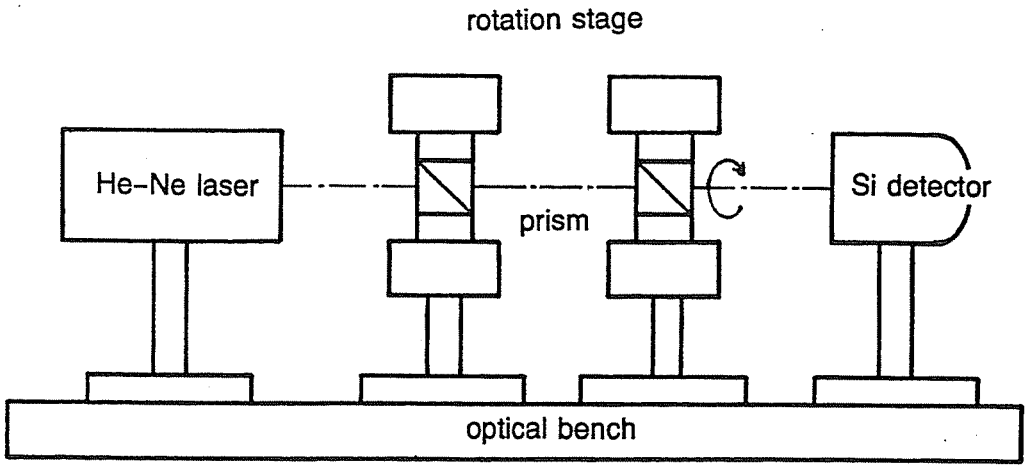

Fig. 1. Basic alignment for the measurement of the extinction ratio of the prisms.

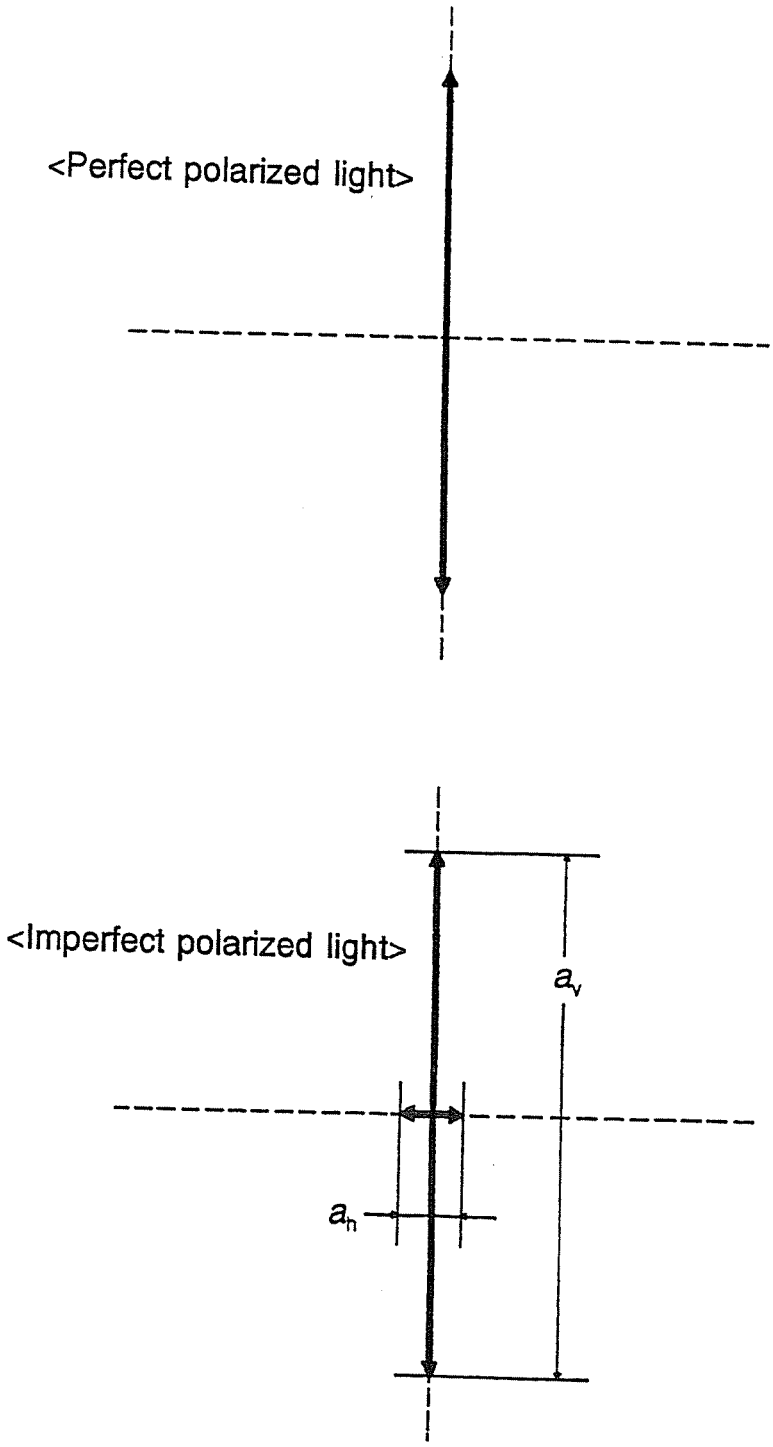

Fig. 2. Vibration direction of perfect polarized light (a) and imperfect polarized light (b).

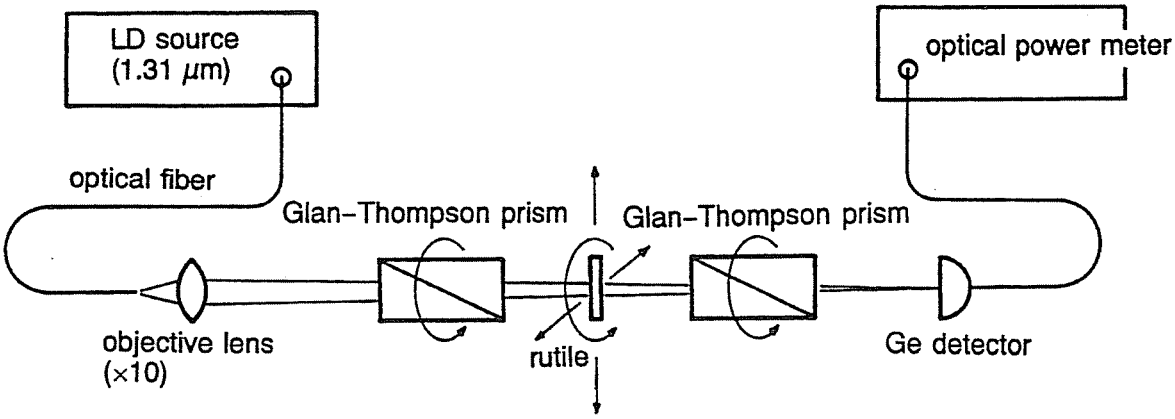

Fig. 3. Basic alignment for the measurement of the extinction ratio of a parallel plate.

phenomenon is caused by the imperfection of the crystal. Therefore, the extinction ratio is a good index to evaluate how imperfect the crystal is.

If two high-quality polarizers (at least 60 dB) are available, the extinction ratio of a crystal can be easily measured without processing the crystal to be two polarizer prisms. In this case, the crystal is just cut to be a parallel plate and then polished to be mirror surface. Fig. 3 shows the alignment for the measurement of extinction ratio of the parallel plate. The anti-reflection coating should be made of both sides of the plate if possible. The polarizer and the analyzer are aligned to be crossed nicols and the plate between them is aligned on the extinction position. If the extinction ratio of the crystal is below that of the polarizer and the analyzer, the total extinction ratio provides that of the crystal. If the extinction ratio is not changed before and after placing the crystal, the extinction ratio of the crystal is equivalent or more than that of polarizers. The advantage of this method is that the extinction ratio for any crystals can be measured, even if the crystal is optically isotropic.

In this study, two Glan-Thompson prisms were fabricated from a pure rutile single crystal grown under a low oxygen partial pressure and their extinction ratio was directly measured by using He-Ne laser as illustrated in fig. 1. Also, parallel plates were processed from Zr- or Al-doped rutile single crystals and their extinction ratio was measured by using commercially available Glan-Thompson prisms of which extinction ratio was above 60 dB and laser diode of 1.3 μm as illustrated in fig. 3.

3. FABRICATION OF PRISMS

3.1 Glan–Thompson prism

The Glan–Thompson prism is widely used in optical measurements. All the disadvantages of the Nicol prism are eliminated in this prism. The most remarkable advantage of this prism is that linearly polarized light of which direction is the same as that of incident light can be produced. The principle of the Glan–Thompson prism is illustrated in fig. 4. This prism is constituted of two triangle prisms, between which adhesive such as Canada balsam is used. The incident light normal to the surface of the prism is divided to the ordinary and extraordinary rays, which vibrate perpendicularly and parallel to the optic axis, respectively. The ray of which refractive index is larger than other's is completely reflected at the surface which is diagonally cut. In the case of rutile, extraordinary ray is completely reflected. The ordinary ray is also reflected to some extent at the same surface and the reflectance is determined by the difference in the refractive index between the prism and the adhesive. At this stage, linearly polarized light can be obtained, but its direction is remarkably different from that of the incident light. The direction of the ordinary ray is modified by the second prism to be the same as that of the incident light.

The geometry of the Glan–Thompson prisms fabricated from a rutile single crystal is 5×5×3.5 mm, which is appreciably smaller than that fabricated from a calcite single crystal as shown in table 1. That is because the refractive indices of rutile are much higher than those of calcite. The larger refractive indices mean larger reflectance, but reflection loss can be minimized by making anti–reflection coating.

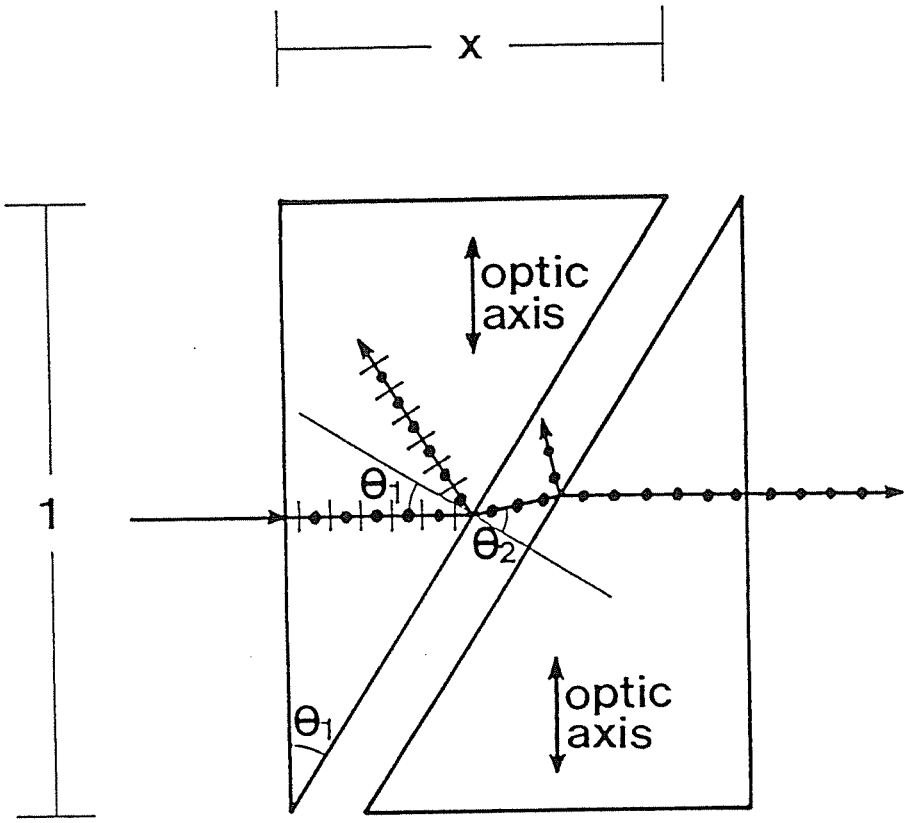

Fig. 4. Principle of the Glan–Thompson prism.

Table 1. Geometry of Glan–Thompson prism fabricated from different materials

material	θ_1 in fig. 4	x
rutile	32.3	0.63
calcite	69.2	2.63
quartz	86.4	15.9

* refractive index of the adhesive: 1.55

3.2. Parallel plate

The Glan–Thompson prism certainly has excellent features, but this prism can not be used in the optical communication since large insertion loss is inevitable. In practical optical isolator, parallel plates of which surface is inclined to the optic axis are often used as polarizers as shown in fig. 5. The laser beam is divided through the parallel plate into two waves, i.e. ordinary and extraordinary rays, which vibrate perpendicularly each other, since the extraordinary ray does not follow the Snell's law. The divided width is desired to be as large as possible to make the device size small. The divided width, S, is determined by following equation:

$$S=\frac{D(n_e^2-n_o^2)}{2(n_o^2\sin^2\phi+n_e^2\cos^2\phi)}$$

where D is the thickness of the plate and ϕ is the angle between the optic axis and the normal to the plate surface. When D is constant, the maximum division is obtained, if

$$\tan\phi=\frac{n_e}{n_o}$$

is met. The maximum divided width for rutile is comparable to that for calcite as shown in table 2.

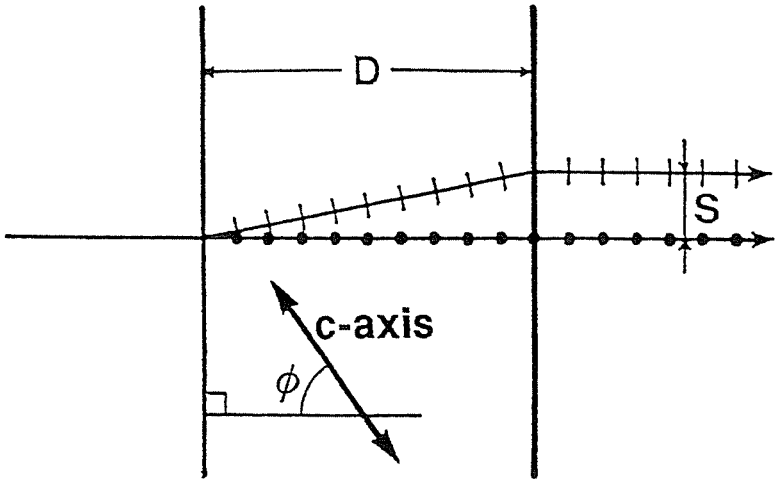

$$S=\frac{D(n_e^2-n_o^2)\sin 2\phi}{2(n_o^2\sin^2\phi+n_e^2\cos^2\phi)}$$

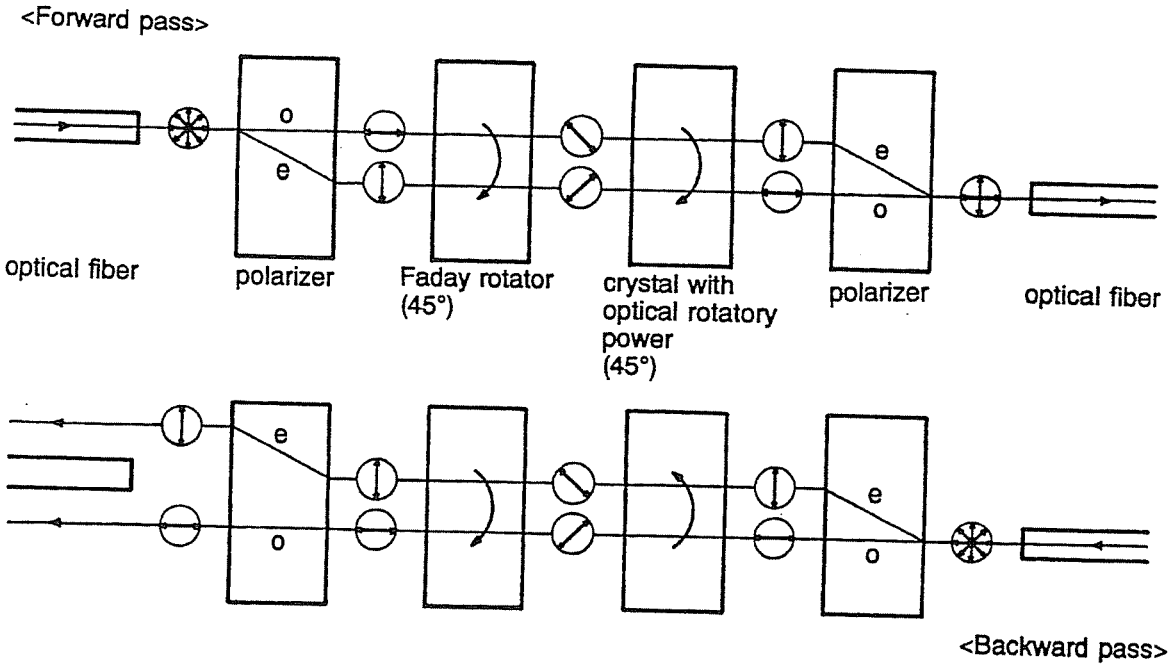

Fig. 5. Principle of an optical isolator using parallel plates as polarizers.

Table 2. Comparison of the maximum light splitting by a parallel plate made of different materials

material	ϕ	S_{max}
rutile	47.98	0.104
calcite	41.87	0.110
quartz	45.17	0.006

* D = 1 mm in fig. 5

4. RESULTS AND DISCUSSION

4.1. Glan–Thompson prism

In fig. 1, when the polarizer is fixed and the analyzer is rotated, the energy of the light emerged from the analyzer should be represented by a sine (or cosine) curve as a function of the rotation angle. There is no essential difference between the sine and cosine curves, that is, if the measurement is started with crossed nicols, a sine curve should be obtained, and if parallel, a cosine curve.

Fig. 6 shows the relation between the rotation angle of analyzer and the transmitted light power through two Glan–Thompson prisms, which were fabricated from a pure rutile single crystal grown by the floating zone method under a relatively low oxygen partial pressure. As expected, cosine curve relation is obtained between the rotation angle and the transmitted light power. The ratio of the maximum power of 28.4 μW to the minimum power of 0.1 nW gives the extinction ratio of the prisms:

$$R_{ext}(dB) = 10 \cdot \log \frac{I_{\max}}{I_{\min}} = 10 \cdot \log \frac{28.4 \times 10^{-6}}{0.1 \times 10^{-9}} = 55(dB)$$

The extinction ratio of commercial Glan–Thompson prisms which are fabricated from calcite single crystals is 53–60 dB (cited from the catalog of Karl Lambrecht Ltd.). Accordingly, the Glan–Thompson prisms fabricated in this study has comparable extinction ratio to commercial prisms.

The anti–reflection coating was not made on the Glan–Thompson prisms, and the reflection loss was consequently 85 %. The reflection may cause stray light, which will increase the extinction ratio. Considering this point, the optical quality,

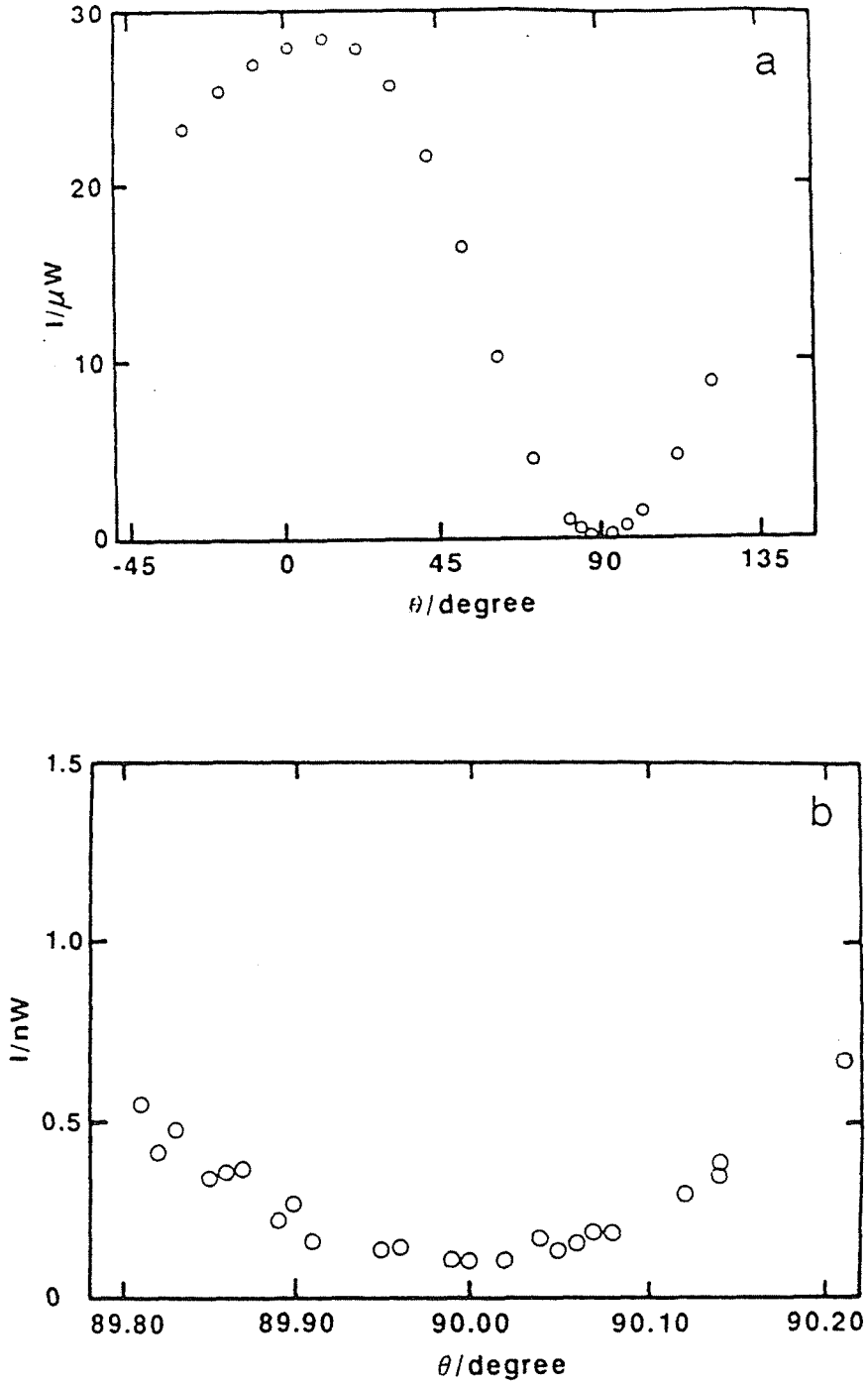

Fig. 6. Result on the measurement of the extinction ratio of Glan–Thompson prisms made of a pure rutile single crystal grown by the floating zone method under a low–oxygen partial pressure: (a) overall; (b) magnification around 90 ° in (a) (rotation angle of one prism (θ) versus transmitted light power through two prisms).

i.e. extinction ratio, of the floating zone grown rutile single crystals is probably higher than that measured in this experiment.

4.2. Parallel plates

A parallel plate was initially set so as to obtain the maximum extinction ratio at the center of the crystal and then translated in Y and Z directions to measure the distribution of the extinction ratio. Therefore, the extinction ratio obtained at other measuring point is not necessarily the maximum value at that point. However, this method is the best way to quantitatively evaluate the optical uniformity of the crystal.

Figs. 7 and 8 show the distribution of the extinction ratio of the parallel plates made of Zr- and Al-doped rutile single crystals, respectively. The measurement was done at intervals of 0.5 mm. The central gray region represents the position of the measured crystal and the outer black part represents therefore the extinction ratio of Glan-Thompson prisms made of calcite single crystals. The darker region represents higher extinction ratio. The maximum extinction radio of 58 dB was obtained for both the Zr- and Al-doped crystals. This extinction ratios of the parallel plates are comparable to that of the Glan-Thompson prisms made of the undoped rutile single crystal. For the Zr-doped crystal, the extinction ratio is more than 50 dB at any measuring positions, whereas for the Al-doped crystal extinction ratios less than 50 dB are observed at some positions. Accordingly, the Zr-doped crystal is more optically uniform than Al-doped crystal. This is obvious from the polarized microphotographs of cross sections as shown in fig. X and Y in Chapter 2. The Al-doped crystal certainly has few low-angle grain boundary, but some strain, which will deteriorate the optical uniformity, can be observed. On the other hand, the Zr-doped crystal has little strain. This result proves that ZrO_2

		Z																			
		0.5	1.0	1.5	2.0	2.5	3.0	3.5	4.0	4.5	5.0	5.5	6.0	6.5	7.0	7.5	8.0	8.5	9.0	9.5	10.0
Y	0.5	63.5	70.7	67.8	67.6	66.5	67.6	68.2	68.7	65.1	67.5	67.3	67.5	67.6	67.3	67.5	67.5	67.5	67.4	67.3	67.5
	1.0	70.3	69.0	70.2	69.5	68.3	62.1	70.3	69.3	67.4	67.4	67.5	67.4	67.5	67.5	67.5	67.4	67.4	67.3	67.3	67.5
	1.5	71.3	69.6	71.3	70.5	69.3	66.7	62.7	66.0	67.3	67.3	67.3	67.4	67.3	67.5	67.4	67.3	67.3	67.3	67.5	67.4
	2.0	67.0	61.2	67.8	71.3	70.3	68.1	63.4	57.2	58.0	58.5	60.0	63.8	65.8	67.3	67.3	67.4	67.4	67.3	67.3	67.4
	2.5	67.2	67.5	66.5	65.5	63.8	54.9	52.7	53.7	55.2	55.5	55.0	54.2	54.9	59.0	65.3	67.4	67.4	67.5	67.6	67.4
	3.0	67.3	67.5	67.3	67.3	53.8	51.4	53.9	55.6	57.1	57.1	56.9	56.5	55.9	54.1	57.3	62.3	67.5	67.4	67.2	67.4
	3.5	67.5	67.4	67.5	63.6	50.9	53.4	54.6	55.4	55.7	56.4	55.8	55.3	56.7	56.4	54.0	56.3	67.3	67.3	67.3	67.4
	4.0	67.5	67.5	67.3	52.7	52.7	52.3	54.1	58.6	57.8	57.4	57.4	57.2	55.7	56.7	55.4	52.8	56.2	67.3	67.2	67.5
	4.5	67.3	67.5	67.3	50.4	52.5	54.2	54.7	57.0	57.4	56.8	56.7	57.3	57.3	55.1	55.8	52.5	57.3	67.3	67.6	64.8
	5.0	67.3	67.4	63.0	50.9	52.7	53.5	55.6	57.3	57.6	57.2	57.0	57.3	57.7	55.0	55.6	54.9	55.7	67.5	62.3	69.7
	5.5	67.3	67.3	54.7	51.5	52.6	53.0	56.0	57.9	57.7	57.5	57.4	57.5	57.8	55.1	55.9	56.0	57.7	62.2	67.2	69.1
	6.0	67.3	67.3	51.9	52.1	53.2	53.2	56.5	57.6	57.9	58.0	57.9	58.0	57.6	54.6	55.7	56.2	57.6	70.3	69.7	67.3
	6.5	67.3	67.5	52.0	52.6	54.1	53.6	56.3	58.0	58.2	58.3	58.1	58.1	56.8	54.5	55.5	55.6	62.6	68.7	69.0	67.3
	7.0	68.7	67.3	52.0	53.2	54.9	53.7	56.3	58.0	58.2	58.3	58.2	57.7	55.5	55.6	55.7	54.7	64.0	67.3	66.6	67.9
	7.5	67.5	67.2	52.4	53.3	54.9	53.6	56.7	58.2	58.1	58.2	57.9	56.6	54.6	55.7	55.9	54.8	61.8	67.0	67.3	66.8
	8.0	67.4	67.1	53.7	53.4	53.9	53.9	56.3	57.6	57.6	57.4	56.7	54.9	55.7	55.2	56.0	56.1	63.9	67.0	67.3	68.5
	8.5	67.3	67.3	57.0	52.3	53.9	56.1	54.1	55.2	55.5	55.1	54.3	55.3	54.8	55.7	54.9	60.1	67.1	55.5	67.0	69.5
	9.0	66.8	69.8	55.5	52.5	53.6	54.2	55.6	55.5	54.9	55.3	56.2	54.3	55.0	55.3	55.7	67.3	67.4	61.3	60.9	64.8
	9.5	71.0	71.3	67.5	52.9	53.5	54.2	54.4	54.2	54.3	54.7	54.6	54.6	54.6	54.4	59.7	67.3	67.4	67.6	67.3	67.5
	10.0	70.3	71.3	70.8	69.0	57.7	53.5	53.1	53.7	54.0	54.1	54.2	54.3	54.7	60.1	67.6	67.2	67.4	67.2	67.4	67.4

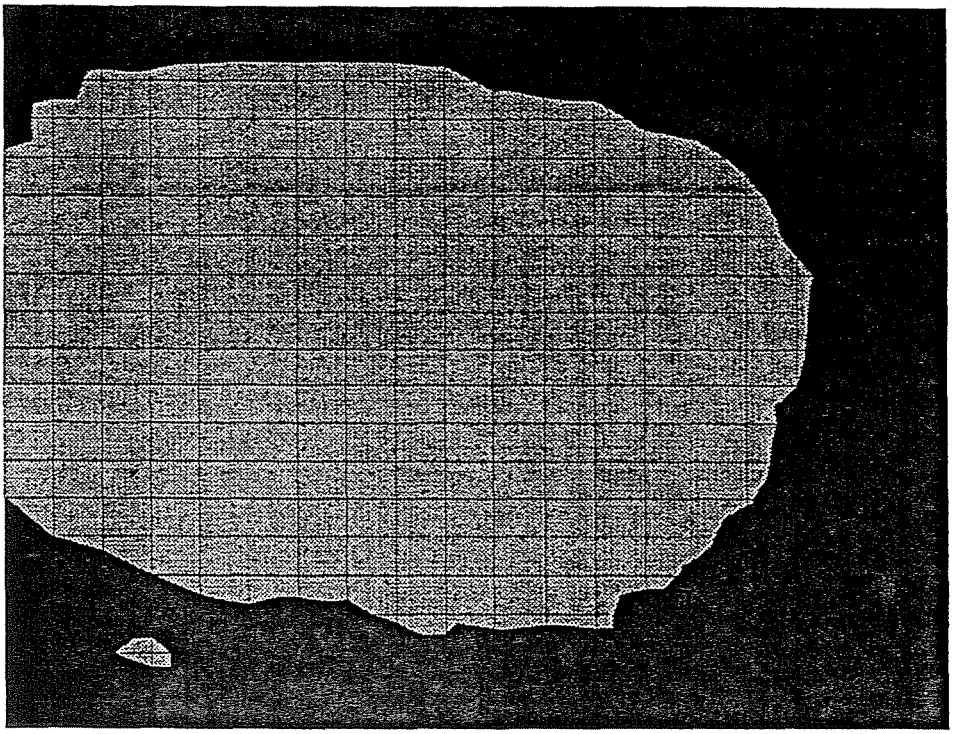

Fig. 7. Distribution of the extinction ratio in the parallel plate made of Zr-doped rutile single crystal grown by the floating zone method.

Y \ Z	0.5	1.0	1.5	2.0	2.5	3.0	3.5	4.0	4.5	5.0	5.5	6.0	6.5	7.0	7.5	8.0	8.5	9.0	9.5	10.0
0.5	57.3	58.6	69.3	69.4	69.5	69.5	69.3	69.3	69.4	56.2	57.3	57.3	57.3	57.3	57.3	57.3	57.3	57.3	57.3	57.3
1.0	58.7	64.4	69.2	69.2	69.2	69.4	69.4	69.4	69.4	58.1	57.3	57.3	57.3	57.3	57.3	57.3	57.3	57.3	57.3	57.3
1.5	69.5	68.6	69.3	69.2	69.5	69.5	69.3	69.4	69.4	57.5	57.3	57.3	57.3	57.3	57.3	57.3	57.3	57.3	57.3	57.3
2.0	63.9	68.6	68.4	69.4	69.5	69.5	69.1	68.1	60.3	57.0	57.3	57.3	57.3	57.3	57.3	57.3	57.3	57.3	57.3	57.3
2.5	57.3	57.3	56.4	60.2	69.1	69.4	60.5	56.5	49.6	53.0	56.3	57.3	57.3	57.3	57.3	57.3	57.3	57.3	57.3	57.3
3.0	57.2	57.3	57.3	57.2	57.4	58.8	59.7	55.8	44.1	53.3	51.2	52.7	55.5	57.3	57.3	57.3	57.3	57.3	57.3	57.3
3.5	57.3	57.3	57.2	57.3	59.9	53.0	57.8	53.9	50.5	53.4	51.7	54.1	56.6	57.2	57.2	57.3	57.3	57.3	57.3	57.3
4.0	57.2	57.3	57.3	60.9	60.0	53.3	49.9	51.3	52.3	50.5	50.8	47.4	56.9	58.5	57.0	57.2	57.3	57.3	57.3	58.0
4.5	57.3	57.3	57.7	60.5	56.2	48.0	49.4	51.9	51.9	50.8	53.8	58.1	57.6	56.7	59.3	56.5	57.3	57.3	58.1	69.4
5.0	57.3	57.3	58.0	57.3	47.6	44.6	51.2	52.2	52.8	56.0	56.1	58.1	57.0	55.9	57.1	57.0	57.2	58.4	58.0	69.4
5.5	57.3	57.3	53.2	59.1	51.7	45.6	54.7	52.7	52.3	53.8	58.9	57.1	56.0	55.2	55.6	55.8	60.7	69.1	69.5	69.6
6.0	57.3	57.3	53.6	62.2	62.2	58.3	54.9	53.1	52.8	54.4	56.5	58.4	56.7	55.2	52.7	54.7	68.3	69.1	69.4	69.5
6.5	57.3	57.3	51.6	60.0	61.1	57.8	55.4	54.5	54.1	55.2	55.8	54.6	55.0	53.9	52.9	52.5	68.9	69.1	69.3	69.3
7.0	57.3	57.3	53.8	55.3	59.6	56.8	55.7	55.5	55.6	56.6	55.5	53.4	52.6	52.0	55.2	58.7	69.0	69.2	69.3	69.4
7.5	57.3	57.3	54.5	56.1	56.2	55.2	55.0	56.2	56.1	56.8	55.3	53.3	51.8	51.3	57.2	58.3	69.1	69.1	69.2	69.3
8.0	55.4	56.3	56.2	56.9	57.0	54.4	55.4	57.2	57.2	56.5	54.6	52.9	51.7	57.1	55.4	57.0	69.2	69.1	69.3	69.4
8.5	65.4	69.3	68.5	53.9	56.1	56.2	56.0	57.2	57.1	57.2	56.2	53.3	56.3	57.1	57.4	57.3	56.9	65.4	69.2	69.4
9.0	69.2	69.4	69.2	68.8	46.8	51.6	53.4	52.5	49.8	50.5	54.6	56.3	57.6	57.4	57.3	57.3	57.3	57.2	57.5	58.1
9.5	69.0	69.3	69.2	69.3	69.1	55.5	56.7	55.0	53.6	54.9	58.0	57.5	57.3	57.3	57.3	57.3	57.3	57.3	57.3	57.3
10.0	69.4	69.5	69.5	69.3	69.4	58.3	57.3	57.3	57.3	57.3	57.3	57.3	57.2	57.3	57.3	57.3	57.3	57.3	57.3	57.3

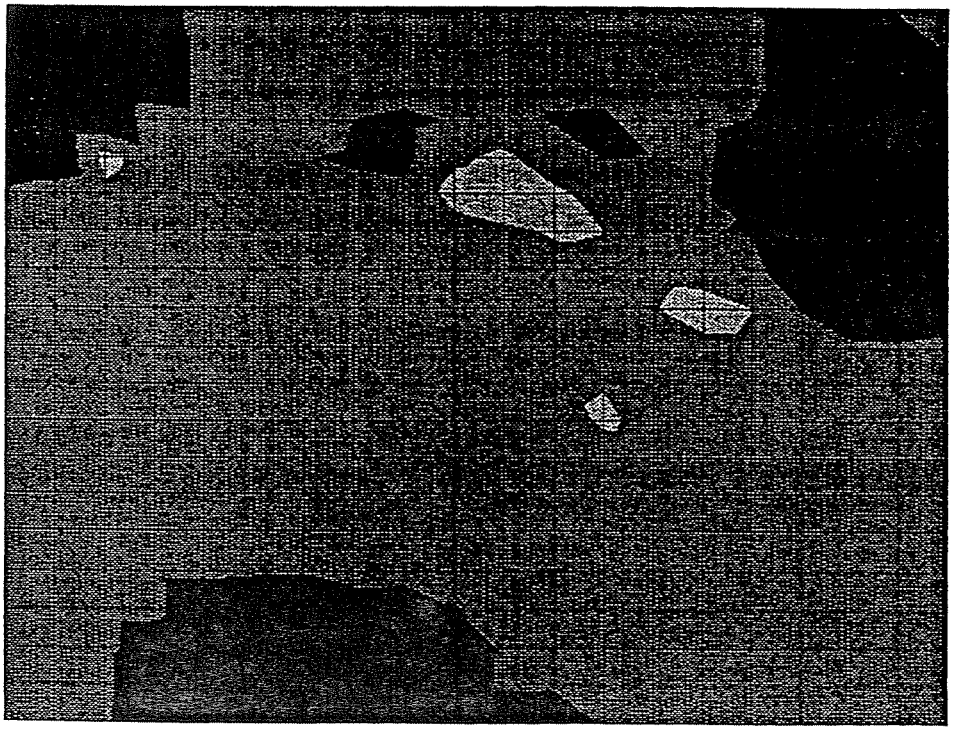

Fig. 8. Distribution of the extinction ratio in the parallel plate made of Al-doped rutile single crystal grown by the floating zone method.

is the most effective dopant to obtain optically uniform rutile single crystals by the floating zone method.

5. SUMMARY AND CONCLUSIONS

Glan–Thompson prisms and parallel plates were fabricated from the floating zone grown rutile single crystals and their extinction ratios were measured in order to evaluate the optical quality of the crystals as practical optical devices. The extinction ration of the Glan–Thompson prisms fabricated from a pure rutile single crystal which was grown under a low oxygen partial pressure was 55 dB, which is comparable to that of commercial Glan–Thompson prisms made of calcite single crystal. The maximum extinction ratios of 58 dB was obtained for both the Zr– and Al–doped crystals. The optical uniformity of the Zr–doped crystal was superior to that of the Al–doped crystal.

The optical quality of the undoped and doped crystals are comparable. In the case of the undoped crystal, however, the growth direction is limited to along the c–axis to obtain low–angle grain boundary free rutile single crystals, while the Zr–doped crystals can be grown along any directions. In accordance with the application, therefore, if the c–axis growth is better, the addition of any dopant is not necessary, and if the c–axis should be greatly inclined, the crystal growth should be done with a small amount of ZrO_2.

The extinction ratios of any prisms fabricated from the rutile single crystals which were grown in this study were slightly less than 60 dB, which is highest grade specification for long distance optical communication devices. However, the minimum desired extinction ratio is 30 dB for simple devices like polarized–light

dependant isolator. Therefore, the optical quality of the floating zone grown rutile single crystals is high enough for the practical use as polarizer.

Chapter 6

Floating Zone Growth and Characterization of $MgTa_2O_6$ and $NiTa_2O_6$ Single Crystals

1. INTRODUCTION

Although there are a great number of optically uniaxial crystals, the only limited crystals, which have special crystal structures, possess large birefringence. The carbonate crystals which have the sodium nitrate ($NaNO_3$) structure is well known to have large birefringence, e.g. $CaCO_3$: 0.17, $MgCO_3$: 0.19, $FeCO_3$: 0.22 and so on [1]. Also, sodium nitrate itself has large birefringence (0.25). From this fact, it is expected that the magnitude of birefringence is dependable to crystal structure rather than chemical composition.

As stated in Chapter 1, rutile (TiO_2) single crystals are one of the most promising materials because of large refractive indices and large birefringence, i.e. for ordinary ray $n_o = 2.616$, for extraordinary ray $n_e = 2.903$ and birefringence $\Delta n = 0.287$. Cassiterite (SnO_2), which adopts the rutile structure, also has appreciably large refractive indices and birefringence, i.e. $n_o = 1.997$, $n_e = 2.093$ and $\Delta n = 0.096$ [2]. Paratellulite (TeO_2) has distorted rutile structure. The refractive indices of paratellulite are 2.274 and 2.430 for ordinary and extraordinary rays, respectively, and thus birefringence is 0.156 [3]. Tapiolite ($FeTa_2O_6$) is known to adopt the trirutile structure [4], which is superstructure of rutile. Also, tapiolite has large refractive indices and birefringence, i.e. $n_o = 2.27$, $n_e = 2.42$ and $\Delta n = 0.15$ [5]. From these facts, the oxides which adopt the rutile or trirutile structure are expected to have large refractive indices and birefringence on the basis of their structures.

$MgTa_2O_6$ and $NiTa_2O_6$ are also known to have the trirutile structure [6,7]. A few researcher have tried to grow those single crystals by the chemical vapor reaction and slow cooling flux method [8,9], but any crystals grown by such

methods are small. Accordingly, the optical properties of those materials have not been clarified.

In this study, $MgTa_2O_6$ and $NiTa_2O_6$ single crystals have been successfully grown by the floating zone method. This chapter deals with the optimum conditions for the floating zone growth, some important optical properties such as refractive indices and transmittance, and miscellaneous properties of the $MgTa_2O_6$ and $NiTa_2O_6$ single crystals.

2. EXPERIMENTAL

MgO (Kojundo Kagaku Kenkyusho, 99.9%), NiO (Kojundo Kagaku Kenkyusho, 99.9%) and Ta_2O_5 (Kojundo Kagaku Kenkyusho, 99.9%) powders were used as starting materials. After the determination of ignition loss, the powders were mixed stoichiometrically for 2 hours in the ethanol medium with an agate mortar or, in the case of $NiTa_2O_6$, 5 mol% excess NiO was added to compensate the loss of NiO by evaporation. The mixed powder was calcined in a platinum crucible at 1000 °C for 10 hours to obtain the single phase of trirutile. After grinding, the powder was molded under a hydrostatic pressure of 100 MPa to be a rod typically 10 mm in diameter and 60 mm long. The molded specimen was sintered at 1400 °C for 3 hours in a vertical tube furnace.

The growth apparatus and procedure was the same as for rutile single crystals described in Chapter 2. Growth conditions were as follows: growth rate was 5 mm/hr, rotation rate was 30 rpm for both a feed rod and a seed crystal (counter–rotation), and atmosphere was an O_2 or Ar stream of 2 dm^3/min.

The grown crystals were annealed in air from 1200 to 800 °C at a cooling rate of 8 °C/hr for $MgTa_2O_6$ and 14 °C/hr for $NiTa_2O_6$. After the determination of the crystal orientation, the crystals were cut to plates at various angles with the c–axis, which is optical axis of trirutile structure, and polished to be mirror finish. For the determination of refractive indices, a parallel plate which was cut parallel to the c–axis was used. The refractive indices for both ordinary and extraordinary rays were determined distinctively by the direct focalizing method (Fig. 1) using a polarizing microscope with a tungsten–filament lamp as light source. An interference (conoscopic) figure of the crystal which was cut perpendicularly to the c–axis was also observed with the polarizing microscope. Transmittance in a range of wavelength from 200 to 2000 nm was measured with a spectrophotometer (Hitachi–330). Temperature dependance of dielectric constant was measured from room temperature to 150 °C by three probe method using an LCR meter (HP–4285A). Chemical durability for a variety of acids was evaluated by the weight loss after immersing for 1 day. Vickers hardness on (001) plane was examined under the load of 300–500 g using a hardness tester (Shimazu type M).

3. RESULTS AND DISCUSSION

3.1. Floating zone growth of $MgTa_2O_6$ and $NiTa_2O_6$ single crystals

When the sintered $MgTa_2O_6$ feed rod was directly used for the floating zone growth, a number of bubbles were easily formed in the melt zone. The amount of the bubbles was sensitive to the atmosphere, that is, the O_2 stream accelerated the formation of bubbles whereas the Ar stream was effective to suppress the formation of the bubbles. Nevertheless, the bubbles were gradually accumulated with proceeding growth run even if the Ar stream was used, and the melt zone

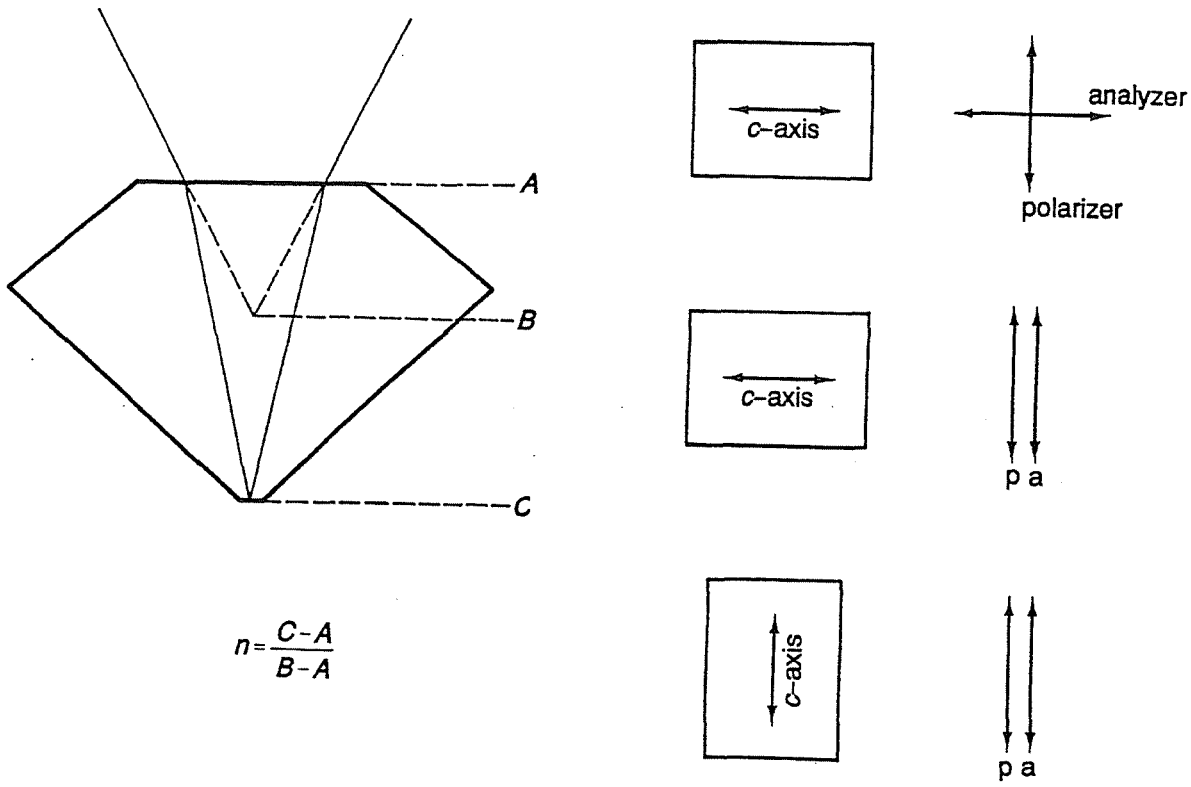

Fig. 1. Schematic illustration of direct focalizing method for the measurement of refractive index of optically uniaxial crystals. When the c–axis is perpendicular to the polarizer and analyzer, the refractive index for ordinary ray can be determined; when parallel, for extraordinary ray.

consequently became unstable. The origin of the bubbles must be residual pore in the feed rod, since $MgTa_2O_6$ is difficult to densify. In order to avoid this problem the sintered rod was once passed through the melt zone at a relatively high rate of 27 mm/hr in the Ar stream to prepare a dense rod, in which few pores are exist. A stable growth run was effected in the Ar stream without introducing the bubbles into the melt zone using the premelted feed rod.

The formation of bubbles in the melt zone is a serious problem also in the case of $NiTa_2O_6$ when the sintered feed rod was used directly for the floating zone growth. Moreover, in this case, the Ar stream is not favorable as the growth atmosphere because the evaporation of NiO from the melt zone is very intensive under such a low oxygen partial pressure. It was thus difficult to keep the stoichiometry in the Ar stream even if the 5 mol% excess NiO was added to the feed rod. By using a dense feed rod premelted in the O_2 stream, as well as $MgTa_2O_6$, a stable growth run was performed without the bubble formation even in the O_2 stream.

The as–grown $MgTa_2O_6$ and $NiTa_2O_6$ single crystals obtained by the floating zone method was black and opaque as shown in figs. 2(a) and 3(a). The reduction of Ta^{5+} to Ta^{4+} would occur to form oxygen vacancies at high temperatures even in the O_2 stream. Subsequent annealing in air rendered the crystals transparent as shown in figs. 2(b) and 3(b). The color of the $MgTa_2O_6$ and $NiTa_2O_6$ was pale–yellow and pale–green, respectively.

Growth direction was an important factor for both $MgTa_2O_6$ and $NiTa_2O_6$ to prevent the grown crystals from cracking on cooling to room temperature after the growth run. If the growth direction was perpendicular to (110) plane, many cracks were formed parallel to the (110) plane, which is cleavage plane of the trirutile

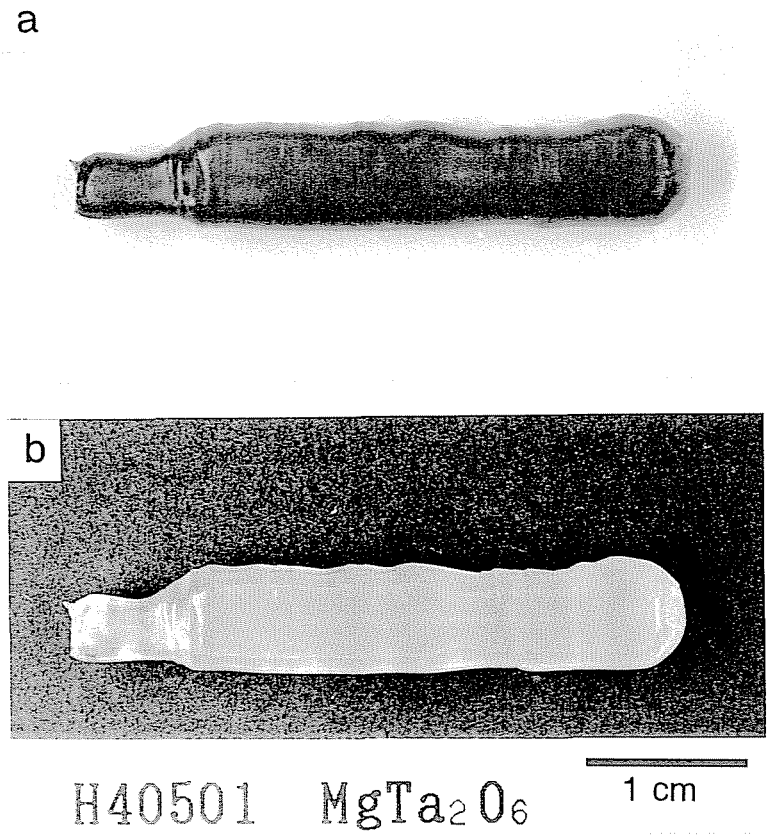

Fig. 2. Floating zone grown $MgTa_2O_6$ single crystal: (a) as-grown; (b) annealed at 1200–800 °C for 50 h.

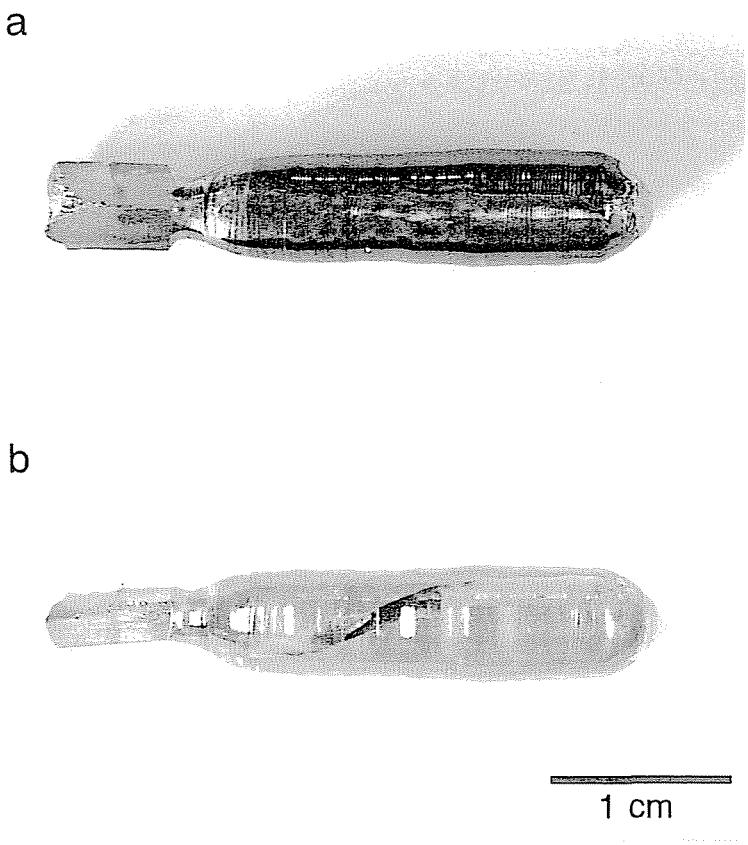

Fig. 3. Floating zone grown $NiTa_2O_6$ single crystal: (a) as-grown; (b) annealed at 1200–800 °C for 30 h.

structure. The growth along the c–axis was effective to suppress the cracking; in particular crack–free single crystals were obtained in the case of $MgTa_2O_6$ growth as shown in fig. 2(b). In the case of $NiTa_2O_6$, however, completely crack–free single crystals were not obtained. The cracks typically propagate parallel to (110) cleavage plane from the tip to the seed in the $NiTa_2O_6$ crystal as shown in fig 3(b).

The $MgTa_2O_6$ crystals grown along the c–axis had strong crystal habit, which is nearly square–prism morphology covered with four facets consisted of {110} planes. This morphology is the same as that of a rutile single crystal grown along the c–axis. On the other hand, the crystal habit of the $NiTa_2O_6$ was not so strong as $MgTa_2O_6$, and only small facets, which are also consisted of {110} planes, were observed on the side of the crystals.

Fig. 4 shows orthoscopic figures of vertical sections of $MgTa_2O_6$ and $NiTa_2O_6$ crystals observed under the polarizing microscope with crossed nicols. There are an appreciable number of low–angle grain boundaries in the $NiTa_2O_6$ crystal, whereas no low–angle grain boundary is observed in the $MgTa_2O_6$ crystal.

As mentioned in the previous chapter, the formation of low–angle grain boundary is the most serious problem in the rutile single crystal growth by the floating zone method. One of the methods to suppress the formation of the low–angle grain boundaries is to use a relatively low oxygen partial pressure of up to 10^{-2} as growth atmosphere. The $MgTa_2O_6$ single crystal was grown in the Ar stream, which provides the oxygen partial pressure of about 10^{-4}. Under such a low oxygen partial pressure, Ta^{5+} will be strongly reduced to form an appreciable number of Ta^{4+}. Since the ionic radius of Ta^{4+} is larger than that of Ta^{5+}, i.e. Ta^{4+}: 0.074 nm and Ta^{5+}: 0.068 nm, Ta^{4+} may act as the pinning center to restrict the

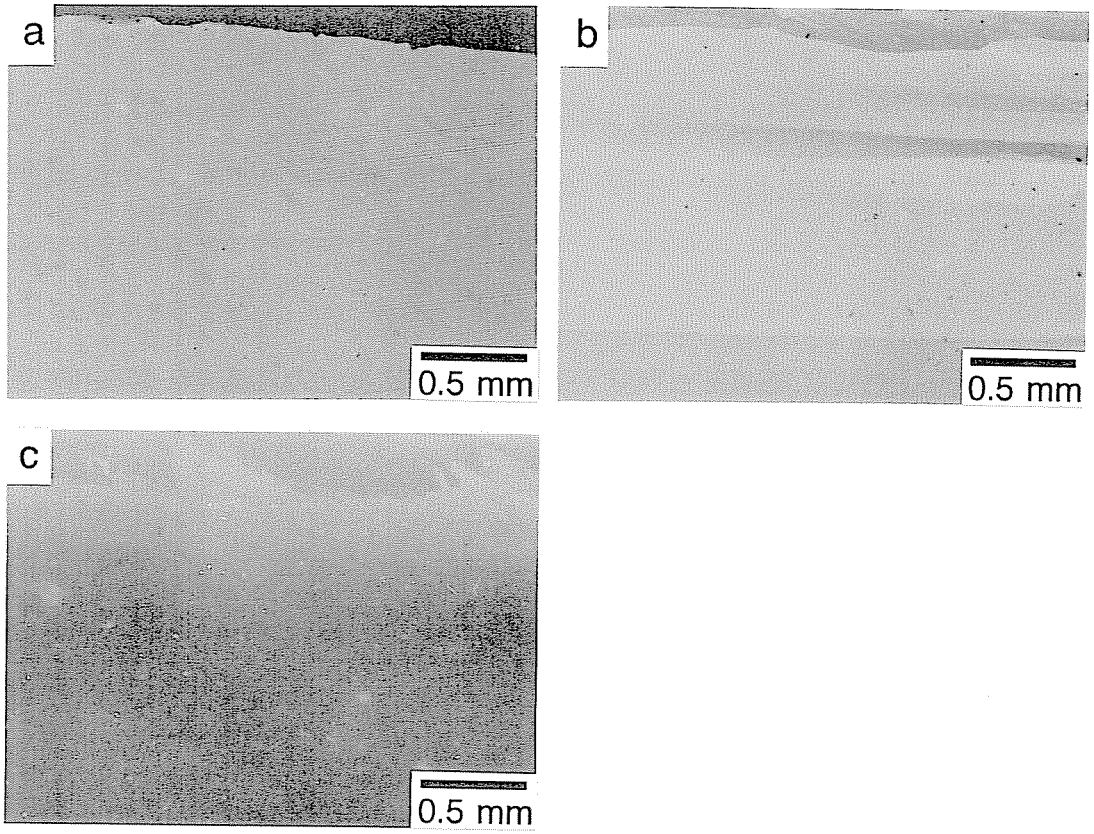

Fig. 4. Polarized microphotographs of the vertical sections of $MgTa_2O_6$ and $NiTa_2O_6$ crystals: (a) $MgTa_2O_6$; (b) $NiTa_2O_6$ (pure); (c) $NiTa_2O_6$ (Zr–doped).

migration of dislocations so that low-angle grain boundaries were not formed in the $MgTa_2O_6$ single crystals.

In the case of $NiTa_2O_6$, however, the Ar stream can not be used because of the intensive evaporation of NiO. It is expected that the $NiTa_2O_6$ crystal grown in the O_2 stream does not contain enough Ta^{4+} to suppress the formation of low-angle grain boundaries. Accordingly, the addition of ZrO_2 to $NiTa_2O_6$ was tried in the same way for rutile single crystals as mentioned in Chapter 2. Fig. 4(c) shows the vertical section of ZrO_2-doped (1 mol%) $NiTa_2O_6$ crystal. Although a few low-angle grain boundaries can still be observed, the number of the boundaries were considerably decreased. However, more addition of ZrO_2, e.g. 2 mol%, resulted in the nucleation of other grain, which had different direction from the seed crystal, on the surface of the crystal, so that a single crystal could not be obtained.

Fig. 5 shows an interference figures of the floating zone grown $MgTa_2O_6$ and $NiTa_2O_6$ crystals observed with the polarizing microscope. For $NiTa_2O_6$, a section which contained few low-angle grain boundaries was used for the conoscopic observation. In both figures, the isogyers cross perpendicularly at approximately one point, and all the isochromatic curves are concentric circles. These figures are typical for an optically uniaxial crystal, and accordingly the $MgTa_2O_6$ and $NiTa_2O_6$ crystals obtained in this study would be optically uniform and would have little stress birefringence.

3.2. Optical properties of $MgTa_2O_6$ and $NiTa_2O_6$

Refractive indices of $MgTa_2O_6$ and $NiTa_2O_6$ are give in table 1. Since the light source was a tungsten-filament lamp, which emits approximately white light,

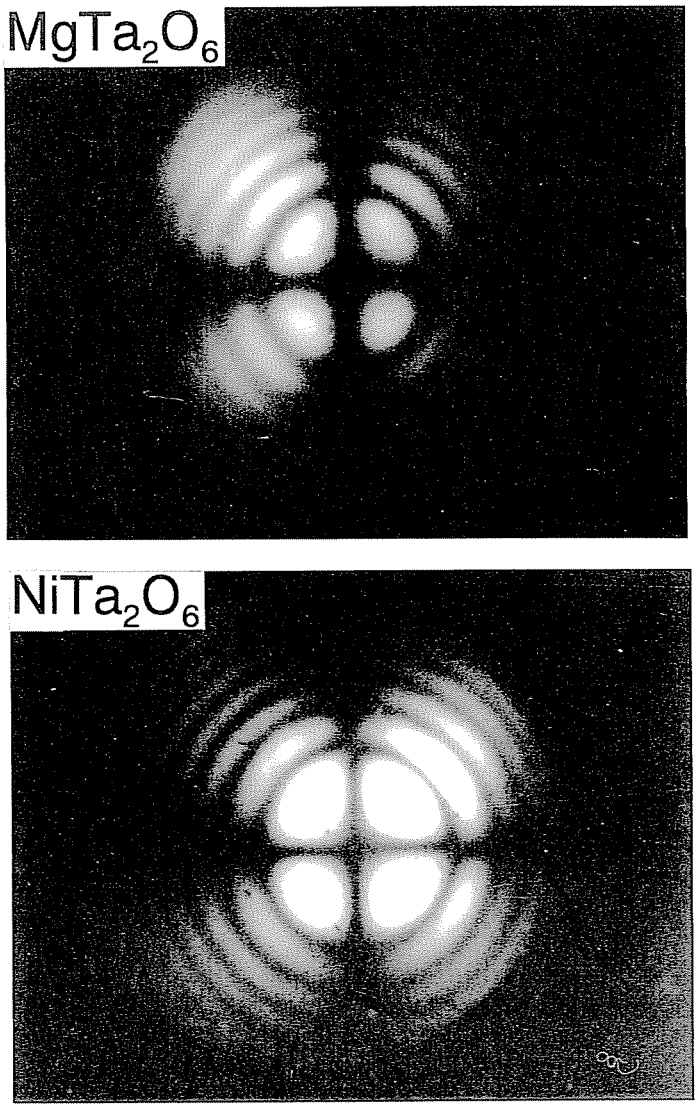

Fig. 5. Conoscopic figures of $MgTa_2O_6$ and $NiTa_2O_6$ single crystals grown by the floating zone method.

Table 1. Refractive indices of trirutile and rutile type materials

	n_o	n_e	Δn
$MgTa_2O_6$	2.07	2.18	0.11
$NiTa_2O_6$	2.29	2.44	0.15
$FeTa_2O_6$	2.27	2.42	0.15
TiO_2	2.616	2.903	0.287
SnO_2	1.997	2.093	0.096

the refractive indices measured would be average over the range of visible light. The optic character was positive as well as rutile. The refractive indices and the birefringences are not so large as compared with those of the rutile, but as shown in fig. 6 they are considerably larger than those of the other optically uniaxial crystals, e.g. quartz (SiO_2), which has conventionally been used for polarizing devices.

The reason why the rutile or trirutile type oxides have large birefringence is explained as follows: Rutile or trirutile structure involves AO_6 octahedra which align along the c–axis, namely optic axis, sharing edge consisted of O–O bond as shown in fig. 7. On the basis of the Pauling's fifth rule, the length of the sharing edge is shorter than other edges which do not share with other octahedra because the repulsion occurs between like charges of like cations. In fact, the shearing edge of rutile is 0.025 nm, which is shorter than the normal O–O length of 0.028 nm. This difference in the O–O length may result in the difference in the polarization of oxide ions between parallel and perpendicular to the optic axis. Refractive index in an oxide crystal is significantly affected by the polarization of the oxide ions. The refractive index, namely the velocity of electromagnetic wave, is determined by the interaction between the electromagnetic wave and polarization of oxide ions. Accordingly, there is difference in the velocity of the electromagnetic waves which vibrate parallel and perpendicular to the optic axis. Similar situation occurs in the calcite–type crystal, in which plane–like CO_3^{2-} ions is perpendicular to the optic axis.

Fig. 8 shows a typical double refraction image through the $MgTa_2O_6$ single crystal which was cut at an angle of 45 degrees with the c–axis. An appreciable split of light–beam can be observed between ordinary and extraordinary rays. The

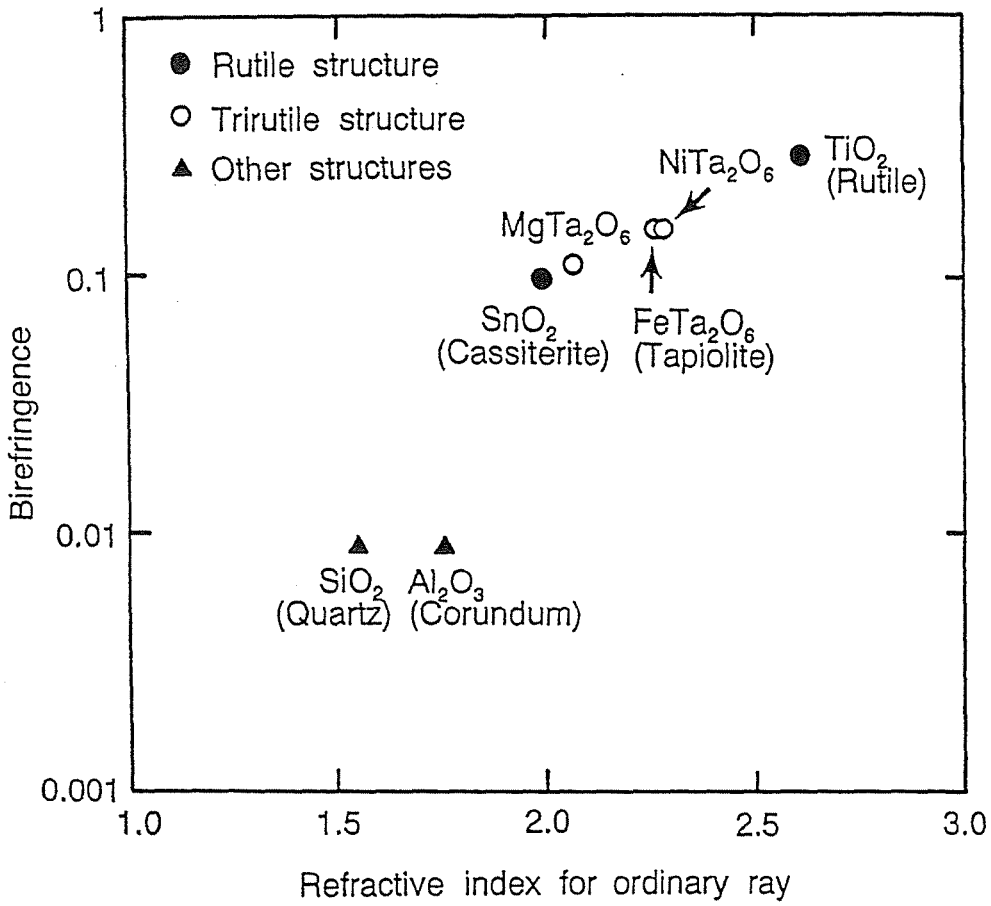

Fig. 6. Refractive index for ordinary ray and birefringence of optically uniaxial crystals.

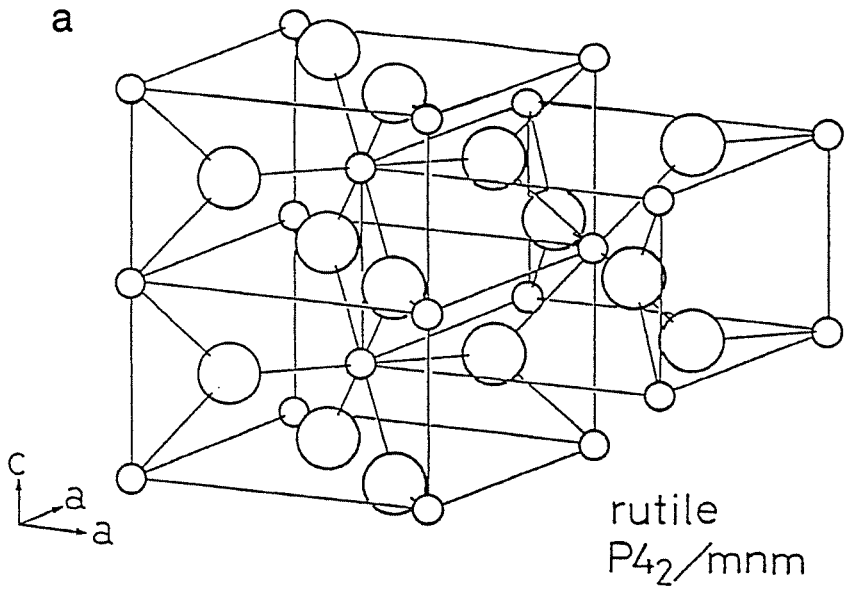

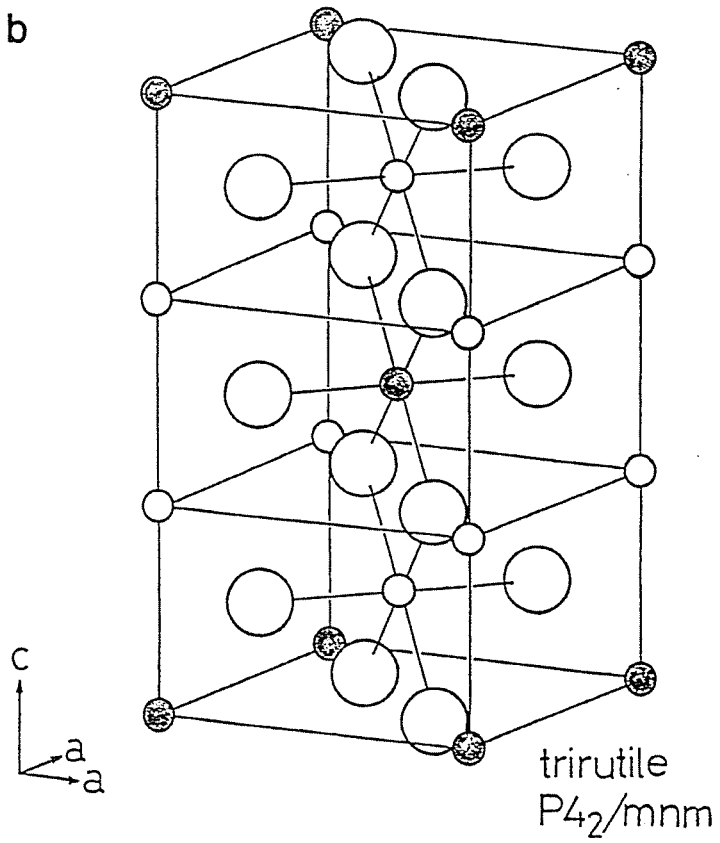

Fig. 7. Crystal structures of rutile (a) and trirutile (b). Large open circles represent oxide ions and small circles represent cations.

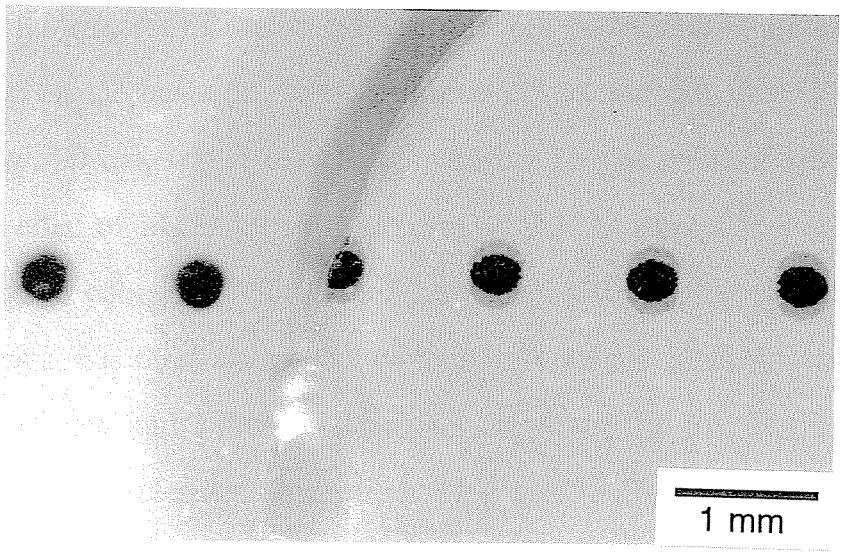

Fig. 8. Double refraction images through a $MgTa_2O_6$ single crystal. The crystal was cut at an angle of 45 ° with the c–axis and polished to be 1.6 mm thick.

ratio of the split width to crystal thickness is 1:20, which is close to theoretical value calculated from the refractive indices. The magnitude of the split is about a half of that of rutile but about eight times larger than that of quartz. Accordingly, the $MgTa_2O_6$ single crystal has the possibility to serve in practical polarizing devices.

The $MgTa_2O_6$ single crystal does not have remarkable absorption spectra in a range of wavelength from 500 to 2000 nm as shown in fig. 9. The transmittance through the crystal perpendicular to the c–axis is about 75%, which approximately corresponds to the theoretical value calculated from the refractive index of 2.07 for ordinary–ray on the basis of Fresnel's formula. The transmittance is gradually decreased below 500 nm, which may be responsible for the color of pale–yellow. The absorption edge of $MgTa_2O_6$ is at 290 nm, which is appreciably extended to ultraviolet region as compared with that of the rutile (420 nm). On the other hand, the $NiTa_2O_6$ crystal has three strong absorptions in the wavelength ranges of 400–500 nm, 650–900 nm and 1100–1500 nm as shown in fig. 10. Borromei et al reported the same characteristic absorptions of the $NiTa_2O_6$ single crystal grown by the flux method [10], and they concluded that the origin of those absorptions is attributable to distorted NiO_6 octahedra. The absorptions in 400–500 nm and 650–900 nm correspond to blue and red color in the visible region, respectively, and they are responsible to the characteristic pale–green color of $NiTa_2O_6$ because blue and red are complementary color for green. The transmittance in the wavelength range of 500–650 nm is about 72%, which corresponds to the calculated value from the refractive index of 2.29 for ordinary–ray.

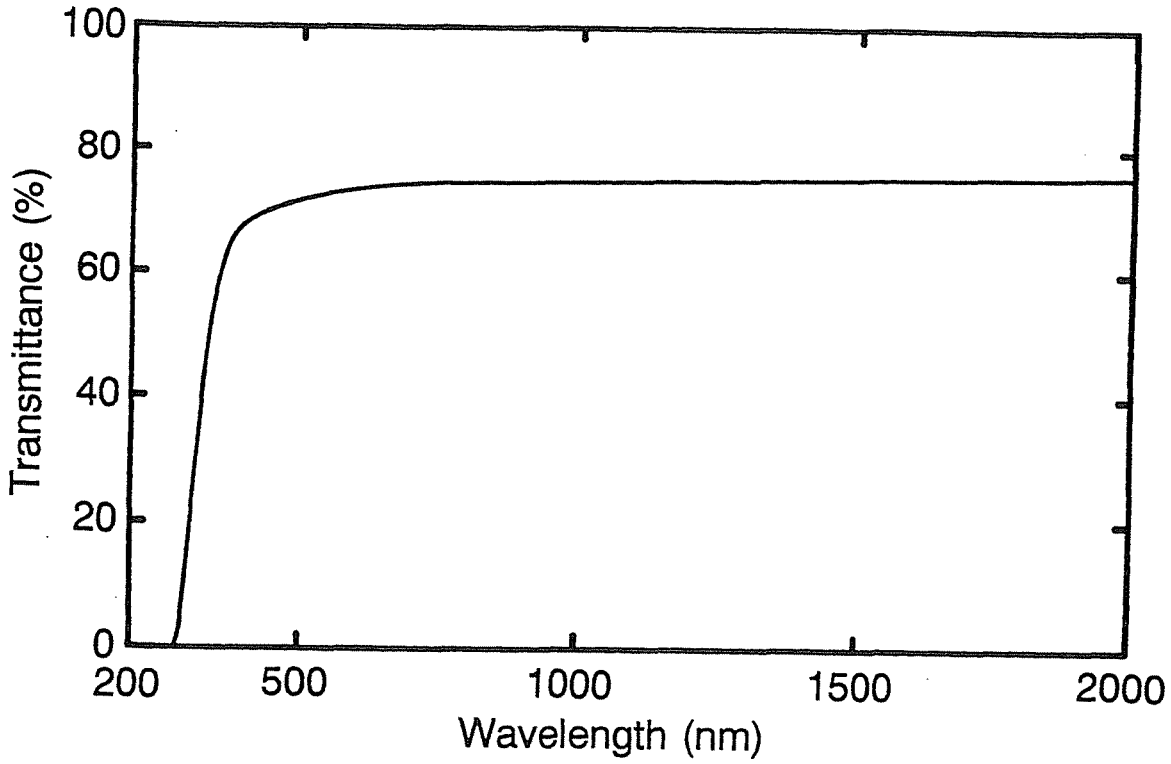

Fig. 9. Transmittance of the $MgTa_2O_6$ single crystal in visible and near infrared regions.

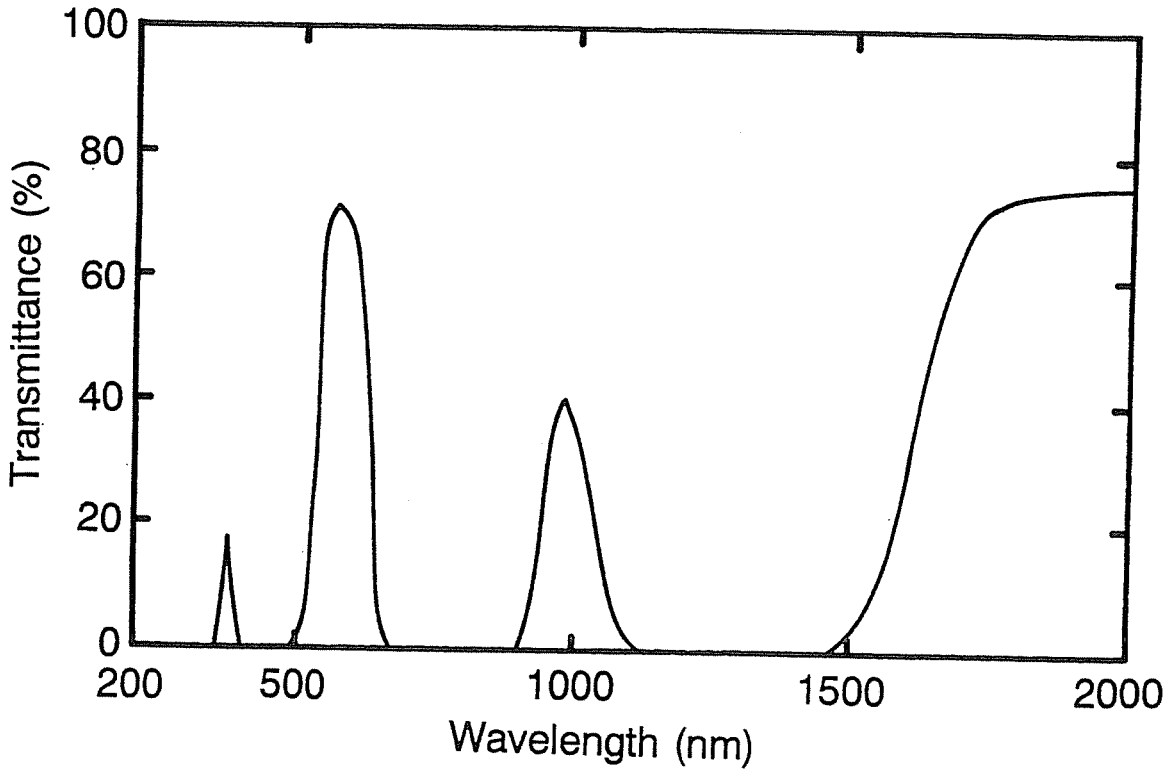

Fig. 10. Transmittance of the $NiTa_2O_6$ single crystal in visible and near infrared regions.

3.3. Miscellaneous properties of $MgTa_2O_6$ and $NiTa_2O_6$

Every optical devices must be processed as precisely as possible to keep the quality of signal, i.e. laser beam. Although calcite single crystals have comparable birefringence to rutile, the processing of the calcite single crystals is very difficult because of the strong cleavage and low hardness. Rutile single crystals also have cleavage plane of {110}, but this plane is not easily cloven by the mechanical shock. Moreover the hardness of rutile is moderate, i.e. not so hard as alumina and not so soft as calcite, to process. Although the $MgTa_2O_6$ single crystal also has {110} cleavage plane, the plane is not easily cloven as well as rutile. On the other hand, the $NiTa_2O_6$ single crystal is easily cloven as compared with $MgTa_2O_6$ so that a completely crack free crystal was not obtained. The values of Vickers hardness for $MgTa_2O_6$ and $NiTa_2O_6$ are given in table 2. $MgTa_2O_6$ and $NiTa_2O_6$ have comparable vickers hardness, which is just larger than that of rutile. These moderate hardness will contribute to relatively easy processing of the crystals.

The chemical stability is one of the important properties required for practical devices. Calcite single crystals are dissolved a little in water and are easily attacked by all the acids. On the contrary, rutile has excellent chemical stability. This is the reason why rutile single crystal is more favorable in recent optical device than calcite. Thus, the $MgTa_2O_6$ and $NiTa_2O_6$ crystals were immersed in water, hydrochloric acid, nitric acid and sulfuric acid for one day to examine the chemical durability. No weight loss was observed after immersing water and any acids. Therefore, the $MgTa_2O_6$ and $NiTa_2O_6$ single crystals have good chemical stability, which is comparable to rutile.

The dielectric properties of $MgTa_2O_6$ and $NiTa_2O_6$ are summarized in table 3. The dielectric constant (ε_r) perpendicular to the c–axis for both $MgTa_2O_6$ and

Table 2. Vickers hardness (H_V) of $MgTa_2O_6$, $NiTa_2O_6$ and rutile

	H_V	load (N)
$MgTa_2O_6$	980 ± 40	4.9
$NiTa_2O_6$	970 ± 30	2.9
TiO_2	940 ± 10	4.9

Table 3. Dielectric properties of trirutile and rutile type materials

		ε_r	TC_{ε_r}	n_o and n_e
$MgTa_2O_6$	($\perp$c)	25	−100	n_o: 2.07
	(//c)	29	−70	n_e: 2.18
$NiTa_2O_6$	($\perp$c)	27	−50	n_o: 2.29
	(//c)	35	−30	n_e: 2.44
TiO_2	($\perp$c)	85.3		n_o: 2.616
	(//c)	170		n_e: 2.903
SnO_2	($\perp$c)	9.6		n_o: 1.997
	(//c)	13.5		n_e: 2.093

$NiTa_2O_6$ are larger than that parallel to the c–axis as well as rutile. This is consistent with the anisotropy of refractive indices although the difference in ε_r between parallel and perpendicular to the c–axis is also not so large as rutile. In trirutile and rutile type materials, there is qualitative correlation between refractive index and dielectric constant, i.e. a material having larger refractive index has large dielectric constant. The sign of temperature coefficient of dielectric constant (TC_{ε_r}) is negative for both $MgTa_2O_6$ and $NiTa_2O_6$ as similar as other dielectrics. The relation between ε_r at room temperature and TC_{ε_r} departs from the linear relation, which is empirically proposed by Harrop [11], for both $MgTa_2O_6$ and $NiTa_2O_6$, that is, the values of TC_{ε_r} are less than that expected from ε_r.

4. SUMMARY AND CONCLUSIONS

$MgTa_2O_6$ and $NiTa_2O_6$ single crystals were successfully grown by the floating zone method. The use of the premelted feed rod was important to suppress the formation of bubbles in the melt zone so that a stable growth run was performed in both cases of $MgTa_2O_6$ and $NiTa_2O_6$. In the case of $NiTa_2O_6$, the O_2 stream as growth atmosphere was essential to avoid the evaporation of NiO to keep the stoichiometry in the melt zone. The as–grown $MgTa_2O_6$ and $NiTa_2O_6$ crystals were black and opaque, and subsequent annealing in air rendered the crystals transparent. The color of the $MgTa_2O_6$ and $NiTa_2O_6$ crystals were pale–yellow and pale–green. The $MgTa_2O_6$ crystals contained no low–angle grain boundaries, whereas the $NiTa_2O_6$ crystal comprised an appreciable number of low–angle grain boundaries since the crystal growth for $NiTa_2O_6$ was done in the O_2 stream. The addition of a small amount of ZrO_2 was effective to reduce the number of the low–angle grain boundaries as well as rutile. The conoscopic figures clarified that the $MgTa_2O_6$ and $NiTa_2O_6$ single crystals grown by the floating zone method had

good optical uniformity.

The optical and miscellaneous properties of the $MgTa_2O_6$ and $NiTa_2O_6$ single crystals were revealed in this study as follows:

(1) For $MgTa_2O_6$, n_o = 2.07 and n_e = 2.18 under white light, and birefringence was thus 0.11. For $NiTa_2O_6$, n_o = 2.29 and n_e = 2.44 and thus Δn = 0.15. The optic character of $MgTa_2O_6$ and $NiTa_2O_6$ was positive as well as the other rutile or trirutile type oxides.

(2) The $MgTa_2O_6$ crystal did not have marked absorption spectra in the wavelength range of 500–2000 nm, and the transmittance was about 75%. The absorption edge was at 290 nm. On the other hand, the $NiTa_2O_6$ crystal had tree major absorptions in 200–2000 nm, and two of them in the visible region are responsible to the characteristic pale–green color of the $NiTa_2O_6$ crystals.

(3) The Vickers hardness of $MgTa_2O_6$ and $NiTa_2O_6$ is comparable and is just larger than that of rutile.

(4) The $MgTa_2O_6$ and $NiTa_2O_6$ crystals had good chemical stability.

(5) The dielectric constant of $MgTa_2O_6$ and $NiTa_2O_6$ crystals was 25–30, which was considerably smaller than that of rutile, and anisotropy of the relative dielectric constant is also smaller than that of rutile.

In the survey of optical properties of $MgTa_2O_6$ and $NiTa_2O_6$ single crystals, both crystals were found to have relatively high birefringence as expected. The $NiTa_2O_6$ single crystal can probably not be used practical devices since this crystal has strong absorptions in visible and near infrared region. On the other hand, the $MgTa_2O_6$ single crystal is transparent in wider wavelength region than rutile is. The other properties of $MgTa_2O_6$ are comparable to those of rutile. Moreover,

low-angle grain boundaries are not so easily formed in $MgTa_2O_6$ as in rutile. Although the exact melting temperature of $MgTa_2O_6$ is not known, it is surely lower than that of rutile since the lamp power necessary for steady floating zone growth of $MgTa_2O_6$ is about 80% that for rutile. From this fact, the Czochralski growth of $MgTa_2O_6$ might be possible to obtain large-diameter crystals. If this is realized, the $MgTa_2O_6$ single crystals may be used in a variety of optical devices although the birefringence of $MgTa_2O_6$ is less than that of rutile.

REFERENCES

1. A. Miyashiro and I. Kushiro, "Gansekigaku", Kyoritsu Shuppan, (1972) 199.
2. Г. B. Camcohoba, "Sankabutsu-binran", Nisso Tsushin-sha, (1969) 306.
3. M. Kimura, "Hikari Erekutoronikusu Zairyo Manyuaru", Optronics-sha, (1986) 419.
4. T. Osaka and T. Nakayama, *Trans. Japan. Inst. Metals*, **10** (1969) 437.
5. JCPDS file No. 23-1124.
6. Von G. Bayer, *Ber. Dtsch. keram. Ges.*, **59** (1962) 535.
7. H. Mullar-Busschbaum and R. Wichmann, *Z. Anog. Allg. Chem.*, **536** (1986) 15.
8. K. Kawajiri, Y. Yamasaki and Y. Sugitani, *Nihon Kagakukai-shi*, No. 8 (1986) 15.
9. R. Kremer and J. Greeden, *J. Solid State Chem.*, **73** (1988) 1244.
10. R. Borromei, E. Cavalli and L. Oleari, *Inorg. Chim. Acta*, **204** (1993) 159.
11. P. J. Harrop, *J. Mater. Sci.*, **4** (1969) 370.

Chapter 7

Conclusions

This thesis has described on the growth of rutile (TiO_2) and trirutile ($MgTa_2O_6$ and $NiTa_2O_6$) single crystals by the floating zone method. In the case of rutile, for which most part of this thesis is devoted, the study object has been targeted to grow optical grade single crystals to use as practical polarizers. In the case of trirutile, the purpose was directed to clarify their optical properties, which have been unknown. The following is the conclusions of this thesis.

Chapter 1 has dealt with the background for this study. The importance of the rutile single crystals in the optical communication has been described on the basis of their properties. Some new candidates for polarizer materials have also given. The outline of the floating zone method has been described comparing with the Verneuil method, which has conventionally been employed to grow rutile single crystals.

Chapter 2 has dealt with the floating zone growth of rutile single crystals free from low-angle grain boundaries, which deteriorate optical quality of the crystals. The effects of oxygen partial pressure and dopant were examined to suppress the formation of low-angle grain boundaries. A relatively low oxygen partial pressure as growth atmosphere was effective to suppress the formation of low-angle grain boundaries except peripheral region. The addition of a small amount of ZrO_2 or Al_2O_3 was also effective to reduce the number of low-angle grain boundaries. The formation of low-angle grain boundaries would be based on the polygonization mechanism, that is, edge dislocations are migrated and rearranged linearly to reduce the thermal stress which occurs during cooling. In the case of the ZrO_2 or Al_2O_3 addition, Zr^{4+} ions of which radius is larger than that of Ti^{4+} and Al^{3+} ions of which radius is smaller than that of Ti^{4+} would substitute the Ti^{4+} sites to pin down the migration of the dislocations by reducing the strain energy around the

dislocations so that the polygonization did not occur. When a low oxygen partial pressure was used, Ti^{3+} ions would have a role as pinning center for dislocations. When growth direction was inclined to the c-axis, for example 48°, low-angle grain boundaries were formed more readily than when the c-axis growth. More intensive thermal stress would occur when the c-axis was inclined. The addition of ZrO_2 of 1.0 at% was the only means to suppress the formation of low-angle grain boundaries in such a case.

Chapter 3 has dealt with the effects of aliovalent cations on decoloration of floating zone grown rutile single crystals. The aliovalent cation free rutile crystal after the melt growth is usually colored due to the residual Ti^{3+} ions which are formed by the reduction at a high temperature. The addition of a small amount of trivalent or divalent cation was very effective to obtain pale-yellow and transparent rutile single crystals in the as-grown state. The electrical conductivity of the Al-doped rutile single crystal was higher by one order of magnitude than that of the undoped crystal in AC field, but DC conductivity of both crystal was much the same. From these facts, it is concluded that the aliovalent cations would substitute the Ti^{4+} sites to form oxygen vacancies, via which oxide ions easily diffuse to oxidize Ti^{3+} to Ti^{4+} in the rutile crystal during cooling to room temperature for 30 min.

Chapter 4 has dealt with the solid-liquid interface shapes in the floating zone growth of rutile single crystals. The interface shapes are an important factor not only to influence crystal quality but also to examine the possibility to grow large diameter crystals by the floating zone method. An extremely convex interface should be avoided to prevent the contact between a feed rod and a growing crystal. In the case of 10 mm diameter crystal, the height of the interface was

drastically lowered by increasing crystal rotation rate because of enhanced force convection. In the case of 13 mm diameter crystal, however, the height of the interface was not significantly lowered only by the increased rotation rate of up to 60 rpm. The temperature of the central part of the melt zone for the 13 mm diameter crystal would be much lower than that for the 10 mm diameter crystal due to increased melt volume. This phenomenon indicates the difficulty to grow large diameter rutile single crystals by the floating zone method.

Chapter 5 has dealt with the optical quality of the floating zone grown rutile single crystals as practical polarizers. Glan–Thompson prisms and parallel plates were fabricated from undoped and doped rutile single crystals, respectively, and their extinction ratio was measured. The extinction ratio of the Glan–Thompson prisms was 55 dB, which is comparable to high grade commercial Glan–Thompson prism made of calcite single crystals. The maximum extinction ratio of the parallel plates was 58 dB for both Zr– and Al–doped rutile single crystals. The optical uniformity of the Zr–doped crystal was superior to the Al–doped crystal. From these results, the optical quality of the rutile single crystals grown by the floating zone method is high enough to be served in practical optical devices.

Chapter 6 has dealt with the floating zone growth and characterization of trirutile ($MgTa_2O_6$ and $NiTa_2O_6$) single crystals, which are expected to have large birefringence because of their crystal structure. The $MgTa_2O_6$ and $NiTa_2O_6$ single crystals were successfully grown by the floating zone method using a premelted feed rod. The birefringence of $MgTa_2O_6$ and $NiTa_2O_6$ was determined to be 0.11 (n_o: 2.07, n_e: 2.18) and 0.15 (n_o: 2.29, n_e: 2.44), respectively, which are significantly large as expected. The $MgTa_2O_6$ single crystal does not have any characteristic absorptions in visible and near infrared region and has the absorption

edge of 290 nm, which is appreciably shorter than that of rutile (420 nm). On the other hand, the $NiTa_2O_6$ single crystal has three absorption bands in the wavelength range of 400–500 nm, 650–900 nm and 1100–1500 nm. The chemical and mechanical properties of $MgTa_2O_6$ are similar to those of rutile. Accordingly, the $MgTa_2O_6$ single crystal has the potentiality to be served in practical optical devices.

In conclusion, the optical grade rutile single crystals were successfully grown by the floating zone method, and the double oxides with trirutile structure were revealed to have large birefringence as had been expected.

ACKNOWLEDGEMENTS

The research work written in this thesis was initiated at Research and Development Division, Chichibu Cement Co., Ltd. It has been continued at Department of Applied Chemistry, Faculty of Engineering, Hokkaido University. It is nothing to say that this work has been supported by the cooperation, understanding and encouragement of many people. I would like to express my sincere gratitude to following people:

Prof. Kohei Kodaira (Hokkaido University) for his strict and instructive check of my papers, fruitful suggestions and discussions, and continuous encouragement;

Drs. Shigeyuki Kimura and Kenji Kitamura (National Institute for Research in Inorganic Materials) for their kind guidance to the floating zone growth and the optical characterization of single crystals and their informative advice and discussions;

Prof. Toru Matsushita (Kumamoto Institute of Technology) for his lecture of the ceramic science and continuous encouragement;

Dr. Junichi Takahashi (Hokkaido University) for his collaboration, especially in electrical characterization of rutile single crystals, valuable discussion and continuous encouragement;

Dr. Keiichi Minegishi (Sintering Metal Co., Ltd.) for providing me with an

opportunity to study the crystal growth by the floating zone method;

Dr. Tadatoshi Hosokawa (Chichibu Cement Co., Ltd.) for his kind guidance to the crystal optics, especially characterization using a polarizing microscope;

Dr. Katuyuki Asaumi (Sumitomo Cement Co., Ltd.) for teaching me how to work as a scientist;

Messrs. Junji Saito and Hideaki Kaneda (Mitubishi Kagaku Corporation) for measurements of the extinction ratio of rutile single crystals;

Mr. Tsuyoshi Furusaki (Hokkaido University) for his helpful collaboration and encouragement;

Mr. Kazuto Ando (Sumitomo Cement Co., Ltd.) for his assistance of growing trirutile single crystals by the floating zone method;

Mr. Kazuhito Hatta (Graduate Student of Hokkaido University) for his assistance of growing rutile single crystals by the floating zone method;

and

My family for their lots of smiles, which have let me forget anything troubled and have given me relaxation.